

CHARACTERISATION OF METABOLITE
CONCENTRATION IN THE LATERAL GENICULATE
NUCLEUS AND VISUAL CORTEX OF PATIENTS
WITH DIFFERENT SEVERITY OF GLAUCOMA USING
MAGNETIC RESONANCE SPECTROSCOPY

BY

LIYANA BINTI MUSA

A thesis submitted in fulfilment of the requirement for the
degree of Doctor of Philosophy in Health Sciences

Kulliyyah of Allied Health Sciences
International Islamic University Malaysia

OCTOBER 2023

ABSTRACT

Glaucoma is an ocular disease that results progressive damage of the retinal nerve fibre layer which result to irreversible visual deterioration. Glaucoma impact on the brain is not conclusive. Even the magnetic resonance spectroscopy (MRS) findings in the visual pathway areas shown incoherent findings. This study aimed to investigate and measure the concentration of metabolites in the lateral geniculate nucleus (LGN) and visual cortex (VC) of subjects with glaucoma using MRS. The MRS measurement using a single-voxel spectroscopy (SVS) was performed using 1.5 Tesla MRI, on healthy young adults, healthy older adults, mild glaucoma, and severe glaucoma. A standardised volume of interest of 13mm x 13mm x 13mm was placed in the region of LGN and VC. Five metabolites were extracted and quantified from raw spectra using the AMARES (Advanced Method for Accurate, Robust, and Efficient Spectral Fitting) method within the Java-based magnetic resonance user interface (jMRUI). The quantification process yields amplitudes in arbitrary units of N-acetyl aspartate (NAA), glutamate-glutamine (Glx), creatine (Cr), choline (Cho), and Myo-Inositol (mI). Two consecutive scans were performed on each LGN and VC from both brain hemispheres of young healthy adults. The repeatability of MRS measurement in the LGN and VC were analysed. The LGN and VC of young healthy subjects and healthy elderly subjects were scanned. The metabolites were compared between groups. The metabolites in the LGN of healthy elderly subjects, participants with mild glaucoma and severe glaucoma were compared. The metabolites in the VC of healthy elderly subjects, participants with mild glaucoma and severe glaucoma were compared. The metabolites concentration in the LGN and VC showed no significant differences between consecutive scan ($p > 0.05$). Analysis showed good agreement and small variability between the consecutive MRS measurements (bias in LGN: -0.46 to 1.17; bias in VC: -0.61 to -0.22). Healthy older adults have lower levels of NAA and higher levels of Glx, Cr, and Cho in the LGN compared to healthy young adults ($p < 0.05$). In the VC, healthy older adults have higher levels of Cr, Cho and mI compared to healthy young adults ($p < 0.05$). Severe glaucoma group has higher level of NAA (65.03 ± 14.66 ; Tukey HSD, $p = 0.03$) and lower level of Cho (14.09 ± 5.07 ; Games-Howell, $p = 0.016$) in the LGN compared to healthy group. Glx (604.93 ± 93.55 ; Games-Howell, $p = 0.031$) level in the VC was lower in severe glaucoma compared to healthy group while Cho/Cr (0.030 ± 0.06 ; Tukey HSD, $p = 0.031$) level in the VC was lower in severe glaucoma group compared to mild glaucoma group. The single voxel MRS using 1.5 Tesla MRI is repeatable in determining metabolites concentration in the LGN and VC. Age affects the NAA, Glx, Cr and Cho concentrations in the LGN, and Cr, Cho and mI concentrations in the VC. Metabolites analysis should consider aging into factor. Glaucoma may cause shift in the NAA and Cho concentration amplitudes and ratio in the LGN. Glaucoma may cause shift in the Glx and Cho/Cr concentration amplitudes and ratio in the VC. Further research in this area may help elucidate the underlying mechanisms of glaucoma and potentially aid in the development of novel diagnostic or therapeutic approaches.

ملخص البحث

الجلوكوما هو مرض يصيب العين، ويؤدي إلى تلف تدريجي لطبقة الألياف العصبية في شبكية العين مما يؤدي إلى تدهور بصري لا رجعة فيه. إن تأثير الجلوكوما على الدماغ ليس قاطعاً، حتى أظهرت نتائج التحليل الطيفي بالرنين المغناطيسي (MRS) نتائج غير مترابطة لمناطق المسار البصري. تهدف هذه الدراسة إلى اكتشاف تركيز المستقلب وقياسه في النواة الركبية الجانبية (LGN) والقشرة البصرية (VC) للأشخاص المصابين بالجلوكوما باستخدام التحليل الطيفي بالرنين المغناطيسي (MRS). ويشير قياس هذا التحليل باستخدام التحليل الطيفي أحادي فوكسل (SVS) إلى تطبيق 1.5 تسلا MRI على الشباب والكبار الأصحاء، والرزق الخفيف والشديد. قد تم وضع حجم موحد من الاهتمام يبلغ 13 x 13 x 13 مم في منطقة LGN و VC. تم استخراج خمسة مستقلبات وقياس كميتها من الأطياف الخام باستخدام الطريقة المتقدمة للتركيب الطيفي الدقيق القوي الفعال (AMARES) داخل واجهة مستخدم الرنين المغناطيسي القائمة على جافا (jMRUI). قد استنتجت عملية القياس الكمي وحدات تعسفية لـ N-أسيتيل الأسبارتات (*N-acetyl aspartate*) (NAA)، والغلوتامات الجلوتامين (Glx)، والكرياتين (Cr)، والكولين (Cho)، ميو-إينوزيتول (ml). تم إجراء فحصين متتاليين على كل من VC و LGN من نصفي الكرة المخية للكبار الأصحاء. وتم تحليل إمكانية تكرار قياس MRS لـ LGN و VC. وتم فحص LGN و VC للشباب وكبار السن الأصحاء. قد قورنت المستقلبات الموجودة بين المجموعات التي أُجريت على LGN لكبار السن الأصحاء، والمعانين بخفيف وشديد الجلوكوما، وعلى VC لكبار السن الأصحاء، والمشاركين الذين يعانون من خفيف وشديد الجلوكوما. أظهر تركيز المستقلبات في LGN و VC عدم وجود فروق ذات دلالة إحصائية بين الفحص المتتالية ($P > 0.05$). وأظهر التحليل اتفاقاً جيداً وتبايناً صغيراً بين قياسات MRS المتتالية (التحيز في LGN: -0.46 إلى 1.17؛ التحيز في VC: -0.61 إلى -0.22). يتمتع كبار السن الأصحاء بمستويات أقل من NAA ومستويات أعلى لـ Glx و Cr و Cho في LGN مقارنة بالشباب الأصحاء ($P < 0.05$). وأما في VC، فيتمتع كبار السن الأصحاء بمستويات أعلى لـ Cr و Cho و ml مقارنة بالشباب الأصحاء ($P < 0.05$). تتمتع مجموعة الجلوكوما الشديدة بمستوى أعلى لـ NAA (65.03 ± 14.66)؛ (14.09 ± 5.07)؛ Games-Howell، $p = 0.03$) ومستوى أقل لـ Cho (604.93 ± 93.55)؛ (0.016) في LGN مقارنة بالمجموعة الصحية. كان مستوى Glx (604.93 ± 93.55)؛ Games-Howell، $p = 0.031$) في VC أقل في الجلوكوما الشديدة مقارنة بالمجموعة الصحية، بينما كان مستوى Cho/Cr (0.030 ± 0.06 ؛ Tukey HSD، $p = 0.031$) في VC أقل في الجلوكوما الشديدة مقارنة بمجموعة الجلوكوما الخفيفة. يمكن تكرار فوكسل MRS واحد باستخدام التصوير بالرنين المغناطيسي بقوة 1.5 تسلا لتحديد تركيز المستقلبات في LGN و VC. إن العمر يؤثر على تركيزات NAA، و Glx، و Cr في تركيزات LGN، و Cr، و Cho، و ml في VC. فيجب أن يأخذ تحليل المستقلبات في عين اعتباره عامل العمر. قد يتسبب الجلوكوما في حدوث تحول في اتساع ونسبة تركيز NAA و Cho في LGN، وفي اتساع ونسبة تركيز NAA و Cho في Cho في LGN، وفي اتساع ونسبة Glx و Cho/Cr في VC. قد يساعد إجراء المزيد من الأبحاث في هذا المجال لمعرفة الآليات الأساسية لمرض الجلوكوما، وربما يساعد في تطوير أساليب تشخيصية أو علاجية جديدة.

APPROVAL PAGE

The thesis of Liyana binti Musa has been approved by the following:



Asst. Prof. Dr. Firdaus bin Yusof @ Alias
Supervisor



Dr. Mazuin binti Mohd Razalli
Co-Supervisor



Dr. Azlan Azha Musa
Co-Supervisor



Dr. Iqbal bin Jamaludin
Internal Examiner



Associate Professor Dr. Ahmad Nazlim Yusoff
External Examiner



Chairman
Professor Dr. Mohd. Zulfaezal bin Che Azemin

DECLARATION

I hereby declare that this dissertation is the result of my own investigations, except where otherwise stated. I also declare that it has not been previously or concurrently submitted as a whole for any other degrees at IIUM or other institutions.

Liyana binti Musa

Signature 

Date 10th October 2023



INTERNATIONAL ISLAMIC UNIVERSITY MALAYSIA

**DECLARATION OF COPYRIGHT AND AFFIRMATION OF
FAIR USE OF UNPUBLISHED RESEARCH**

**CHARACTERISATION OF METABOLITE CONCENTRATION
IN THE LATERAL GENICULATE NUCLEUS AND VISUAL
CORTEX OF PATIENTS WITH DIFFERENT SEVERITY OF
GLAUCOMA USING MAGNETIC RESONANCE
SPECTROSCOPY**

I declare that the copyright holder of this thesis/dissertation are jointly owned by the student and IIUM.

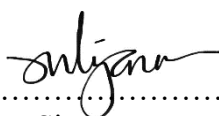
Copyright © 2023 Liyana binti Musa and International Islamic University Malaysia. All rights reserved.

No part of this unpublished research may be reproduced, stored in a retrieval system, or transmitted, in any form or by any means, electronic, mechanical, photocopying, recording or otherwise without prior written permission of the copyright holder except as provided below

1. Any material contained in or derived from this unpublished research may only be used by others in their writing with due acknowledgement.
2. IIUM or its library will have the right to make and transmit copies (print or electronic) for institutional and academic purpose.
3. The IIUM library will have the right to make, store in a retrieval system and supply copies of this unpublished research if requested by other universities and research libraries.

By signing this form, I acknowledged that I have read and understand the IIUM Intellectual Property Right and Commercialization policy.

Affirmed by Liyana binti Musa



.....
Signature

10th October 2023

.....
Date

DEDICATION

This study is wholeheartedly dedicated to my beloved husband, children and parents who have been my source of inspiration and gave me strength when I thought of giving up, who continually provide their moral, spiritual, emotional, and financial support.



ACKNOWLEDGEMENTS

All glory is due to Allah, the Almighty, whose Grace and Mercies have been with me throughout the duration of my programme. Although it has been challenging, His Mercies and Blessings on me ease the herculean task of completing this thesis. I am most indebted to my supervisor, Asst. Prof. Dr. Firdaus bin Yusof @ Alias, whose enduring disposition, integrity, promptitude, thoroughness, and friendship have facilitated the successful completion of my work. I put this on record and appreciate his detailed comments, useful suggestions, and inspiring queries, which have considerably improved this thesis. His brilliant grasp of the aim and content of this work led to his insightful comments, suggestions, and queries, which helped me a great deal. Despite his commitments, he finds time to listen and attend to me whenever requested. The moral support he extended to me was, without doubt, a boost that helped in building and writing this research work. I am also grateful to my co-supervisors, Dr. Mazuin binti Mohd Razalli, Dr. Azlan Azha Musa, and my former supervisor, Dr. Sabrillahakim Sidek, whose support and cooperation contributed to the outcome of this work.

I would also like to thank Universiti Teknologi MARA (UiTM) for allowing me to conduct the research at the UiTM Specialist Hospital in Sg. Buloh.

Sincere thanks are also extended to Desiree Abdurrachim, someone who resided in Singapore for guiding me on the MRS analysis process, Encik Naim from the Radiological Department (UiTM Sg. Buloh) for helping me with radiological procedures, and Encik Iskandar from the Ophthalmological Department (UiTM Sg. Buloh) for helping me with ophthalmological procedures.

I shall thank Asst. Prof. Dr. Farah Wahida Ahmad Zaki, the Head of Department (HOD) of Diagnostic Imaging and Radiotherapy Department (DDIR), and former HOD, Assoc. Prof. Dr. Sayed Inayatullah Shah, for continually keeping tabs on me, as well as other staff from DDIR specifically and Kulliyah of Allied Health Sciences (KAHS) IIUM generally, for their time and kind assistance with any issues I forwarded during my study tenure.

In addition, I would like to express my gratitude to my friend, Sr. Halimatussa'dah Ahmad Radzi for her unwavering support and encouragement throughout these years of study when I was in turmoil, not to forget to my other postgraduate friends.

Also, sincere thanks to the Ministry of Education Malaysia and IIUM for their continuous financial support.

Lastly, my gratitude goes to my beloved husband, Khairul Asraff bin Abdul Karim, and lovely children, Maryam, Iman, and Maya, for their prayers, understanding, and endurance while away; to both of my parents, Musa Mastor and Siti Julia Ramanoon; to my parents-in-law, Abdul Karim Adam and Anitah Harun; and to my siblings for their prayers and always believing that I could complete this journey.

Once again, we glorify Allah for His endless mercy on us, one of which is enabling us to successfully round off the efforts of writing this thesis. Alhamdulillah.

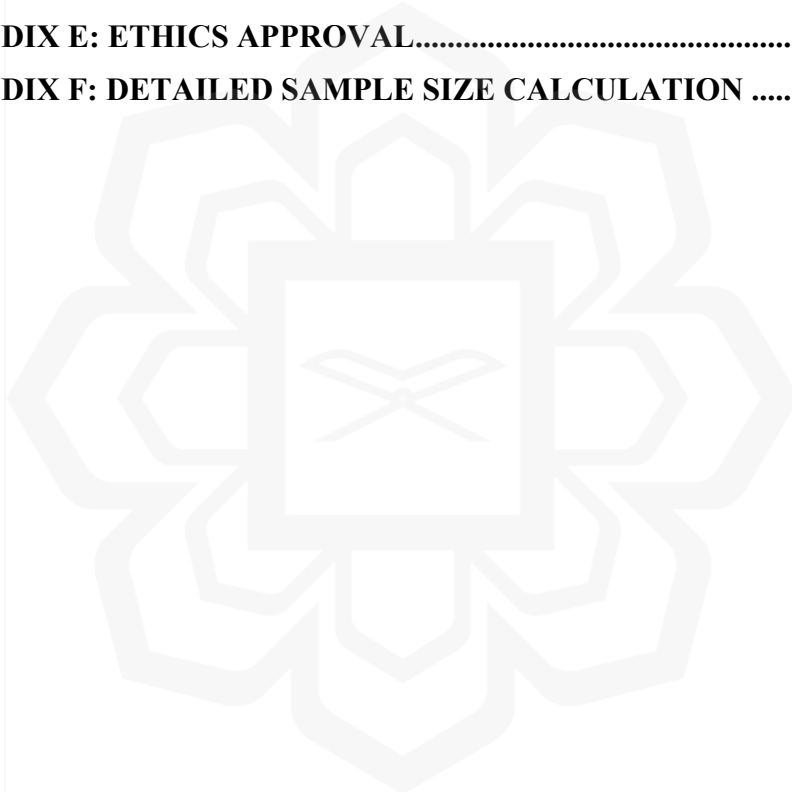
TABLE OF CONTENTS

Abstract	ii
Abstract in Arabic	iii
Approval Page.....	iv
Declaration.....	v
Copyright	vi
Acknowledgements.....	viii
Table of Contents.....	ix
List of Tables	xiii
List of Figures	xv
List of Equations	xix
List of Abbreviations	xx
List of Symbols/ SI Units.....	xxii
CHAPTER ONE: INTRODUCTION	1
1.1 Background Of Study.....	1
1.2 Problem Statement	5
1.3 Research Questions	7
1.4 Research Objective	8
1.4.1 General Objective	8
1.4.2 Specific Objectives	8
1.5 Significance Of Study	9
1.6 Scope Of The Research.....	10
1.7 Organisation Of The Thesis	11
CHAPTER TWO: REVIEW OF LITERATURE	12
2.1 Introduction.....	12
2.2 The Anatomy of Visual pathway	12
2.3 Glaucoma	16
2.3.1 Degeneration and Atrophy in Glaucoma	20
2.4 Metabolomics.....	23
2.5 Magnetic Resonance Imaging (MRI).....	29
2.6 Magnetic Resonance Spectroscopy (MRS).....	31
2.6.1 MRS Acquisition	32
2.6.2 MRS Spectrum	36
2.6.3 Spectroscopy Data Processing.....	37

2.7 MRS In Studies Of Glaucoma	40
2.8 Metabolites Measured By MRS In Glaucoma	46
2.9 Selected Research Approach And Justification	49
2.10 Research Gaps.....	49
2.11 Chapter Summary	50
CHAPTER THREE: GENERAL METHODOLOGY.....	51
3.1 Introduction.....	51
3.2 Research Method Framework	51
3.3 Ethics And Consent Form	54
3.4 Study Group Category Criteria	54
3.5 Eye Screening	56
3.6 Sample Size.....	58
3.7 Magnetic Resonance Imaging (MRI) Procedures.....	59
3.8 Magnetic Resonance Spectroscopy (MRS) Acquisition.....	60
3.9 MRS Analysis	62
3.9.1 Spectral Data Pre-Processing.....	63
3.9.2 Spectral Analysis and Quantification	65
3.10 Patient Care	67
3.10.1 Eye Care	68
3.10.2 MRI Care.....	68
3.11 Statistical Analysis.....	69
3.11.1 Repeatability Test.....	69
3.11.2 Mean Metabolites Differences Test (Independent T-Test)	70
3.11.3 Mean Metabolites Differences Test (One Way-ANOVA).....	70
3.12 Chapter Summary	70
CHAPTER FOUR: REPEATABILITY OF METABOLITES MEASUREMENT IN LATERAL GENICULATE NUCLEUS AND VISUAL CORTEX USING MAGNETIC RESONANCE SPECTROSCOPY IN HEALTHY YOUNG ADULT.....	71
Abstract.....	71
4.1 Introduction.....	73
4.2 Specific Methodology	74
4.2.1 Subjects.....	74
4.2.2 MRS Acquisition	75
4.2.3 MRS Analysis.....	75
4.2.4 Statistical Analysis	76
4.3 Results.....	78

4.4 Discussion	90
4.5 Conclusion	95
CHAPTER FIVE: METABOLITE COMPARISON IN THE LATERAL GENICULATE NUCLEUS AND VISUAL CORTEX OF HEALTHY YOUNG AND HEALTHY ELDERLY SUBJECTS	96
Abstract.....	96
5.1 Introduction.....	98
5.2 Specific Methodology	99
5.2.1 Subjects.....	99
5.2.2 MRS Acquisition	99
5.2.3 MRS Analysis.....	100
5.2.4 Statistical Analysis	101
5.3 Results.....	102
5.4 Discussion	104
5.5 Conclusion	108
CHAPTER SIX: METABOLITES CONCENTRATION IN THE LATERAL GENICULATE NUCLEUS OF GLAUCOMA PATIENTS.....	109
Abstract	109
6.1 Introduction.....	111
6.2 Specific Methodology	112
6.2.1 Subjects.....	112
6.2.2 MRS Acquisition	112
6.2.3 MRS Analysis.....	113
6.2.4 Statistical Analysis	113
6.3 Results.....	114
6.4 Discussion	118
6.5 Conclusion	123
CHAPTER SEVEN: METABOLITES CONCENTRATION IN THE VISUAL CORTEX OF GLAUCOMA PATIENTS.....	124
Abstract	124
7.1 Introduction.....	126
7.2 Specific Methodology	128
7.2.1 Methodological Variation.....	128
7.2.2 Statistical Analysis	128
7.3 Results.....	129
7.4 Discussion	133
7.5 Conclusion	136

CHAPTER EIGHT: CONCLUSION	137
8.1 General Discussion	137
8.2 Contribution And Benefits Of The Research.....	140
8.3 The Limitation Of The Study Resulting From The Impact Of Covid-19.....	141
8.4 Study Limitation And Future Studies	142
REFERENCES.....	144
APPENDIX A: PUBLICATION AND PRESENTATION	173
APPENDIX B: INFORMATION SHEET.....	174
APPENDIX C: CONSENT FORM	177
APPENDIX D: MRI PATIENT SAFETY SCREENING FORM.....	178
APPENDIX E: ETHICS APPROVAL.....	179
APPENDIX F: DETAILED SAMPLE SIZE CALCULATION	181



LIST OF TABLES

Table 2.1 The comparison between STEAM and PRESS (Mandal, 2007).	35
Table 2.2 The location (ppm) of common detectable metabolites.	37
Table 2.3 The summary of MRS glaucoma studies.	45
Table 3.1 Specific criteria of each group	55
Table 3.2 Hodapp-Parrish-Anderson (HPA) classification system	57
Table 4.1 The raw spectrum scan number from healthy young group for analysis after the spectral evaluation	75
Table 4.2 Mean \pm SD metabolite concentration amplitude of the quantified metabolites in the LGN.	78
Table 4.3 Mean \pm SD metabolite concentration amplitude of the quantified metabolites in the VC.	79
Table 4.4 The Bland-Altman bias and limit of agreement in LGN.	80
Table 4.5 The Bland-Altman bias and limit of agreement in VC.	84
Table 4.6 Repeatability statistics for metabolites measurement in LGN.	88
Table 4.7 Repeatability statistics for metabolites measurement in VC.	89
Table 5.1 The raw spectrum scan number in healthy young and elderly groups after the spectral evaluation	100
Table 5.2 Comparison of metabolite concentration amplitude between healthy young group and healthy elderly group in LGN.	102
Table 5.3 Comparison of metabolite concentration amplitude between healthy young group and healthy elderly group in VC.	103
Table 6.1 The demographics of all subjects following the respective groups.	112

Table 6.2 Comparison of metabolites concentration amplitude in the LGN between groups.	114
Table 6.3 Comparison of metabolites ratio in the LGN between groups.	116
Table 7.1 Comparison of metabolites concentration amplitude in the VC between groups.	129
Table 7.2 Comparison of metabolites ratio in the VC between groups.	131



LIST OF FIGURES

- Figure 1.1 Scope of research activities. 10
- Figure 2.1 The diagram shows the connection pathway from the eyes to the brain, where temporal retina fibres pass to the brain on the same side while nasal retina fibres cross over at the optic chiasm (L, left; R, right) (Armstrong & Cubbidge, 2019). 13
- Figure 2.2 A. Diagram in sagittal view shows the location of LGN in brain hemisphere, also the projection from the retina to the visual areas of the thalamus and midbrain, ending in the primary visual cortex. B. Magnified diagram shows the small structure of LGN, showing the terminal connection of the optic tract to the lateral geniculate nucleus (Antimo Buonocore, 2010). 14
- Figure 2.3 Diagram shows the VC in purple. a. the location of VC at the posterior region of the brain from side point of view. b. the location of VC in midsagittal cross point of view, where it is located along the superior and inferior of the calcarine fissure on the medial area of the occipital lobe (Sheffield, 2022). 15
- Figure 2.4 The diagram shows the areas involved in visual information processing in brain side point of view and midsagittal cross section view. Red arrow shows the dorsal stream visual pathway. Blue arrow shows the ventral stream visual pathway (Sheffield, 2022). 16
- Figure 2.5 The anatomy of the eye with magnified view of retina area that contain the RGCs ('Anatomy of the Eye | Biology for Majors II', n.d.). 17
- Figure 2.6 Illustration of visual pathway from the retina through the lateral geniculate nucleus to the primary visual cortex (Bressloff, 2005). 18
- Figure 2.7 The spectrum that shows the multiplets of Gln and Glu that commonly combined as Glx, the smaller Cr at 3.9 ppm, primary Cr at 3.02 ppm, edited from (Shevelev et al., 2017) 25

Figure 2.8 The glutamate-glutamine cycle (Feng et al., 2022). (1) Glu is released by neuron cells. (2) Glu binds to neuron receptors. (3) Glu dissipates from synapse to astrocytes. (4) Glu in astrocytes is converted to Gln. (5) Gln is shuttled to neurons. (6) Gln is converted to Glu.	25
Figure 2.9 The major component of an MRI system.	30
Figure 2.10 An example volume of interest (VOI) placement measured at 13mm x 13mm x 13mm in the visual cortex.	33
Figure 2.11 The STEAM pulse sequence schematic diagram(Allen D. Elster, 2023b) .	34
Figure 2.12 The PRESS pulse sequence timing diagram (Allen D. Elster, 2023a) .	35
Figure 2.13 An example of a normal metabolite peak in MR spectrum, edited from (McRobbie et al., 2006)	36
Figure 2.14 Published studies by year.	41
Figure 3.1 The research method framework.	53
Figure 3.2 The VOI for LGN was placed at the rear end of the thalamus.	61
Figure 3.3 The VOI for VC was placed as close as possible to the posterior position of the VC.	62
Figure 3.4 Example of unacceptable spectrum due to the undesirably biphasic waveform shown between 1.0 ppm and 2.0 ppm.	64
Figure 3.5 Example of acceptable narrow and upright spectrum.	64
Figure 3.6 Identification of the top and line widths of a metabolite.	65
Figure 3.7 Soft constrains for each metabolite.	66
Figure 4.1 Bland and Altman difference plots using NAA concentration amplitude in the LGN in the first and second sessions of the MRS technique.	81

Figure 4.2 Bland and Altman difference plots using Glx concentration amplitude in the LGN in the first and second sessions of the MRS technique.	82
Figure 4.3 Bland and Altman difference plots using CR concentration amplitude in LGN in the first and second sessions of the MRS technique.	82
Figure 4.4 Bland and Altman difference plots using Cho concentration amplitude in the LGN in the first and second sessions of the MRS technique.	83
Figure 4.5 Bland and Altman difference plots using mI concentration amplitude in the LGN in the first and second sessions of the MRS technique.	83
Figure 4.6 Bland and Altman difference plots using NAA concentration amplitude in the VC in the first and second sessions of the MRS technique.	85
Figure 4.7 Bland and Altman difference plots using Glx concentration amplitude in the VC in the first and second sessions of the MRS technique.	86
Figure 4.8 Bland and Altman difference plots using Cr concentration amplitude in VC in the first and second sessions of the MRS technique.	86
Figure 4.9 Bland and Altman difference plots using Cho concentration amplitude in VC in the first and second sessions of the MRS technique.	87
Figure 4.10 Bland and Altman difference plots using mI concentration amplitude in the VC in the first and second sessions of the MRS technique.	87
Figure 5.1 The VOI (red box) location in the right (a) and left (b) regions of the LGN.	99
Figure 5.2 The VOI (red box) location in the right (a) and left (b) regions of the VC.	100
Figure 6.1 The box and whiskers plot illustrating a significantly higher NAA amplitude in the LGN of severe glaucoma group compared to the healthy group. There is an increase in NAA amplitudes from 53.31 ± 6.83 in the healthy group to 65.03 ± 14.66 in the severe glaucoma group, an increase of 11.72 (95% CI, 0.95 to 22.49) ($p=0.03$).	115

Figure 6.2 The box and whiskers plot illustrating the significant difference in mean of Cho between groups. There is a decrease in Cho amplitudes from 23.91 ± 7.02 in the healthy group to 14.09 ± 5.07 in the severe glaucoma group, a decrease of 9.82 (95% CI, 2.68 to 16.95) ($p=0.008$). There is also a significant decrease in Cho amplitudes from 22.63 ± 4.23 in the mild glaucoma group to 14.09 ± 5.07 in the severe glaucoma group, a decrease of 8.54 (95% CI, 1.82 to 15.26) ($p=0.016$). 115

Figure 6.3 The box and whiskers plot show a lower NAA/Cr ratio in healthy group compared to the mild glaucoma group. There is an increase in NAA/Cr ratio in LGN from 1.49 ± 0.37 in the healthy group to 1.86 ± 0.41 in the mild glaucoma group, an increase of 0.37 (95% CI, 0.02 to 0.73) ($p=0.038$). 117

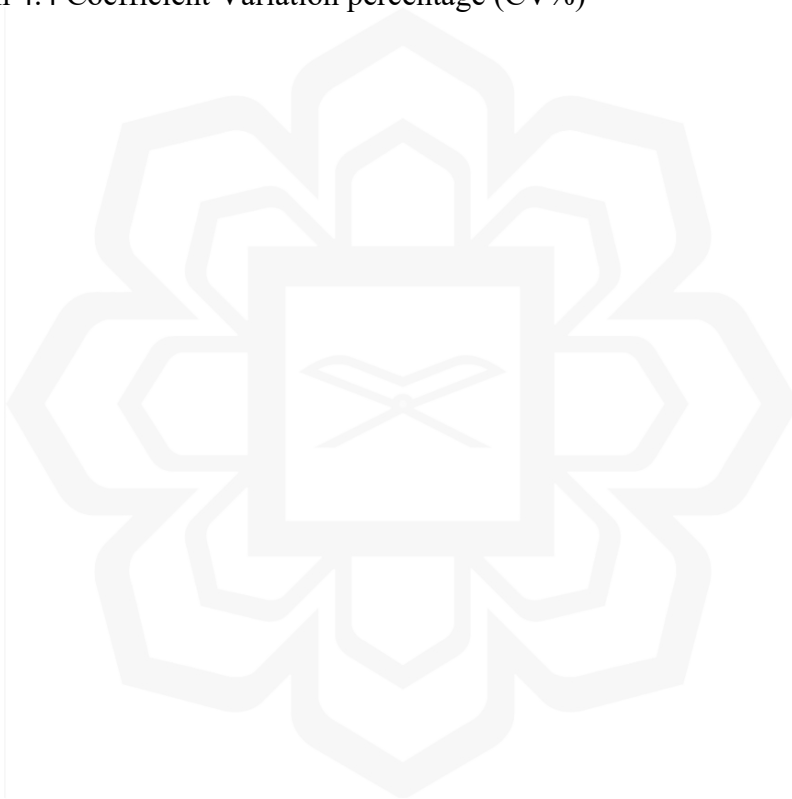
Figure 6.4 The box and whiskers plot show a decrease in Cho/Cr in the severe glaucoma group compared to the mild glaucoma group. There is a decrease in the Cho/Cr ratio in the LGN from 0.70 ± 0.18 in the mild glaucoma group to 0.48 ± 0.14 in the severe glaucoma group, a decrease of 0.22 (95% CI, 0.03 to 0.41), ($p=0.023$). 117

Figure 7.1 The box and whiskers plot illustrate a significantly lower Glx amplitude in the severe glaucoma group compared to the healthy group. There is a decrease in Glx amplitudes in VC from 745.00 ± 109.27 in the healthy group to 604.93 ± 93.55 in the subjects with severe glaucoma group, a decrease of 140.07 (95% CI, 13.13 to 267.03) ($p=0.031$). 130

Figure 7.2 This box and whiskers plot illustrates the significant reduction in the mean Cho/Cr in the severe glaucoma group compared to the mild glaucoma group. There was a decrease in the Cho/Cr ratio in the VC from 0.42 ± 0.11 in the mild glaucoma group to 0.30 ± 0.06 in the severe glaucoma group, a decrease of 0.12 (95% CI, 0.01 to 0.23) ($p=0.031$). 132

LIST OF EQUATIONS

Equation 4.1 Repeatability coefficient (RC)	76
Equation 4.2 Within standard deviation (WSD)	76
Equation 4.3 Repeatability Coefficient percentage (RC%)	77
Equation 4.4 Coefficient Variation percentage (CV%)	77



LIST OF ABBREVIATIONS

3DT1W	3D T1 Weighted
ICH	International Council for Harmonisation of Technical Requirements for Pharmaceuticals For Human Use
SAR	Specific Absorption Rate
UiTM	Universiti Teknologi Mara
3D	Three Dimensional
ACG	Angle Closure Glaucoma
AAHScout	Automated Positioning and Alignment of Slices Using the Anatomical Landmark
AMARES	Advanced Method for Accurate, Robust, And Efficient Spectral
ANOVA	Analysis of Variance
Cho	Choline
CI	Confidence Interval
CPSD	Corrected Pattern Standard Deviation
Cr	Creatine
CV	Coefficient of Variation
dB	Decibel
FA	Flip Angle
FDT	Frequency-Doubling Technology
FOV	Field Of View
GHT	Glaucoma Hemifield Test
Glx	Glutamate-Glutamine
HPA	Hodapp-Parish Anderson
HVFA	Humphrey Visual Field Analyzer
IIUM	International Islamic University Malaysia
IOP	Intraocular Pressure
jMRUI	Java-Based Magnetic Resonance User Interface
LCModel	Linear Combination Model
LGN	Lateral Geniculate Nucleus
LOA	Limit Of Agreement
MD	Mean Deviation

mI	Myo-Inositol
MRI	Magnetic Resonance Imaging
MRS	Magnetic Resonance Spectroscopy
MVS	Multi Voxel Spectroscopy
NAA	N-Acetyl Aspartate
NEX	Number Of Excitation
NTG	Normal Tension Glaucoma
OHT	Ocular Hypertensive
POAG	Primary Open Angle Glaucoma
PRESS	Point Resolved Spectroscopy
PSD	Pattern Standard Deviation
RC	Repeatability Coefficient
RGC	Retinal Ganglion Cell
ROI	Region Of Interest
SD	Standard Deviation
SNR	Signal To Noise Ratio
STEAM	Stimulated Echo Acquisition Mode
SVS	Single Voxel Spectroscopy
TE	Echo Time
TR	Repetition Time
VA	Visual Acuity.
VC	Visual Cortex
VOI	Voxel Of Interest
WMS	Within Means Square
WSD	Within Standard Deviation

LIST OF SYMBOLS/ SI UNITS

mm	Milimetre
mmHg	Millimeters of mercury
ms	Milliseconds
°C	Degree Celsius
ppm	Parts per million
W/kg	Watts per kilogram



CHAPTER ONE

INTRODUCTION

1.1 BACKGROUND OF STUDY

Metabolites are small molecules that are intermediates or final products of metabolism and serve a variety of cellular functions (Aizen, Tao, Rencus-Lazar, & Gazit, 2018). They are produced by the metabolic processes of bacteria, fungi, plants, and animals (Zandavar & Babazad, 2023). They are essential for the proper functioning as fuel, maintain cell structure, participate in signalling and defence mechanisms, and stimulate or inhibit enzymes (Aizen et al., 2018; Y. Liu et al., 2022). To gain insights into the composition and dynamics of metabolites within biological systems, metabolomics, a rapidly advancing field, is employed. Metabolomics encompasses the comprehensive study of metabolites present in a specific biological sample at a given time, providing valuable information about the metabolic state of an organism or a particular tissue (Kaddurah-Daouk, Kristal, & Weinshilboum, 2008). Metabolites quantification can be conducted using methods which include mass spectrometry, and magnetic resonance spectroscopy (MRS) (Barbosa-Breda, Himmelreich, Ghesquière, Rocha-Sousa, & Stalmans, 2018). Mass spectrometry, a widely used approach in metabolomics, requires samples collection from subjects, and samples are discarded after use. The technique is considered invasive due to the need for sample extraction. In ophthalmology, the traditional mass spectrometry for metabolites analysis have been conducted using samples from tear fluid, aqueous humour, vitreous humour, cornea, and lens (Barbosa-Breda et al., 2018). These analyses yield valuable information about the metabolic profiles specific to ocular tissues, offering insights into the physiological and pathological processes occurring within the eye.

The MRS, on the other hand, analyses metabolites in vivo non-invasively, does not require sample collection, and can be repeated over time, allowing for longitudinal studies (Barbosa-Breda et al., 2018). This technique provides a unique non-invasive window into the biochemical composition of tissues, offering valuable insights into physiological and pathological processes (P. Lee, Adany, & Choi, 2017). Moreover, MRS has found applications beyond neurological research. It is extensively utilized in other fields, such as oncology for characterizing tumors, cardiology for assessing myocardial metabolism, and musculoskeletal studies for evaluating muscle metabolism and pathology (Gondim Teixeira et al., 2017; Hudsmith & Neubauer, 2009; Ross, Chenevert, Kim, & Ben-Yoseph, 2015).

The MRS is readily available in most clinical magnetic resonance imaging (MRI) systems, which enables its usage accessible in the clinical setting. The MRS typically begins with the acquisition of MRI images that serve as a guide for tissue volume selection (Hesselink, 2014; Van Der Graaf, 2010). This ensures that the MRS focuses on the region of interest within the body. The procedure then is followed by the acquisition of spectra using specific MRS techniques such as single-voxel spectroscopy (SVS) or multi-voxel spectroscopy (MVS) (Hesselink, 2014; Van Der Graaf, 2010). SVS focuses on a single, specific volume within the tissue, providing detailed information about the metabolites in that localized area (Van Der Graaf, 2010). On the other hand, MVS allows for the simultaneous analysis of multiple volumes, offering a broader view of the metabolic profile across different regions (Van Der Graaf, 2010).

The core of MRS lies in its ability to generate spectra, which are essentially graphs depicting the distribution of different metabolite in the tissue being analyzed (Govindaraju, Young, & Maudsley, 2000; McRobbie, Moore, Graves, & Prince, 2006). These spectra are produced through the detection of radiofrequency signals emitted by atomic nuclei, particularly protons, in response to a magnetic field (Blüml, 2013; Govindaraju et al., 2000; McRobbie et al., 2006). Each metabolite in the tissue emits a unique signal, allowing for the identification and quantification of various compounds. The quantification process involves several steps such as line-broadening, fourier transforms, and phasing (Blüml, 2013; McRobbie et al., 2006).

After acquiring the spectrum, the area under each peak is calculated, which is directly proportional to the concentration of the corresponding metabolite (Blüml, 2013). In recent years, the MRS has been adopted to quantify metabolites in the sensitive tissues in the brain that are related to visual processing. These include studies on neurodegenerative disease involving subjects with glaucoma (Aksoy et al., 2018; Boucard, Hoogduin, van der Grond, & Cornelissen, 2007; Doganay, Cankaya, & Alkan, 2012; Guo et al., 2018; Rucker et al., 2003; Sidek et al., 2016). By employing MRS, researchers can gain valuable insights into the metabolic alterations occurring in related anatomical tissues, contributing to a deeper understanding of the underlying mechanisms of such conditions.

Glaucoma is a major public health issue characterized by progressive deterioration of the optic nerve, stemming from the chronic loss of the nerve fiber layer, which deteriorates vision and the visual field (Gandhi & Dubey, 2013; Hazin, Hendrick, & Kahook, 2009; Kapetanakis et al., 2016). Glaucoma pathogenesis is complex leading to difficulty in its diagnosis. Glaucoma poses a challenging clinical management due to the lack of rapid diagnostic methods and limited therapeutic options (Barbosa-Breda et al., 2018). The standard clinical procedures using clinical reading including intraocular pressure, retinal nerve fiber analysis, optic disc evaluation and visual field analysis often leads to late diagnosis.

The damage caused by glaucoma at the point of its detection may usually have been exaggerated due to the lack of sensitivity of the above clinical parameters. Also, as glaucoma being chronic in nature, the visual function reduction or any deteriorating ocular signs are slow and may be indistinct by patients in its earlier stage. Glaucoma is usually detected late where substantial damage has occurred, and some patients may have developed serious visual problems (Kapetanakis et al., 2016). The study of metabolites has the potential to yield biomarkers that can aid glaucoma diagnostics, classifications, and progression detection methods (Barbosa-Breda et al., 2018). MRS data has been shown to have the merits in detecting glaucoma-related-metabolite changes prior of deterioration in visual clinical data (Murphy et al., 2016).

There are a limited number of studies on glaucoma which employed the MRS, and the reports were generally inconsistent. The literature focuses on different anatomical structures in the brain yet confined to tissues associated with the visual pathway. To note, the MRS glaucoma studies have ventured investigations on the lateral geniculate nucleus (LGN) (Aksoy et al., 2018; Doganay et al., 2012), optic radiation (Sidek et al., 2016; Y. Zhang, Chen, Wen, Wu, & Zhang, 2013), and visual cortex (VC) (Aksoy et al., 2018; Guo et al., 2018; Murphy et al., 2016) . All studies have focused on the key metabolites in the brain, including N-acetyl-aspartate (NAA), glutamate-glutamine (Glx), creatine (Cr), choline (Cho), and myo-inositol (mI) (Soares & Law, 2009). There were some similarities in the technique employed by the studies, yet their unique parameter settings may have consequently borne the variation in the results.

This thesis explores the MRS analysis on glaucoma subjects in the LGN and VC using the SVS technique. The results from the experiments in this thesis may not only contribute to the scientific understanding of glaucoma pathophysiology but also have significant implications for society and the country at large. By shedding light on the metabolic changes associated with glaucoma, this research may pave the way for more targeted and effective treatment strategies, potentially improving the quality of life for individuals affected by this glaucoma. Additionally, a deeper comprehension of glaucoma at the molecular level may lead to advancements in diagnostic techniques, ultimately benefiting healthcare systems and reducing the economic burden of glaucoma-related healthcare costs on the nation.

1.2 PROBLEM STATEMENT

Glaucoma, a chronic and vision-threatening disease, is not limited to the progressive injury of the optic nerve but is increasingly recognized as a complex neurodegenerative disease that can have an impact on the central nervous system, including the brain (Arrigo et al., 2021). Studies have shown that glaucoma can lead to structural and functional changes in the brain. One study found damage to the white matter integrity along the central visual pathway, affecting connections crucial for coordinating vision and movement (V. Trivedi et al., 2019). Other studies have found changes in gray matter volume and disrupted connectivity between visual cortex regions in glaucomatous patients (Nuzzi, Dallorto, & Rolle, 2018a). Another study demonstrated that glaucoma patients may experience cognitive dysfunctions, indicating a broader influence on thinking abilities (Gangeddula, Ranchet, Akinwuntan, Bollinger, & Devos, 2017).

One example of the impact of glaucomatous damage on brain metabolites can be seen in a recent study. The study findings linked glaucoma to decreased GABA levels, causing degrading of neural specificity in the visual cortex, which can impact sensory and cognitive functions (Bang et al., 2023). Certain areas of the visual pathway including the vitreous, optic radiation, lateral geniculate body (LGN), and visual cortex (VC), that have been studied using MRS (Aksoy et al., 2018; Doganay et al., 2012; Rucker et al., 2003; Sidek et al., 2016), also showed conflicting findings as mentioned in section 1.1.

Furthermore, the body of literature on glaucoma using MRS analyzed changes of metabolite concentrations using a variety of spectroscopic parameter settings. For example, the study by (Rucker et al., 2003) pioneered the MRS experiment by comparing metabolite concentrations in the vitreous of four healthy subjects to only one subject with optic neuropathy using size a 10x10x10 mm voxel of interest (VOI). They discovered a high concentration of lactate in the human vitreous and advocated the application of non-invasive MRS to the human vitreous in vivo for the assessment of retinal and optic nerve metabolism.

Both Aksoy et al. (2018) and Doganay et al. (2012) conducted studies to investigate changes in metabolite concentrations in the lateral geniculate nucleus (LGN) in glaucoma patients. However, there were differences in the size of the volume of interest (VOI) used by each study, with Aksoy et al. using a VOI size of 13x13x13 mm and Doganay et al. (2012) using a VOI size of 12x12x12 mm. Additionally, the study populations of the two studies were diverse, with Aksoy et al. (2018) using subjects with several types of glaucoma and Doganay et al. (2012) only comparing healthy groups and groups of primary open-angle glaucoma.

Although the two studies reported conflicting results, where Aksoy et al. (2018) found a significant reduction of NAA and Cho in the diseased group compared to the healthy group and Doganay et al. (2012) found no significant reduction of those metabolites in the diseased group compared to the healthy group, they agreed on the potential of MRS in aiding glaucoma diagnosis and understanding the disease's neurodegenerative process. Meanwhile, Sidek et al. (2016) evaluated the changes in metabolite concentration in optic radiation, another brain region involved in visual processing, with a VOI size of 20x20x20 mm in different glaucoma groups following severity. However, they found no significant changes in optic radiation that could be measured using single-voxel MRS.

The results of all studies mentioned in the previous paragraphs might reveal alterations in the concentrations of certain metabolites in individuals with glaucoma compared to those without. There could be changes in metabolites related to energy metabolism, neurotransmitter levels, or markers of oxidative stress. However, interpreting these findings would require further investigation to understand the specific implications of these altered metabolite concentrations. There is also still a lack of consensus regarding the metabolic changes that occur in this disease. This lack of understanding is compounded by the limited knowledge of its pathophysiology and the variability in the experimental protocols and settings used to study it. It may also indicate potential secondary effects of glaucoma on the central nervous system, potentially influencing aspects of brain function beyond vision. In light of the current state of research, it can be asserted that the full extent of glaucomatous damage on the concentration of metabolites in the brain remains inadequately characterized.

Further investigations into metabolic concentration in glaucoma are crucial to shed light on this disease's underlying mechanisms and potential treatment for a specific biological process. Without a more comprehensive understanding of the metabolic changes in glaucoma, it will be challenging to develop effective treatments that can slow or prevent vision loss. Therefore, continued research is necessary to improve our understanding of this complex disease and develop more effective treatments for those affected by glaucoma.

1.3 RESEARCH QUESTIONS

1. What is the degree of repeatability observed in metabolite measurements obtained from the LGN and VC using MRS within a sample of healthy subjects?
2. How does the metabolite concentrations change in the LGN and VC regions in association with the process of healthy aging?
3. How do metabolite concentrations in the LGN of healthy older adults, patients with mild glaucoma, and patients with severe glaucoma differ?
4. How do metabolite concentrations in the VC of healthy older adults, patients with mild glaucoma, and patients with severe glaucoma differ?

1.4 RESEARCH OBJECTIVE

1.4.1 General Objective

To investigate and characterize the concentration of metabolites in the visual pathway particularly the LGN and VC, of healthy subjects and patients with glaucoma using MRS.

1.4.2 Specific Objectives

1. To quantify the repeatability of metabolites measurements in the LGN and VC using MRS among healthy subjects.
2. To measure the metabolite concentrations in the LGN and VC in healthy aging.
3. To compare metabolite concentrations in the LGN of healthy older adults, patients with mild glaucoma, and patients with severe glaucoma.
4. To compare metabolite concentrations in the VC of healthy older adults, patients with mild glaucoma, and patients with severe glaucoma.

1.5 SIGNIFICANCE OF STUDY

The results of this study are anticipated to contribute to the ongoing MRS investigation of metabolite changes in various glaucoma-related brain regions. In contrast to previously published research, this study is novel in that it examined the concentration of metabolites in the LGN and VC of glaucoma patients with varying degrees of severity while adjusting the parameters of the spectroscopy technique.

One of the most compelling potential impacts lies in its clinical relevance. The findings could pave the way for more targeted and effective treatment strategies, potentially leading to personalised approaches tailored to individual metabolic profiles. Moreover, if successful, this study could advance the cause of early glaucoma detection, with the potential to prevent irreversible vision loss. The benefits could extend to healthcare cost reduction, as timely interventions and tailored treatments may alleviate the burden of managing advanced-stage cases. Additionally, the study's methodology and findings have the potential to be a cornerstone for future research in the field, offering a foundation for further exploration. Furthermore, these insights could be integrated into medical education and training programs, enhancing healthcare professionals' understanding of glaucoma, and ultimately improving patient care. Beyond its immediate implications for glaucoma, the techniques and knowledge gained could have cross-disciplinary applications in studying metabolic changes in other ophthalmic conditions.

It is hoped that the current study will be able to enrich the knowledge of glaucoma pathophysiology. Solidifying the understanding on metabolite changes in glaucoma may pave a path of MRS future use as an adjunct test to the current clinical tests for diagnosis and tracking progression.

1.6 SCOPE OF THE RESEARCH

This study primarily aimed to characterize changes in metabolite concentrations in the LGN and VC of patients with glaucoma, using the 1.5 Tesla MRI system in the Radiology Department of the UiTM Specialist Hospital Sungai Buloh. Subjects' recruitment was restricted to patients with severe and mild glaucoma, healthy elderly volunteers of similar age, and healthy young volunteers. All acquired spectroscopy data were processed using the Java-based magnetic resonance user interface (jMRUI; version 6.0 beta)(Stefan et al., 2009) software. Statistical analysis of the amplitude values of each metabolite were computed using version 23.0 of the Statistical Package for the Social Sciences (SPSS) software (SPSS Inc., Chicago, IL, USA). Chapter three of this thesis provides a detailed explanation of the research methodology. Figure 1.1 summarizes the overall scope and activities of the experimental research.

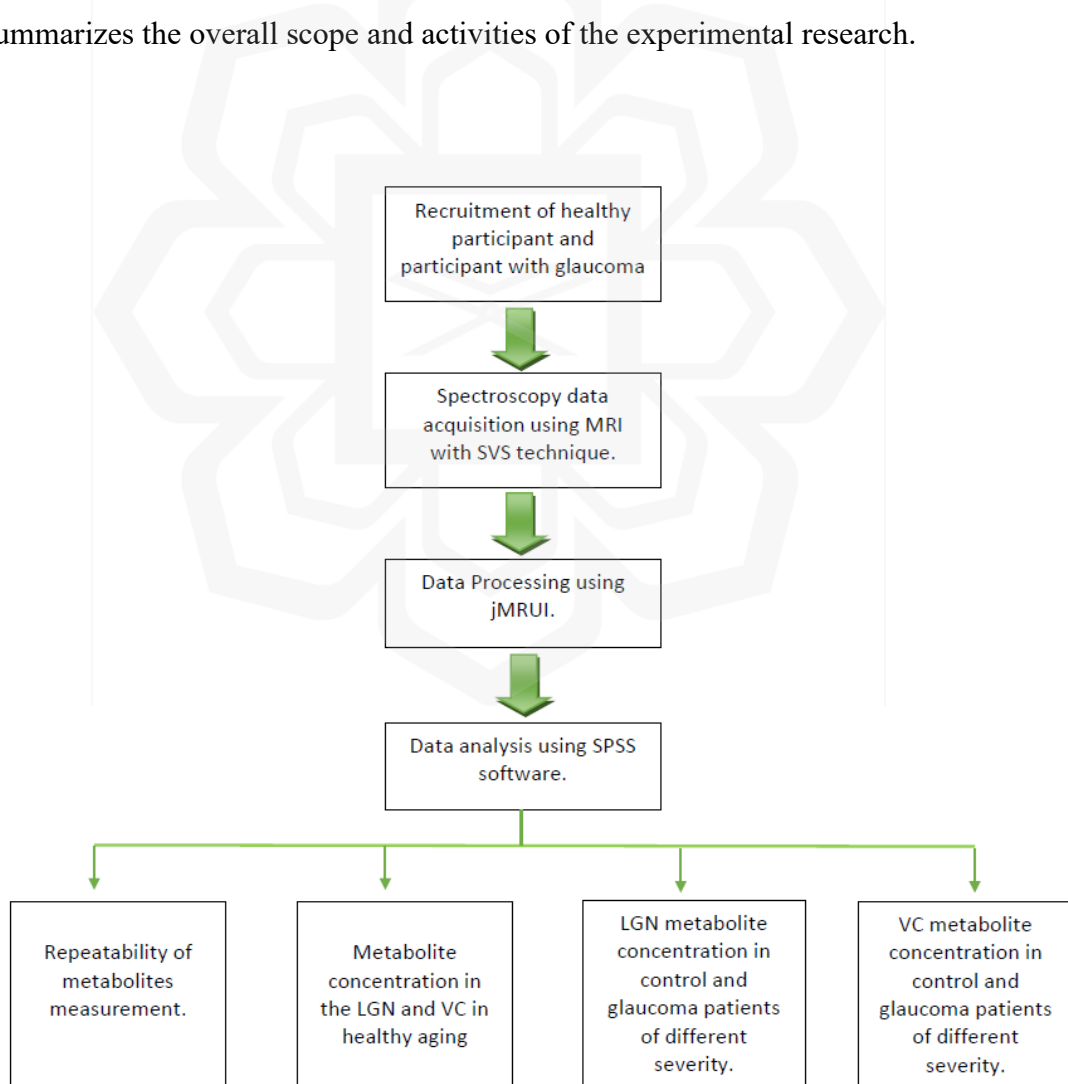


Figure 1.1 Scope of research activities.

1.7 ORGANISATION OF THE THESIS

This thesis consists of eight chapters. Chapter One, the current chapter, provides a brief introduction to the study. In this section, the statement of the problem, research scope, and research objectives are presented.

The literature review is presented in Chapter Two. This section provides a comprehensive review of the relevant literature, focusing on metabolite concentrations, MRS and glaucoma.

The general research methodology used to conduct the experiments in this study is described in Chapter Three. This chapter explains the recruitment of subjects, MRS acquisition and spectrum pre-processing, detailed spectroscopy data processing, and statistical analysis of the processed data.

Chapter Four explains the experiment that concerns the first objective of this study, the repeatability of MRS measurements of selected metabolites in the LGN and VC of healthy subjects. This experiment was conducted to ensure that the results of subsequent experiments were accurate and not random.

The second specific objective of this study is elaborated in Chapter Five. In this chapter, the concentrations of metabolites in the LGN and VC of healthy young and healthy elderly subjects are discussed.

Chapter Six details the experiment of the third specific objective of this study. This chapter covers the investigations of metabolites concentration in the LGN of healthy subjects and glaucoma patients.

Chapter Seven details of experiment on answering the study objective four. The metabolites concentration in the VC of the healthy subjects and glaucoma patients is discussed in this chapter.

Lastly, Chapter Eight concludes all experiments findings and explores some suggestions for further future research on MRS and glaucoma.

CHAPTER TWO

REVIEW OF LITERATURE

2.1 INTRODUCTION

This chapter reviews the literature on metabolite concentration changes in brain structures associated with the visual pathway in glaucoma patients using imaging technology. The chapter discusses the metabolites in the brain, the metabolites study in ophthalmology especially in glaucoma disease, the anatomical brain structure associated with glaucoma, the technology and methodology used for detecting and analysing the metabolites in the brain, and the application of the technology in glaucoma studies. This chapter also includes a critical analysis of previous studies, which assisted in identifying the gaps in knowledge that this study aimed to fill.

2.2 THE ANATOMY OF VISUAL PATHWAY

The visual pathway describes the anatomical course of the visual sensory transmission from the retina to the brain (Armstrong & Cubbidge, 2019). The nerve fibres of the retina, which represent the axons of the ganglion cells, converge at the optic disc to form the optic nerve, which transmits visual information to the brain before leaving the orbital bones. The optic nerves from both eyes meet at the optic chiasm, a structure at the base of the brain, where the nasal retina fibres cross over and combine with temporal retina fibres from the other eye (Figure 2.1) (Armstrong & Cubbidge, 2019). This arrangement ensures that the visual information from the left visual field of both eyes is processed in the right hemisphere of the brain, and vice versa. These fibres travel down the optic tracts and connect to the LGN in the midbrain, where some signal processing occurs. Finally, a series of radiating nerve fibres called the optic radiation carry the visual information to the visual cortex in the brain's occipital lobe for further processing.

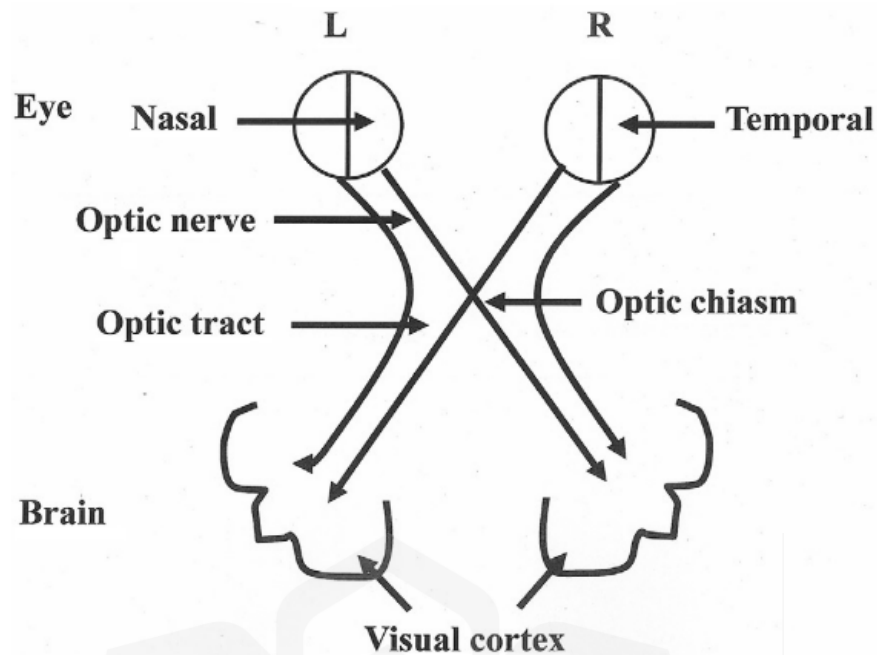


Figure 2.1 The diagram shows the connection pathway from the eyes to the brain, where temporal retina fibres pass to the brain on the same side while nasal retina fibres cross over at the optic chiasm (L, left; R, right) (Armstrong & Cubbidge, 2019).

The LGN is the major relay station between the retina and VC (Bressloff, 2005). In the literature, the LGN may also be termed as corpus geniculatum laterale or lateral geniculate body. A human brain contains a pair of LGN which are located on the left and right sides of the thalamus. LGN is composed of six layers of neurons (grey matter) alternating with optic fibres (white matter). The structure of LGN is a small and mushroom-shaped which receive seventy percent of the optic tract fibers within its six alternating layers of gray and white matter (Brar, 2020). Each LGN receives input from both eyes; from the RGCs of the temporal retinal of the ipsilateral side and from the nasal retinal of the contralateral eye (Figure 2.2). The binocular visual processing begins in the LGN which warrants its importance in the seeing processing (Covington & Khalili, 2022).

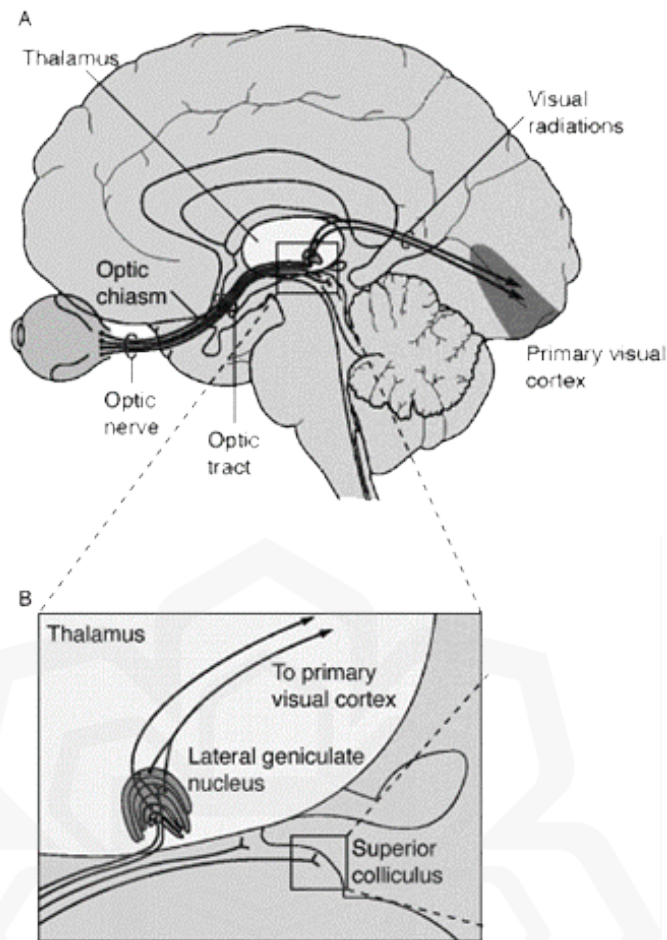


Figure 2.2 A. Diagram in sagittal view shows the location of LGN in brain hemisphere, also the projection from the retina to the visual areas of the thalamus and midbrain, ending in the primary visual cortex. B. Magnified diagram shows the small structure of LGN, showing the terminal connection of the optic tract to the lateral geniculate nucleus (Antimo Buonocore, 2010).

The VC is the visual processing area of the brain, and is located primarily along the superior and inferior sides of the calcarine fissure in the occipital lobe (Figure 2.3), a posterior region of the brain (Huff, Mahabadi, & Tadi, 2022; Sheffield, 2022). The VC is also present in both hemispheres of the brain, where each receives a pre-processed visual information from the LGN of the ipsilateral side (Huff et al., 2022).

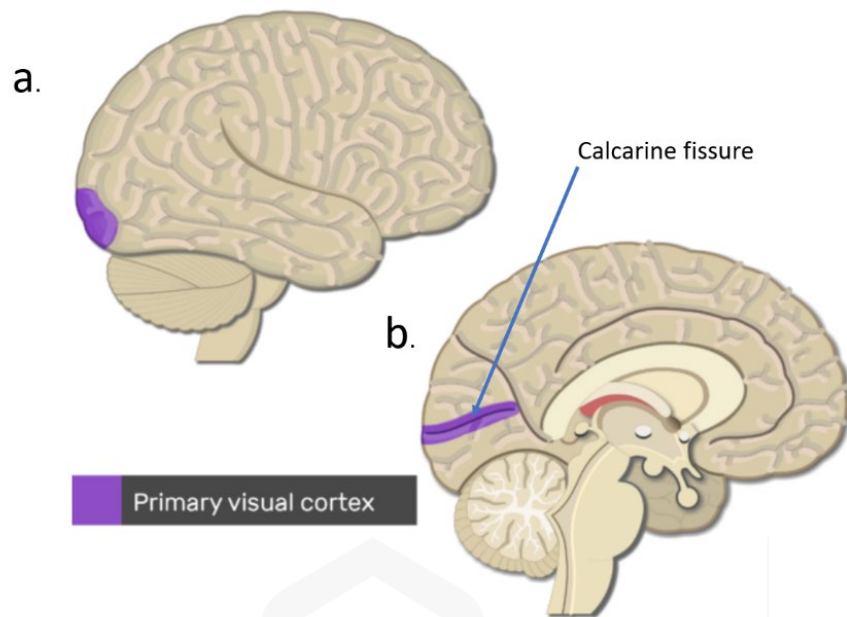


Figure 2.3 Diagram shows the VC in purple. a. the location of VC at the posterior region of the brain from side point of view. b. the location of VC in midsagittal cross point of view, where it is located along the superior and inferior of the calcarine fissure on the medial area of the occipital lobe (Sheffield, 2022).

There are several visual association areas in the VC, specific for certain aspects of visual information. Visual information about face recognition and the size, shape, and colour of an object is processed by neurons in the ventral stream pathway (Sheffield, 2022). The ventral stream pathway occurs when the neuron passes through the secondary visual cortex and extends downward into the inferior temporal gyrus (Sheffield, 2022). Meanwhile, visual information about the motion of an object is processed by the neuron through the dorsal stream pathway, whereby the neuron passes through the secondary visual cortex and extends upward to the posterior parietal cortex (Sheffield, 2022). Figure 2.4 shows the areas involved in visual processing.

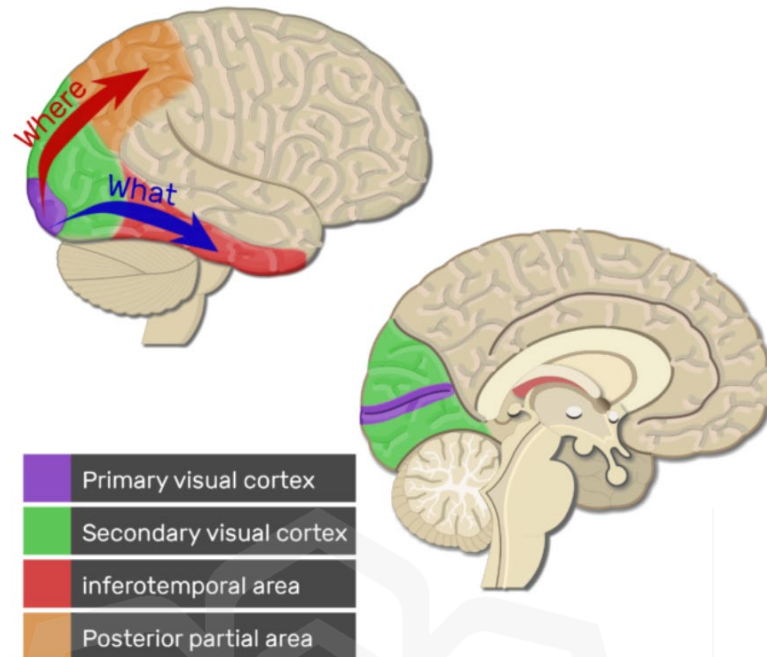


Figure 2.4 The diagram shows the areas involved in visual information processing in brain side point of view and midsagittal cross section view. Red arrow shows the dorsal stream visual pathway. Blue arrow shows the ventral stream visual pathway (Sheffield, 2022).

2.3 GLAUCOMA

Glaucoma is one of the major public health problems and being one of the leading causes of irreversible vision loss worldwide (Abdull, Chandler, & Gilbert, 2016; Kapetanakis et al., 2016). It was estimated that by 2040, the number of people with glaucoma worldwide could increase to 111.8 million (Tham et al., 2014). The large prevalence gives the impression that the number of people who is going to be blind would also increase by the year. Glaucoma is also categorised as a group of chronic diseases that often referred as a 'silent thief of sight' due to its unnoticed eye destruction that cause irreversible damage to the vision of the eye (Abdull et al., 2016). Glaucoma destroys vision starting from the periphery and ultimately involve the central vision which often leads to irreversible blindness (Iester, Telani, Vagge, & Bagnis, 2013). Glaucoma is usually chronic and without any apparent sign and would be only noticed when the diagnosis usually has already indicated a higher degree of glaucoma severity (Tan & Sanders, 2013).

Glaucoma is a chronic optic neuropathy associated with a loss of retinal ganglion cells and their axons (M. Gupta, Ireland, & Bordoni, 2022). Among the clinical manifestations of glaucoma are the excavation of the optic disc, axonal degeneration of retinal ganglion cells (RGC), and apoptotic death of RGC cell bodies (Munemasa & Kitaoka, 2013). RGCs are neuron cells of the central nervous system, with their cell bodies located in the interior retina, whereas their ganglion cells form and locates in the optic nerve (Shahida & Qadir, 2020). The location of RGCs in the retina is illustrated in Figure 2.5.

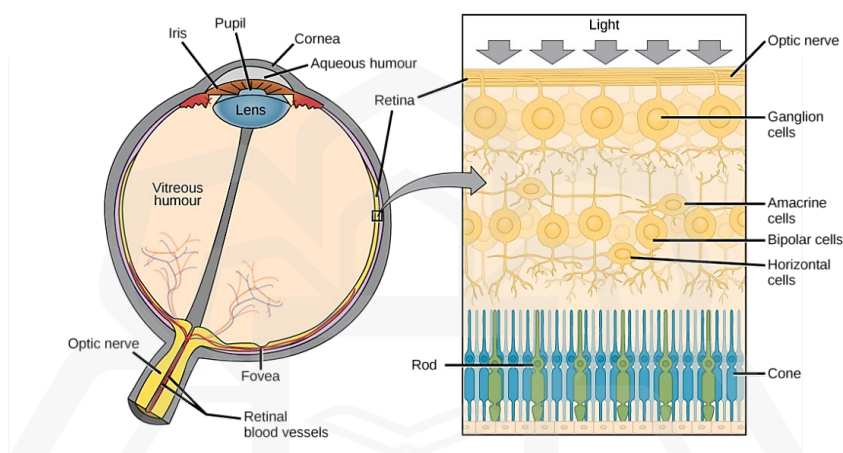


Figure 2.5 The anatomy of the eye with magnified view of retina area that contain the RGCs ('Anatomy of the Eye | Biology for Majors II', n.d.).

The RGCs' axons exit the eye forming the optic nerve, in order to transmit information from the retina to the visual target area in the brain (Peichl, 2009). The optic nerve then acts as the conductor of the RGCs output to the LGN of the thalamus (Bressloff, 2005; M. Gupta et al., 2022). Visual transmission is processed by neurons which begins with the optic nerve in the eye, to the optic chiasm and synapses at the LGN. The visual nerve impulses then continue in the visual pathway to the brain's visual processing area, the VC (M. Gupta et al., 2022). Figure 2.6 illustrates the visual pathway for visual processing.

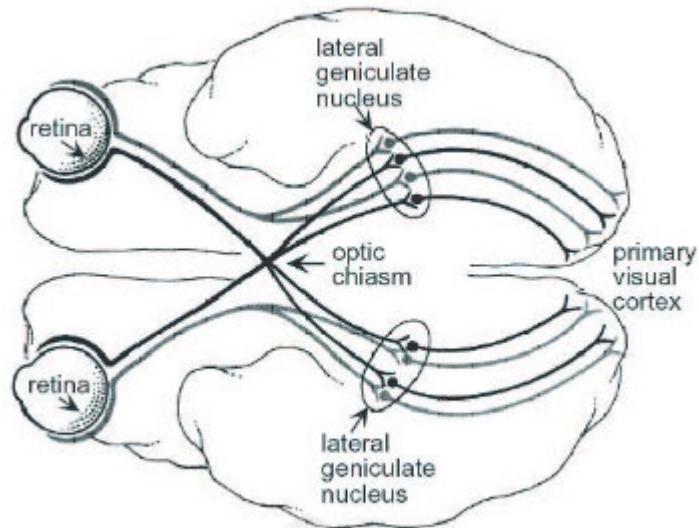


Figure 2.6 Illustration of visual pathway from the retina through the lateral geniculate nucleus to the primary visual cortex (Bressloff, 2005).

Glaucoma is associated with increase in intraocular pressure (IOP) which causes an optic neuropathy, then triggering the optic disc changes and initiating the visual field loss (King, Azuara-Blanco, & Tuulonen, 2013). The normal IOP value is taken between 10 to 21mmHg (Khaw, Shah, & Elkington, 2004). The increase in IOP may be a result of an imbalance between secretion of aqueous humour by the ciliary body and its drainage through trabecular meshwork and uveoscleral outflow pathway (Weinreb, Aung, & Medeiros, 2014). The increased IOP causes a progressive damage to the optic nerve and the RGCs will preliminary affect the peripheral visual field, advancing to the loss of visual acuity and then a permanent blindness if it is left untreated (Hazin et al., 2009; King et al., 2013; Nduaguba & Lee, 2006).

The most common type of glaucoma is primary open angle glaucoma (POAG), which accounts for about 74% of all glaucoma cases worldwide (H. Quigley & Broman, 2006). The term open angle refers to the wide irido-corneal angle which translates to an unhindered excretion of the aqueous humour. Among the many risks factor for POAG includes aging, high IOP, reduced ocular perfusion pressure, thin cornea, myopia, and diabetes mellitus (Grzybowski, Och, Kanclerz, Leffler, & De Moraes, 2020) . POAG usually involves a slow and chronic destruction of RGCs which yield to unnoticeable visual field defects (Yaqub, 2012); which explains the common late detection of the disease (Bussel, Wollstein, & Schuman, 2014). However, there are also glaucoma patients that have the same characteristics associated with POAG but with IOP being constantly in the normal range, who are commonly referred as the normal tension glaucoma (NTG) (King et al., 2013). Nevertheless, some recent literatures categorised NTG as a subset of POAG (Gosling & Meyer, 2022). Meanwhile, some patients may possess high IOP but do not have any characteristics of glaucoma which is categorized as the ocular hypertensives (OHT) (Jonas et al., 2014). POAG, NTG and OHT categorical labelling are based on IOP values, albeit the IOP is exposed to many measurements bias (Machiele, Motlagh, & Patel, 2022). The topic on IOP is out of the scope of this review but can be explored in the journals (Machiele et al., 2022).

The other spectrum of glaucoma is the angle closure glaucoma (ACG)(Khazaeni & Khazaeni, 2023). The global pooled prevalence of ACG was reported as 0.6% for the timeframe of 2001-2022 (N. Zhang, Wang, Chen, Li, & Jiang, 2021). The ACG usually occurs due to blockage of the aqueous humour secretion-excretion pathway, which leads to an extreme increment of the IOP. The ACG can be further be sub-classified with acute ACG and chronic ACG, but both shares the same pathogenesis of glaucoma involving extreme IOP increment (Wormald & Jones, 2015). Different to the POAG, patients with ACG usually present with signs and symptoms such as headache, nausea, eye pain, blurry vision, or redness which also tends to rapidly cause a blindness to the target (Iester et al., 2013). ACG cases are usually attended in the emergency department. Among the risks factor for ACG includes aging, being female, hyperopia, short axial length, and being Asian (N. Zhang et al., 2021). ACG is not in the scope of the current study. Hence, the term glaucoma used in this review is referring to the POAG and its derivatives.

Glaucoma is not understood completely, and all current treatment modalities are directed in reducing the IOP, which includes pharmacological therapy, laser therapy, and filtration surgery (Conlon, Saheb, & Ahmed, 2017). Glaucoma is a difficult disease to diagnose and manage because early symptoms may go unnoticed (Patel & Lighthizer, 2022; Vanoverberghe, 2020). With the increasing prevalence, there is a pressing need for a method for early detection with great diagnostic ability to prevent irreversible blindness due to glaucoma (Soqia et al., 2023; Vanoverberghe, 2020).

2.3.1 Degeneration and Atrophy in Glaucoma

A study on degenerative changes in the brain of patients with glaucoma involving LGN was first reported by (Gupta, Ang, De Tilly, Bidaisee, & Yücel, 2006). They used MRI on dead brains of patients with glaucoma and healthy, evaluating the right cerebral hemisphere of the brains containing the LGN. The coronal MRI scans of patients with glaucoma demonstrated a higher signal intensity and smaller cross section area of the LGN compared to the control (Gupta et al., 2006). Gupta et al. (2006) concluded that the LGN of brains with glaucoma shrunk and had a smaller volume compared to the control brain, as determined by multiple tests using the Nissl-staining method and Cavalieri estimator with Neurozoom software, respectively.

In 2009, Gupta et al. studied LGN once more, but this time with glaucoma patients who were still alive. In this study, an in vivo MRI showed a consistent result to their previous ex-vivo dead brain study. Their MRI study demonstrated a reduction in the height of LGN in glaucoma patients compared to the controls. These findings from both ex-vivo and in-vivo MRI studies demonstrated of the LGN atrophy in glaucoma, which may serve as a biomarker for visual system damage from glaucoma or due the progression of glaucoma.

The volume of the LGN in healthy people and people with glaucoma has also been studied in the past years (Kosior-Jarecka et al., 2020; J. Y. Lee et al., 2014). The previous studies showed that glaucoma has significantly a lower volume of the LGN compared to healthy subjects. Interestingly, Kosior-Jarecka et al. (2020) conducted MRI sequences on healthy, early glaucoma and advanced glaucoma groups. The results of the study revealed that there were significant differences in the LGN volume between the groups, with the healthy group and early glaucoma group having a significantly higher LGN volume than the advanced glaucoma group. Despite the fact that advanced glaucoma has significant findings indicating that there are LGN degenerative processes in the course of glaucoma, the results reported by (Kosior-Jarecka et al., 2020) also indicated that the volume of LGN of the healthy group and early glaucoma groups are literally the same. They have taken precautions steps to ensure that the observed differences in LGN volume were specific to glaucoma and not influenced by unrelated factors by comparing the LGN volume to that of the thalamic nucleus. The thalamic nucleus is not associated with the visual pathway. Importantly, no significant differences were found in the volume of the thalamic nucleus among the groups studied. The non-significant findings of the LGN structural changes between healthy and early glaucoma thus challenges previous assumptions about glaucoma-related changes in the LGN. Kosior-Jarecka et al. (2020) suggested that there may be undiscovered information regarding the pathogenesis of glaucoma, as there were possibly imperceptible differences between healthy individuals and those with early glaucoma.

The confirmation through comparison with the thalamic nucleus underscores the specificity of these findings to glaucoma; however, a notable gap in our understanding persists. The gap in knowledge lies in the difficulty of identifying subtle structural changes in the LGN associated with early-stage glaucoma using conventional MRI sequences. This poses a challenge in accurately diagnosing and understanding the progression of the disease at its early stages. The study by Kosior-Jarecka et al. (2020) suggests that there may be nuances and details regarding the pathogenesis of glaucoma that have yet to be discovered, especially in distinguishing between healthy individuals and those with early-stage glaucoma. This highlights the need for further research and more advanced imaging techniques to better characterize these subtle changes and improve our understanding of the disease.

The neuronal damage in glaucoma and its impact on the VC suggests a trans neuronal degeneration, as evidenced by a decline in neuronal activity in the retinal-LGN-visual cortex pathway (You, Rong, Zeng, Xia, & Ji, 2021). Animal studies using monkeys and marmosets as animal models with glaucoma showed such observations (Noro et al., 2019; Yücel, Zhang, Weinreb, Kaufman, & Gupta, 2003). A significant loss of LGN relay neurons terminating in the main VC was found in the study of induced glaucoma-affected monkeys, resulting in VC damage (Yücel, Zhang, Gupta, Kaufman, & Weinreb, 2000; Yücel et al., 2003). Meanwhile, in the study of glaucomatous marmosets, a significant volume loss was observed in the VC, and further histologic examination of the affected marmosets confirmed degeneration of the LGN and VC (Noro et al., 2019). The expression of brain-derived neurotrophic factor (BDNF) and tropomyosin receptor kinase B (TrkB), which play important roles in neuroprotection, particularly for RGCs in the optic nerve head and retina of affected marmosets also showed a marked decrease. These findings support the reports by You et al. (2021) that atrophy of the central visual system occurs in glaucoma animal models, and trans neuronal degeneration in the visual pathway appears to be one of the sources of damage to the VC.

In human glaucoma study, the evaluation of the area of VC under the sulcus calcarine using the Nissle staining method showed significant thinning of the cortical band (N. Gupta et al., 2006). These results were taken by comparing dead brain with glaucoma to a control brain. Further analysis discovered a correlation between reduced thickness in the VC area below the sulcus calcarine and the inferior border loss of the optic nerve head as well as the superior visual field defect. Gupta et al. (2006) further concluded that VC was subject to neuronal degeneration in advanced glaucoma with 50% visual field loss. A systematic review of visual pathway changes and brain connectivity in glaucoma patients reported that glaucoma patients have decreased thickness and volume of VC, functional abnormalities in VC, and disruption of connectivity within the VC areas (T. Li et al., 2020; Nuzzi, Dallorto, & Rolle, 2018b). In another study, glaucoma has been shown to be the result of neurodegeneration spreading through diffuse structural and functional abnormalities of VC, as evidenced by VC atrophy in the glaucoma brain compared with the non-glaucoma brain (Giorgio, Zhang, Costantino, De Stefano, & Frezzotti, 2018).

In conclusion, the degeneration and atrophy of LGN and VC in relation to glaucoma disease are evident. However, more research needs to be conducted to unwind the complexity of glaucoma pathology ((Martucci, Nucci, & Pinazo-Duran, 2023). Research utilising other robust method such as metabolomic study of the MRS, may expand understanding on glaucoma pathophysiology.

2.4 METABOLOMICS

The emergence of metabolomics i.e., the study of metabolite's interaction within biological system has garnered significant attention over the past decade due to its impact in the analysis of small-molecule components of biological systems and samples (Burgess, Rankin, & Weidt, 2014; R. Liu, Bao, Zhao, & Li, 2021). Despite the fact that a comprehensive analysis of human metabolite interactions within the biological system is still a long way off, it is widely acknowledged that metabolomics has evolved into a powerful method that is proven highly applicable in clinical and biomedical research (Burgess et al., 2014). The development of the metabolomics into a powerful method comprises of two main technologies, which are mass spectrometry and magnetic resonance spectroscopy (MRS) (Barbosa-Breda et al., 2018; Markley et al., 2017). Mass spectrometry is an invasive method involving sample collection for in vitro metabolite analysis. The MRS on the other hand is better alternative than the mass spectrometry in a number of ways as it allows studies of metabolites that are difficult to ionise without the need for any sample preparation or fractionation, directly in a tissue (Markley et al., 2017).

Metabolites are defined as small molecules that act as intermediate in the metabolism and products of metabolism, that is vital for health and proper body functioning (Altaf-Ul-Amin, Kanaya, & Mohamed-Hussein, 2019; Breitling, Cenicerros, Jankevics, & Takano, 2013). Several metabolites in the brain can be detected non-invasively using MRS. The most significant visible metabolites detectable by MRS are N-acetyl-aspartate (NAA), glutamate-glutamine (Glx), creatine (Cr), choline (Cho), and myo-inositol (ml) (Grover et al., 2015).

NAA is the most prominent, concentrated metabolites and largest peak in spectra in a healthy brain (Dandil, 2020; Moffett, Ross, Arun, Madhavarao, & Namboodiri, 2007; Rigotti et al., 2007, 2011). The NAA generates the most prominent peak at 2.02 parts per million (ppm) on an MRS spectrum (Currie et al., 2013; Wootla, Denic, Watzlawik, Warrington, & Rodriguez, 2015). The role of NAA is unclear; however, many agrees that its concentrations reflect to the health of neurons (Currie et al., 2013) and any diversion from the normal concentration may indicate dysfunction (Babourina-Brooks, Wilson, Arvanitis, Peet, & Davies, 2014; Hajek & Dezortova, 2008). Therefore, NAA has been identified as a reliable marker for neuronal death and neuronal dysfunction, which in turn is used clinically to investigate progression of diseases such as multiple sclerosis, and in brain studies (Grover et al., 2015; Hajek & Dezortova, 2008; Moffett et al., 2007). In the brain, NAA is normally more concentrated within the grey matter relative to the white matter (Currie et al., 2013; Hajek & Dezortova, 2008). NAA can also be found in a higher concentration during myelination of brain development and maturation in infancy stage (Currie et al., 2013; Dezortova & Hajek, 2008). The level of NAA concentrations has a certain important diagnostic value especially in neurological disorders (Moffett et al., 2007). For example, the normal NAA value can reach about 10 to 12 mM (millimolar) in healthy adult brains (Hajek & Dezortova, 2008), where reduction in its concentration level indicates neuronal damage or compromised neuronal metabolism (Gujar, Maheshwari, Björkman-Burtscher, & Sundgren, 2005; Moffett et al., 2007). Meanwhile, elevation in the NAA concentration was observed in Canavan diseases ('Canavan disease', n.d.) and in patient with sickle cell disease (Steen & Ogg, 2005).

Glutamate (Glu) and glutamine (Gln) have similar chemical structures, and their proton environments lead to similar coupling patterns, resulting in overlapping signals in the MRS spectrum and thus often referred as Glu-Gln complex (Glx) (Ramadan, Lin, & Stanwell, 2013). In an MRS spectrum, the Glu and Gln signals are not prominent, but they are commonly detectable close together between 2.1 ppm and 2.5 ppm as a result of breaking the signals into multiplets (Faghihi et al., 2017). Figure 2.7 shows the spectrum that have multiplets of Glu and Gln, edited from (Shevelev et al., 2017). In a normal functioning brain, Glu is the most abundant neurotransmitter (Cecil, 2014; Currie et al., 2013) while Gln concentration reading has become an astrocyte marker (Bairwa et al., 2016; Burtscher & Holtas, 2001).

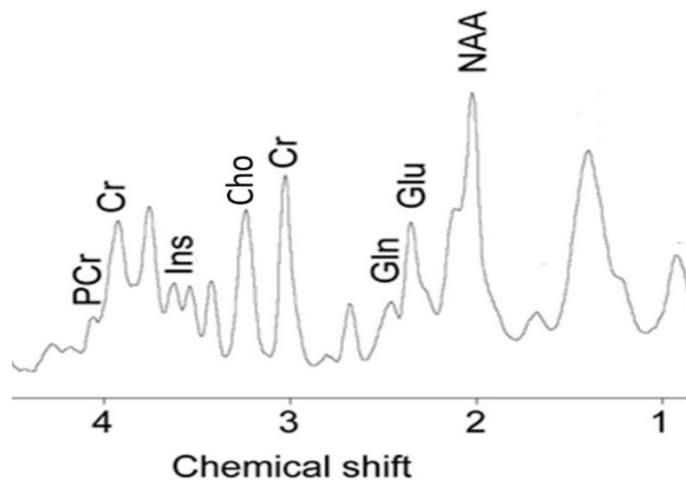


Figure 2.7 The spectrum that shows the multiplets of Gln and Glu that commonly combined as Glx, the smaller Cr at 3.9 ppm, primary Cr at 3.02 ppm, edited from (Shevelev et al., 2017)

To balance Glu in healthy brain, the Glu release by neuronal cells is dissipated by glial glutamate transporters and then converted into Gln and transported back to neurons, where it is converted back into Glu (Ramadan et al., 2013; Zhou & Danbolt, 2014). Figure 2.8 depicts the conversion of Glu to Gln to Glu, which is also known as the glutamate-glutamine cycle (Feng et al., 2022).

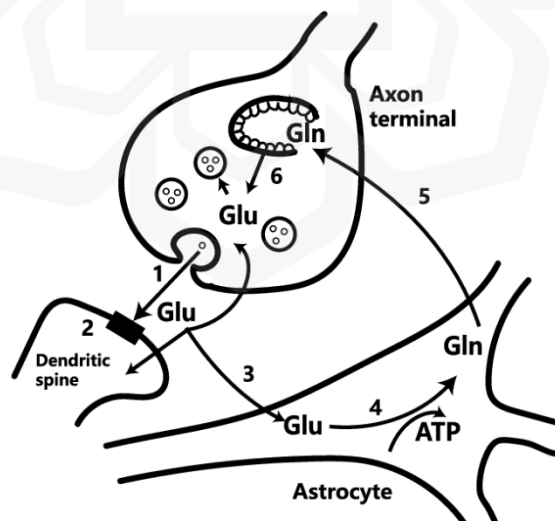


Figure 2.8 The glutamate-glutamine cycle (Feng et al., 2022). (1) Glu is released by neuron cells. (2) Glu binds to neuron receptors. (3) Glu dissipates from synapse to astrocytes. (4) Glu in astrocytes is converted to Gln. (5) Gln is shuttled to neurons. (6) Gln is converted to Glu.

The disruption of Glu uptake and Gln conversion, which can occur in various diseased states, can cause perturbations in Glu and Gln metabolism and result in an excessive buildup of Glu in the extracellular space (Brief, 2000; Ramadan et al., 2013). This excessive buildup of Glu can potentially have neurotoxic effects due to its ability to overstimulate and damage neurons (Danbolt, 2001). In certain pathological conditions, such as traumatic brain injury, stroke, or neurodegenerative diseases, disruptions in Glu metabolism can contribute to neuronal dysfunction and cell death (Danbolt, 2001).

The combination of primary Cr which contains Cr and phosphocreatine (PCr) is necessary for energy supply for bio-chemical processes (Hajek & Dezortova, 2008; Hesselink, 2014). The primary Cr thus is considered as the marker for energy metabolism (Cecil, 2014; Hajek & Dezortova, 2008; Soares & Law, 2009). In a normal MRS spectra, the primary Cr represented by the third highest peak which resonates at 3.02 ppm and located to the right side of Cho (Castillo, Kwock, & Mukherji, 1996; Cecil, 2014; Currie et al., 2013). In the same normal spectra, there is also smaller Cr that resonates at 3.9 ppm (Cecil, 2014; Currie et al., 2013; Soares & Law, 2009). A normal and healthy brain's primary Cr concentration is estimated at 8.6 mM (Currie et al., 2013). Cr concentration value is relatively constant across the brain with little variation even in different pathologies (Currie et al., 2013). The invariability and considerably fixed Cr concentration, hence, is used as a reference metabolite for metabolite ratio calculation (Currie et al., 2013; Dezortova & Hajek, 2008; Faghihi et al., 2017; Soares & Law, 2009). However, (B. S. Y. Li, Wang, & Gonen, 2003) caution that when using reference metabolites in MRS studies, careful consideration should be given to their stability, as assuming the stability of creatine (Cr) may confound metabolite quantifications. It is proven by studies that have reported brain Cr concentration changes in individuals exposed to drugs of abuse, in depressed individuals, and in Alzheimer's disease, indicating differences in energy metabolism in comparison to healthy individuals (D'Anci, Allen, & Kanarek, 2011; Lewandowska, Steinborn, Borkowski, Chlebowska, & Karmelita-Katulaska, 2018).

The MRS also allows measurement of Cho which resonates at 3.2 ppm in an MRS spectrum. Cho represents the amount of choline-containing compound that may be contributed from the concentration of glycerophosphocholine (GPC), phosphatidylcholine and phosphocholine (PCho). PCho involves in glial cell phospholipid metabolism and osmotic regulation (Grover et al., 2015). Since PCho are released during degradation of membrane phospholipids, Cho has become the metabolic marker of membrane density and integrity (Gujar et al., 2005; Hajek & Dezortova, 2008; Minati, Aquino, Bruzzone, & Erbetta, 2010).

It is interesting to note that Cho exhibited high peaks in the MRS spectrum in neonates because their brains are undergoing active myelination (Gujar et al., 2005). Once the cerebral reaches the stage of maturation, the Cho metabolite demonstrates a lower peak, similar to that of adults (Dezortova & Hajek, 2008). The normal concentration of choline in normal healthy brain is estimated at 7 mM (Trihadijaya, Abimanyu, & Darmini, 2019). It is also expected that Cho concentration being higher in the grey matter as compared to the white matter (Gujar et al., 2005). In brain studies, Cho is signified as the marker for brain tumour as Cho is often elevated in malignant cancer event (McRobbie et al., 2006). In cancer cases, the elevated Cho levels indicates of increased cellularity, gliosis, and membrane degradation due to myelin breakdown (Grover et al., 2015; Soares & Law, 2009). In the meantime, it has been reported that decreases in Cho are associated with osmoregulatory alterations in hepatic encephalopathy (Bluml, Zuckerman, Tan, & Ross, 1998).

The peak of mI is primarily found at 3.56 ppm on an MRS spectrum. The mI peak is obtained at short echo-times when performing the MRS (Currie et al., 2013; Gujar et al., 2005; Minati et al., 2010). The mI concentration is prominent in a newborn at a highest peak of 3.5 ppm, and the concentration swiftly decreases with age (Castillo et al., 1996; Dezortova & Hajek, 2008; Hesselink, 2014). Along with myo-inositol-monophosphate and the alpha-protons of glycine, mI have normal concentration of 5 mM in a healthy brain (Cecil, 2014). Changes in the concentration of mI is correlated to the osmolarity condition in the brain which is important in balancing the intracellular sodium content and glial activation (Cecil, 2014). Due to this fact, mI has been known as osmolyte and astrocyte marker (Gujar et al., 2005). An increase in mI concentration can be observed in central nervous system autoimmune disease such as multiple sclerosis, metabolic disorder diseases, degenerative disease (such as Alzheimer disease and frontotemporal dementia), and HIV infection (Faghihi et al., 2017; Gujar et al., 2005; Hesselink, 2014). Meanwhile, a decrease in mI can be seen in cases of brain trauma such as in brain hyponatremia (Moffett et al., 2007) and in meningioma (Faghihi et al., 2017).

This section has highlighted the importance of studying metabolite interactions for comprehensive characterization of metabolites in specific brain regions. This is particularly evident when employing MRS as the metabolomic investigation tool, as it allows for a holistic assessment of the metabolic profiles and their interplay within these regions. Changes in metabolites can help determine whether a tissue is in a normal or pathological state. Overall, previous studies shows that MRS has the potential to advance the study of metabolites interaction, particularly those involving complex diseases such as Alzheimer's, multiple sclerosis, and autoimmune disease (Craig, 2008), and glaucoma (Barbosa-Breda et al., 2018; Patel & Lighthizer, 2022).

2.5 MAGNETIC RESONANCE IMAGING (MRI)

Since Dr. Raymond Damadian's initial discovery of magnetic resonance imaging (MRI) in 1969 (Healthcare, 2019; Lynette, 2020), the continued progress and enhancement of this technology, with significant contributions from Lauterbur, (1973) and Mansfield, (1977), have transformed MRI into one of the most advanced imaging techniques employed in the field of medicine (Graves & Zhu, 2015; Saman & Jamjala Narayanan, 2019). In 1971, Lauterbur published a groundbreaking paper, introducing the new concept that was to use magnetic field gradient to create images that would allow doctors to see detailed images of the inside the body without using harmful radiation (Danilova, Grigorieva, & Komisarenko, 2023). The use of magnetic field gradient was further developed by Mansfield in 1970, to encode spatial information and developed fast imaging techniques that significantly reduced scan times, thereby paving the way for the practical application of MRI (Danilova et al., 2023). In addition, Richard Robert Ernst made substantial contributions to MRS and was recognized with the Nobel Prize in Chemistry in 1991 (Shampo, Kyle, & Steensma, 2012). His breakthroughs revolutionized the precision and depth of chemical analysis possible within NMR spectroscopy encompassing the development of high-resolution NMR methodologies, encompassing Fourier Transform NMR, multi-dimensional NMR spectroscopy, and sophisticated pulse sequences (Shampo et al., 2012).

MRI is also one of the widely utilised non-ionizing diagnostic imaging technologies that permits non-invasive evaluation of the structure and function of the human body (Graves & Zhu, 2015; Van Geuns et al., 1999). In contrast to diagnostic imaging modalities that use ionising radiation, such as computed tomography (CT) scan and x-ray imaging, MRI uses a static magnetic field and radiofrequency (RF) waves to provide clear and detailed image of wide range of organ structures and tissues (Saman & Jamjala Narayanan, 2019). The MRI image produced represents the RF signal intensities of a tissue, and the contrast in the image is dependent on the characteristics of the individual tissues (Sprawls, 2001). Figure 2.9 demonstrates the major components of MRI system and its process of image generation (Sprawls, 2001).

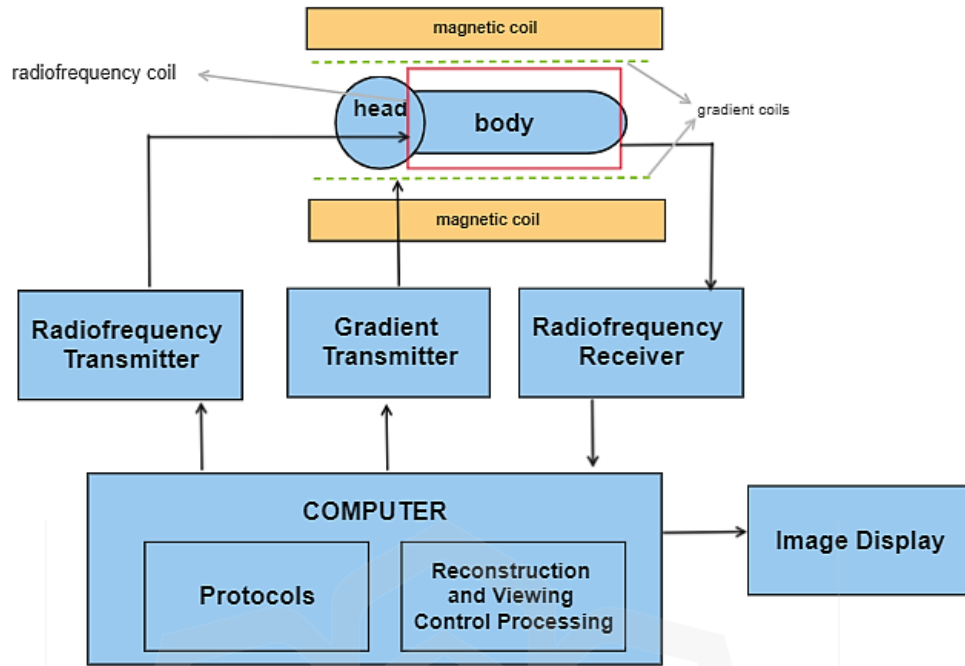


Figure 2.9 The major component of an MRI system.

A common MRI system comprises a superconducting magnet that operates at 1.5 Tesla to 3.0 Tesla to generate a stable and spatially homogeneous magnetic field over a specified volume (Laader et al., 2017). Although MRI systems with a magnetic field strength of 3.0 Tesla and 7.0 Tesla are also becoming increasingly common especially in research setting a, an MRI system with 1.5 Tesla strength is also mostly used for clinical research (Grover et al., 2015; Kagawa et al., 2017; Laader et al., 2017; McGowan, 2008; Saman & Jamjala Narayanan, 2019). Higher magnetic field improves the signal-to-noise ratio (SNR), spectral, spatial, and temporal resolution, as well as quantitative accuracy (Grover et al., 2015).

In addition to producing images of structures and tissues, MRI technology can also be used to produce images of blood in motion and to analyse the metabolites in tissue (Sprawls, 2001). The generation of images involving blood in motion corresponds to functional imaging, while analyses of tissue metabolites simply refer to MRS utilisation (Grover et al., 2015; Sprawls, 2001). The current availability of MRI technology in the clinical setting provides better opportunities for a variety of clinical diagnostic procedures that have been shown as appropriate and efficient.

2.6 MAGNETIC RESONANCE SPECTROSCOPY (MRS)

MRS is an MRI-based method that allows non-invasive examination of metabolic processes in-vivo. The MRS has been used to examine changes in metabolite concentration which can be correlated with structural and functional alterations (Hashemi, Bradley, & Lisanti, 2012). Despite advancements in MRI technology, such as improved contrast resolution, higher magnetic field strength, and better contrast media, MRS was developed as a complementary technique to MRI, specifically for investigating tissue characterization, which cannot be accomplished using MRI alone (Soares & Law, 2009).

MRI primarily aims to generate detailed anatomical images, whereas MRS focuses on analysing the chemical composition and concentrations of specific molecules within a localized region, both utilizing radiofrequency signals for their respective purposes. (Soares & Law, 2009). For instance, while frequency in MRS is determined by the chemical environment of the tissue and presented as a spectrum, frequency in MRI is determined by spatial location and generated as an image (Currie et al., 2013; McRobbie et al., 2006; Soares & Law, 2009; Sprawls, 2001; Tognarelli et al., 2015). MRS and MRI differ in one major aspect: MRS does not use external frequency encoding gradients, which are essential during signal acquisition for producing detailed images in MRI (R. W. Brown, Cheng, Haacke, Thompson, & Venkatesan, 2014; Lambert, Mazzola, & Ridge, 2019; Mandal, 2007; Poser & Setsompop, 2018; Sharma & Lagopoulos, 2010). Instead, frequency encoding in MRS relies on the intrinsic properties of the molecules (Mandal, 2007). Gradients create spatial encoding, allowing for the differentiation of signals from various locations within the body (R. W. Brown et al., 2014; Poser & Setsompop, 2018; Sharma & Lagopoulos, 2010). On the other hand, MRS sequences do not necessitate the same level of spatial encoding as imaging sequences (Keeler, 2010; Lambert et al., 2019). Instead, they rely on specific radiofrequencies to extract metabolic or chemical information (Keeler, 2010; Lambert et al., 2019).

The clinical magnetic strengths of the MRI scanner are usually between 0.2 Tesla to 3.0 Tesla (McRobbie et al., 2006). In clinical MRS, a 1.5 Tesla magnetic field is considered sufficient to measure metabolites signal other than water and fat (Van Der Graaf, 2010). The high natural abundance of hydrogen (^1H), commonly called proton and its high nuclear magnetic sensitivity compared to other magnetic nuclei, has made proton the most common nuclei used to obtain MRS spectrum (Faghihi et al., 2017). Not only that, the proton has become the principal nucleus to a spectroscopic investigation because the proton MRS method can be performed using standard MRI scanner and does not require other unique MRI scanner (Currie et al., 2013).

2.6.1 MRS Acquisition

The two main technique of MRS acquisition are single-voxel spectroscopy (SVS) and multi-voxel spectroscopy (MVS), sometimes referred to as chemical shift imaging (CSI)(Grover et al., 2015). The SVS technique is applied by locating a single voxel (volume of tissue) within region of interest (Faghihi et al., 2017; Grover et al., 2015; Tognarelli et al., 2015). Meanwhile, MVS locates a larger volume consisting of several smaller divided voxels in a region of interest to simultaneously generate all voxels' spectrum (Faghihi et al., 2017; Grover et al., 2015).

The advantage of SVS lies in its ability to achieve a high SNR per unit volume and unit time, making it ideal for obtaining detailed metabolic information from a specific area (Dyda, Weiger, Pruessmann, Meier, & Boesiger, 2001). This heightened sensitivity allows for precise characterization of metabolites within the defined region. However, precise localization requires meticulous attention to voxel placement (Fayad, Barker, & Bluemke, 2007).

Conversely, MVS offers the benefit of simultaneously providing quantitative information from multiple voxels (Chianca et al., 2021). This capability proves invaluable in studies aiming for a broader assessment of metabolite distribution. However, it does have its limitations, particularly in terms of susceptibility to field inhomogeneity and reduced SNR when compared to SVS (Teixeira et al., 2015). These considerations underscore the importance of selecting the appropriate technique based on the specific research objectives and spatial requirements of the study.

The procedures for MRS acquisition using SVS technique begin with the acquisition of MRI images of the region of interest. Prior to running the spectroscopy, the water signal is suppressed using the chemical shift selective (CHESS) technique (Hoa, 2016). This step is essential so that the peak of the metabolite of interest is not obscured by the abundant hydrogen signal in the human body's water signal (Hoa, 2016). Subsequently, a tissue volume would be meticulously chosen from the images from which the MRS spectrum is acquired (Hoa, 2016). Figure 2.10 illustrates an example of the region involved in the selection of the voxel of interest (VOI).

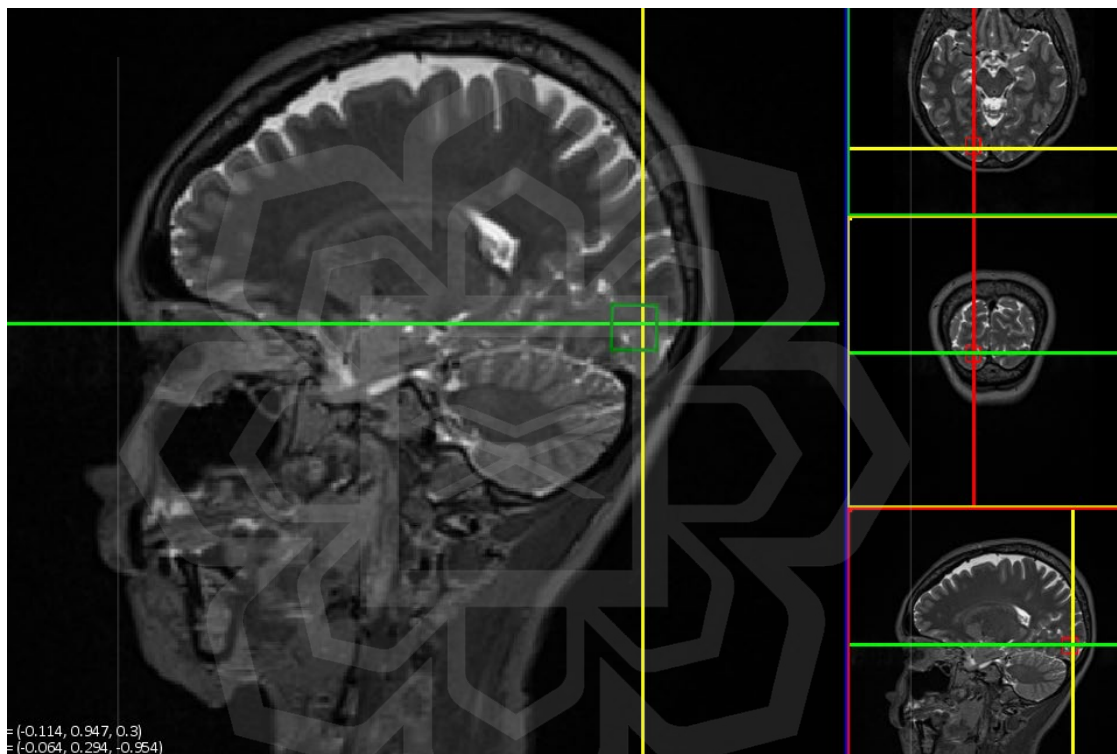


Figure 2.10 An example volume of interest (VOI) placement measured at 13mm x 13mm x 13mm in the visual cortex.

The MRS signal from the selected voxel can be acquired using two distinct sequences: stimulated echo acquisition mode (STEAM) or point resolved spectroscopy (PRESS) (Grover et al., 2015; Hoa, 2016; Tognarelli et al., 2015). STEAM and PRESS generate signals differently, with STEAM generating a stimulated echo signal and PRESS generating a spin echo signal (Tognarelli et al., 2015; Wilson et al., 2019). In the STEAM sequence, three slice-selective 90-degree radiofrequency pulses are simultaneously applied in conjunction with three orthogonal gradients (x, y, z) (Allen D. Elster, 2023b; Mandal, 2007). The collected stimulated signals originate exclusively from protons that have undergone all three radiofrequency pulses (Mandal, 2007). Figure 2.11 illustrates the timing diagram of STEAM pulse sequence.

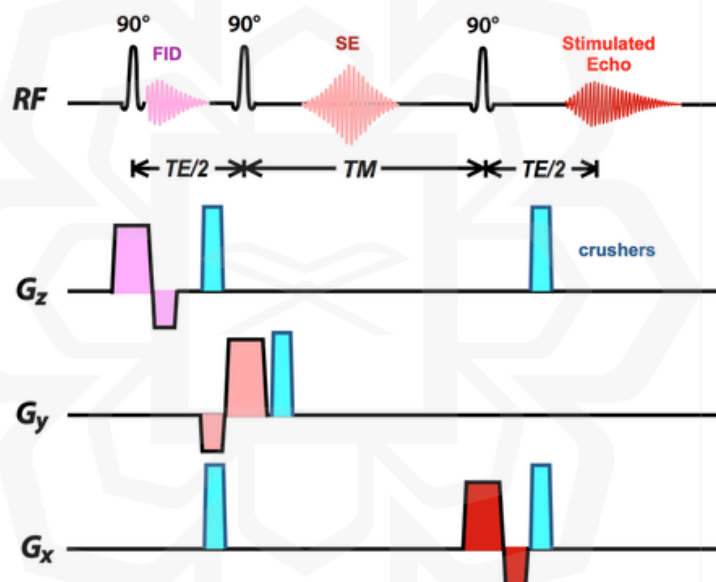


Figure 2.11 The STEAM pulse sequence schematic diagram(Allen D. Elster, 2023b) .

In the PRESS sequence, three slice selective radiofrequency pulses of 90 degrees, 180 degrees, and 180 degrees are applied simultaneously with three orthogonal gradients (x, y, z) (Allen D. Elster, 2023a). At time TE, the PRESS signal is a double spin echo that has experienced all the three radiofrequency pulses (Mandal, 2007). Figure 2.12 The PRESS pulse sequence timing diagram (Allen D. Elster, 2023a) .illustrates the timing diagram of PRESS pulse sequence.

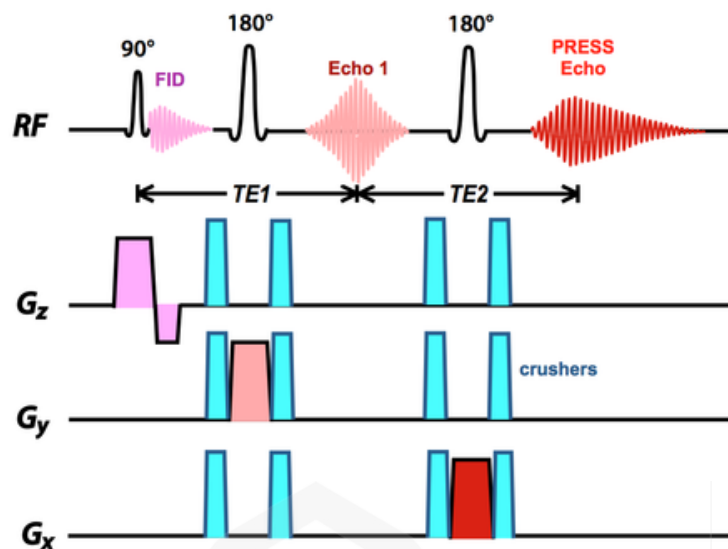


Figure 2.12 The PRESS pulse sequence timing diagram (Allen D. Elster, 2023a) .

The signal intensity of PRESS is double to that of STEAM, resulting in a spectrum with a higher SNR than that of STEAM (Mandal, 2007; McRobbie et al., 2006; Tognarelli et al., 2015). However, with the same hardware as PRESS, STEAM produces a shorter echo time, which subsequently allows more metabolites to be reliably detected than a longer echo time (Bulakbasi, 2004; Mandal, 2007; McRobbie et al., 2006). The comparative details of STEAM and PRESS sequences are presented in Table 2.1.

Table 2.1 The comparison between STEAM and PRESS (Mandal, 2007).

STEAM	PRESS
Similarities	
<ul style="list-style-type: none"> • Both pulse sequences involve three orthogonal gradients to select slices. • Both can be applied with phase encoding gradients 	
Differences	
<ul style="list-style-type: none"> • Less sensitive to T2 relaxation effects (no T2 relaxation occurs) 	<ul style="list-style-type: none"> • Higher sensitivity by factor of two, given the same echo time.
<ul style="list-style-type: none"> • With same hardware, STEAM can achieve shorter TE than PRESS. 	<ul style="list-style-type: none"> • Amount of power deposited (SAR) twice as high for PRESS compared to STEAM.
<ul style="list-style-type: none"> • Better water suppression 	
<ul style="list-style-type: none"> • Less spurious water signals 	

The comparison of the methods and sequences for MRS data acquisition discussed in this section may enable researchers to select the most appropriate techniques for the conduct of research, particularly in situations where different MRI protocols are available.

2.6.2 MRS Spectrum

The MRS spectrum comprises a set of peaks that denote the resonance of metabolites in the structure or location being probed (McRobbie et al., 2006). Each metabolite has its pattern of resonance in the spectrum which provides *in vivo* metabolite information (Soares & Law, 2009). The x-axis represents the frequency chemical shift in parts per million (ppm) of metabolites in a tissue (Soares & Law, 2009). The varying height of the peaks plotted on the y-axis of the graph, which is arbitrary, represents the strength of the detected signal from metabolites (Blüml, 2013; Gujar et al., 2005). The detected signal signifies the concentration of the detected metabolites (McRobbie et al., 2006; Sprawls, 2001). Figure 2.13 depicts the resonances that are distributed along the x-axis and labelled as ppm, while Table 2.2 provides the value of the chemical shift of several resonances. The most common metabolites resonances, as shown in the graph, are the NAA, Cr, Cho, and ml (Grover et al., 2015; McRobbie et al., 2006). The graph usually is shown up until 4.0 ppm only, as anything beyond 4.7 ppm is considered unreliable. Beyond that, the neighbouring portion of the spectrum will be destroyed by water suppression (McRobbie et al., 2006).

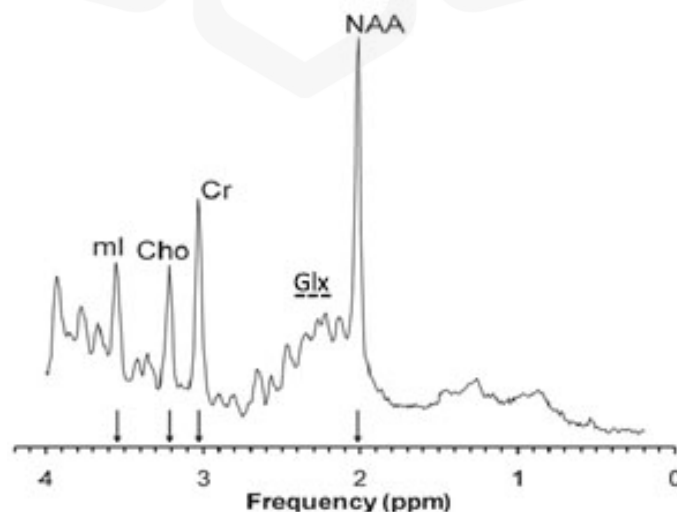


Figure 2.13 An example of a normal metabolite peak in MR spectrum, edited from (McRobbie et al., 2006)

Table 2.2 The location (ppm) of common detectable metabolites.

Metabolite	Chemical shift (ppm)
N-acetyl Aspartate	2.02
Glutamate Glutamine	2.1-2.5
Creatine	3.02
Choline	3.2
Myo-Inositol	3.56

2.6.3 Spectroscopy Data Processing

Processing the MRS's raw data is necessary for non-expert users to interpret or draw conclusions by technically determining the signal strength of each metabolite in a spectrum (Ernst & Linda, 2006). In an MRS spectrum, the area beneath a metabolite peak that represents the signal strength of a metabolite is directly proportional to the concentration of the metabolites being measured (Buonocore & Maddock, 2015; Jansen, Backes, Nicolay, & Kooi, 2006). The process of determining the concentration of metabolite signal is commonly referred to as quantitation, and it can be accomplished with MRI scanner manufacturer software or advanced software such as linear combination model (LCModel) or jMRUI (Blüml, 2013; Near et al., 2021).

There are several approaches that can be used to describe, and report quantified metabolite concentration values (Buonocore & Maddock, 2015; Jansen et al., 2006; Lin et al., 2021; Near et al., 2021). Commonly, metabolite peak integration is used to give a value from the process of summation and subtraction of a frequency range containing the metabolite peak of interest (Buonocore & Maddock, 2015; Lin et al., 2021; Near et al., 2021). Typically, this metabolite peak integration process can be performed in manufacturer software immediately after MRS data acquisition in order to determine the integral value of each metabolite (Buonocore & Maddock, 2015).

Second most used approach is by using the metabolite fitting method that can provide more accurate quantitation value (Buonocore & Maddock, 2015). This method matches the integral value of the important metabolite in the spectrum to a mathematically defined model metabolite spectrum (Buonocore & Maddock, 2015). The optimal combination value from the matched spectrum is then calculated iteratively for each metabolite in the set (Buonocore & Maddock, 2015). Analyses of this metabolite fitting can be performed with the jMRUI-integrated Advanced Method for Accurate, Robust, and Efficient Spectral (AMARES) algorithm, which generates the amplitude as the main parameter of interest of fitted metabolite signal intensity that scales in direct proportion to concentration (Buonocore & Maddock, 2015; Near et al., 2021).

The other approach is by using the LCModel software (Provencher, 2001), which is widely used commercially, employs the most comprehensive method which requires simulation of the exact scanning using in-vitro phantoms (Buonocore & Maddock, 2015). The simulation scanning will generate basis spectra that constrain the iterative peak fitting calculation used to quantify metabolite signal intensity values in the actual in vivo scanning (Buonocore & Maddock, 2015; Ernst & Linda, 2006).

The value derived from the quantitation approaches described above can directly represent metabolite concentration or can be further quantified to obtain absolute metabolite concentration and metabolite ratio (Buonocore & Maddock, 2015; Ernst & Linda, 2006; Jansen et al., 2006). The absolute metabolite concentration requires additional steps during data acquisition and calculations during data quantitation, thus require more time and setting (Buonocore & Maddock, 2015; Jansen et al., 2006). These steps include acquiring a reference signal from a phantom solution of known metabolite concentrations, using this reference signal to calibrate the MRS data and calculate absolute concentrations of the metabolites of interest (Buonocore & Maddock, 2015; Near et al., 2021). Despite requiring more steps to calculate, absolute metabolite concentration is preferred to metabolite ratio for use in scientific research because it provides more accurate and clear measurements (Ernst & Linda, 2006; Jansen et al., 2006).

Meanwhile in clinical setting, the metabolite concentration is usually represented as integral value and metabolite ratio (Blüml, 2013; Ernst & Linda, 2006). On the assumption that the Cr pool is relatively constant in both healthy and diseased individuals, Cr has been used as the reference metabolite in the ratio normalisation method (Blüml, 2013; Buonocore & Maddock, 2015). This metabolite ratio will enable the evaluation of changes in the balance of different metabolites in the body that may be caused by certain diseases (Holmes & Nicholson, 2007). The interpretation of the metabolites' concentration in the form of ratio has been claimed as the fastest and the most employed method in clinical practices (Currie et al., 2012). In contrast to absolute metabolite concentration, which can be affected by factors such as the quantitation method employed, the type of tissue analysed, and the characteristics of the study's subject, metabolite ratios are less sensitive to the differences in the aforementioned factors; as a result, metabolite ratios can be more robust and standardised for comparisons across studies (Wishart, 2008; Wishart et al., 2022). The arguments that absolute concentration has more advantages than metabolite ratio continues to fuel debates regarding the optimal method for interpreting the spectrum (Blüml, 2013; Ernst & Linda, 2006; Jansen et al., 2006).

While the methods for quantifying metabolite concentrations in MRS studies have advanced significantly, the choice of approach introduces important considerations. The widely used metabolite peak integration method, despite being convenient and straightforward, may overlook fine details in the spectral data. This raises questions about its sensitivity to subtle shifts in metabolite concentrations, especially in cases where metabolite peaks may overlap or exhibit non-standard shapes. In contrast, the metabolite fitting method, which employs mathematically defined models, offers a more refined approach to quantification. However, this method relies heavily on the accuracy of the chosen model, which may not always perfectly match with the in vivo spectrum.

Additionally, the application of LCModel, despite being comprehensive, demands meticulous simulation steps with in-vitro phantoms, potentially introducing an additional layer of complexity and room for error. Moreover, the preference for absolute metabolite concentration over ratios in scientific research is well-founded, given its potential for higher accuracy. However, the practicality of implementing absolute quantification in clinical settings may be limited due to the additional time and resources required. Therefore, the choice of quantitation method should be carefully considered in light of the specific research objectives, available resources, and the level of precision required for the study.

2.7 MRS IN STUDIES OF GLAUCOMA

The ability of the MRS method to non-invasively assess the level of metabolites in the brain in neurodegenerative diseases has become an essential option for metabolite assessment in glaucoma studies. Whilst published studies on the application of MRS to evaluate metabolites in brain diseases have been available for some time, the published studies on the application of MRS to evaluate metabolites in glaucoma diseases remain inconclusive.

Relevant articles from database such as MEDLINE, CINALH and SCOPUS were screened by keywords, title, abstract or text words containing the search terms: “metabolites concentration” OR “metabolites”, “magnetic resonance spectroscopy” OR “proton magnetic resonance spectroscopy” OR “¹H-MRS” OR “spectroscopy” OR “MR spectroscopy”, “ocular disease” OR “glaucoma” OR “chronic glaucoma” OR “open-angle glaucoma” OR “suspected glaucoma”, “vitreous” OR “visual cortex” OR “optic nerve” OR “radiation optic”. The Boolean term “AND” and “OR” were employed with the search term in the ‘Advanced Search’ section in each database for comprehensive retrieval.

The systematic search of the mentioned electronic databases pertaining to the use of MRS in studies of human glaucoma diseases then yielded 178 relevant articles. From the 178 reports, only eight articles are genuinely related to the empirical application of MRS in human glaucoma diseases (Table 2.2). Three of the included articles were from Europe (37.5%), three from Asia (37.5%) and two from the United States of America (USA) (25%). In keeping with bibliometric trends in this research area, Figure 2.14 highlights a substantial chronological increase in the number of published studies including review article relating to glaucoma and MRS. The trend shows that studies in this research area continue and keep expanding with times.

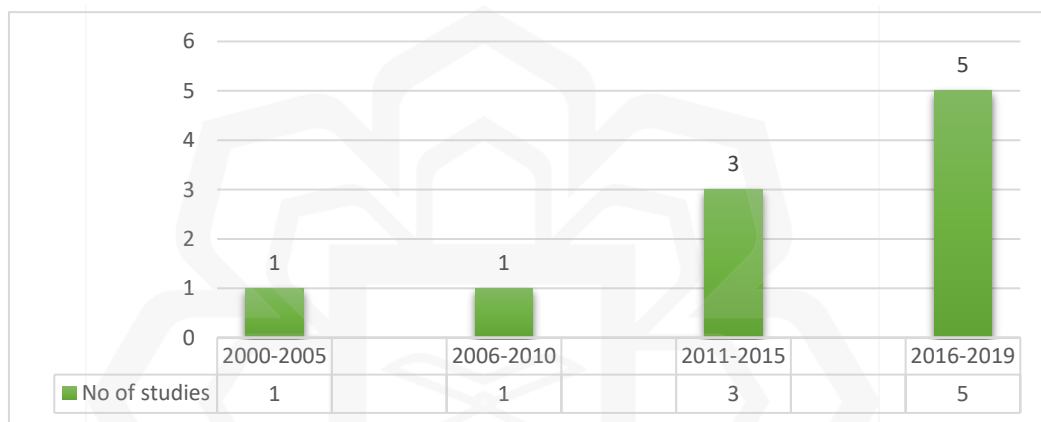


Figure 2.14 Published studies by year.

Each of the eight studies had its own participant group category combination. Former study by Rucker et al., (2003) consisted of only five subjects, one of whom was a patient with optic neuropathy, because its purpose was to explore the feasibility of using MRS in glaucoma studies. Majority of the studies (Aksoy et al., 2018; Boucard et al., 2007; Doganay et al., 2012; Murphy et al., 2016; Sidek et al., 2016) however, focused on the changes of metabolite concentration between control groups and glaucoma group with different type and severity.

In most of the cited studies, the number of subjects was greater than in the feasibility study, but the number of subjects in each group was unequal. Study conducted by Sidek et al., (2016) for example, investigated on the possibility of metabolites concentration changes in optic radiation between group of healthy, mild glaucoma and severe glaucoma with initial recruited subjects were fifteen for each group. Nevertheless, due to issues in their acceptable MRS spectrum, a substantial reduction to only 7 subjects in healthy group, 11 subjects in mild glaucoma group and 5 subjects in severe glaucoma group were used for their statistical analysis.

Fiedorowicz, Dyda, Rejdak, & Grieb, (2011) suggested the visual pathway as options to study glaucoma using MRS, giving alternatives than the usual optic nerve and RGC location. Most of the studies chose the occipital region as the region of investigation (Aksoy et al., 2018; Boucard et al., 2007; Guo et al., 2018; Y. Zhang et al., 2013), while a few chose the vitreous (Doganay et al., 2012; Rucker et al., 2003), LGN (Aksoy et al., 2018; Doganay et al., 2012) and geniculocalcarine, also known as optic radiation related area (Sidek et al., 2016; Y. Zhang et al., 2013). All regions of interest identified in the eight aforementioned studies were anatomical areas within the visual pathway, including the optic radiation, LGN, and VC. None of the studies utilised the MRS method on the optic nerve or RGC, most likely due to the small size of these structures, which made them less likely to fit within the minimum VOI size available in the MRS measurement setting.

The two types of spectroscopy technique that can be applied during the MRI scanning are SVS and MVS. Of all included studies, only one study (Y. Zhang et al., 2013) used MVS technique while the remainder (Aksoy et al., 2018; Boucard et al., 2007; Doganay et al., 2012; Guo et al., 2018; Murphy et al., 2016; Rucker et al., 2003; Sidek et al., 2016) used SVS technique. As anticipated, many studies preferred to use SVS method due to its short acquisition time and higher signal to noise ratio, hence provides good spectral quality (Anith Alfred J, Abubacker Sulaiman F, Divya Shree, Ashraf Ahmed & Prabhu, 2018). It was then argued that MVS also could offer more accurate information through its capability of yielding data from multiple adjacent voxels in a single measurement, thus avoiding error caused by multiple acquisitions times (Yang et al., 2011). The particularly small voxels within the multivoxel also enable the localisation of region of interest individually and independently, thus the metabolites concentration is relatively unaffected by adjacent different tissue (Yang et al., 2011).

Even though some of the studies conducted experiments on the same region of interest, one of the important parameters that differ across all studies is the VOI size. For instance, Murphy et al. (2016), Guo et al. (2018), and Aksoy et al. (2018) used different VOI sizes of $20 \times 20 \times 20 \text{ mm}^3$, $20 \times 30 \times 20 \text{ mm}^3$, and $20 \times 25 \times 30 \text{ mm}^3$ respectively, but those studies aimed to study the changes of metabolites in the VC. While Aksoy et al. (2018) and Doganay et al. (2012) studied metabolite changes in LGN using VOI sizes of $13 \times 13 \times 13 \text{ mm}^3$ and $12 \times 12 \times 12 \text{ mm}^3$, respectively. With the smallest and quickest measurement time, high spatial resolution and a sufficient SNR remain the goals of optimization in MRS, but in reality, it is difficult to obtain a perfect result with ideal parameters' values (Hartmann et al., 2017). Therefore, the choice of spectroscopy will usually be based on the readily available MRS configuration at the location where the researchers are conducting their studies, with some consideration given to adjusting the experiment's parameters in order to achieve the optimum results.

A processing software could enable the raw spectroscopy data being presented in an interpretable or quantitative data (Ernst & Linda, 2006). Almost all studies (Aksoy et al., 2018; Boucard et al., 2007; Doganay et al., 2012; Guo et al., 2018; Rucker et al., 2003; Y. Zhang et al., 2013) used a variety of embedded scanner manufacturer software except one study (Sidek et al., 2016) which used external processing software, named LCModel that apparently could yield more metabolites during the MRS spectrum processing. The variation types of manufacturer scanner software implies that the findings of these studies must be interpreted with caution as it might not be directly transferable or extrapolated to other studies.

Majority of the included studies measured the concentration of NAA, followed by Cr, Cho, Glx, and mI. Cr concentration is stable in normal or in pathological tissues, hence it is taken as a reference for normalisation. For that, these four studies (Doganay et al., 2012; Guo et al., 2018; Sidek et al., 2016; Y. Zhang et al., 2013) took Cr as a reference and thus used metabolite ratio to Cr for their study measurement and interpretation. Although other studies did not use this metabolites ratio to Cr as their study measurement, they do have their own justification. For instance, the other two studies (Aksoy et al., 2018; Boucard et al., 2007) might use the theory of an abnormal tissue could still have different level of Cr than normal tissue and that made them to only consider perhaps the integral value of each metabolite displayed on the spectrum from MRI console.

Based on the findings of the earlier research, there are several important factors that need to be taken into consideration. Table 2.3 provides a concise overview of the previous studies discussed in this section. The components that are included should make it easier to compare the analysis of different studies and provide a roadmap for creating a research design that is more innovative and useful.

Table 2.3 The summary of MRS glaucoma studies.

Authors	Participants	Aim	Region studied with VOI size	MRS Method	Processing Software	Metabolites studied	Magnetic strength
Rucker et al. (2003)	4 healthy, 1 optic neuropathy	feasibility	Vitreous (10x10x10 mm ³)	SVS (PRESS)	Philips NT software	Lactate	1.5 T
Boucard et al. (2007)	7 POAG, 7 AMD	changes	occipital region (elongated PRESS box)	SVS (PRESS)	Philips Intera software	NAA, Cho, Cr	3.0 T
Doganay et al. (2012)	29 Glaucoma, 13 controls	changes	Vitreous (13 x 13 x 13 mm ³) & laterale geniculate body (12 x 12 x 12 mm ³)	SVS (PRESS)	Philips Gyroscan software	NAA, Cho, Cr, Glx,	1.5 T
Zhang et al. (2013)	20 controls 20 primary Glaucoma	changes	Geniculo-calcarine & striate area of occipital lobe	MVS FOV (18x18cm)	GE Signal Excite software	NAA, Cho, Cr, Glx	3.0 T
Sidek et al. (2016)	15 controls 15 mild POAG, 15 severe POAG	comparison	optic radiation (20 x 20x 20 mm ³)	SVS (PRESS)	LCModel Version 6.2	NAA, NAAG, Cr, PCr, GPC, PCh, Gln, Glu	3.0 T
Aksoy et al. (2018)	30 controls, 25 OAG, 16 GS 16 OHT	changes	corpus geniculatum laterale (13 x 13 x 13 mm ³) & visual cortex (20 x 20x 20 mm ³)	SVS (PRESS)	Siemens Syngo MR version B17 software	NAA, Cho, Cr,	1.5 T
Guo et al. (2018)	23 POAG, 21 controls	changes	visual cortex (20 x 30 x20 mm ³)	SVS (PRESS)	Siemens Syngo MR software	NAA, Cho, Cr, Glx, mI,	3.0 T
Murphy et al., 2016	13 early glaucoma, 13 advanced glaucoma 9 healthy	changes	Visual cortex (20x25x30 mm ³)	SVS (STEAM)	Syngo MR software	NAA, Cr, Cho	3.0 T

Abbreviations: AMD = age-related macular degeneration; POAG = primary open angle glaucoma; OAG = open angle glaucoma; OHT = ocular hypertension; GS = glaucoma suspect; SVS = single voxel spectroscopy; MVS = multi-voxel spectroscopy; NAA = N-Acetyl Aspartate; Cho = Choline; Cr = Creatine, Glx = Glutamate-Glutamine; mI = Myo-Inositol; NAAG = N-acetyl aspartyl glutamate; PCr = Phosphocreatine; GPC = Glycerophosphocholine; PCh = Phosphocholine; Gln = Glutamine; Glu = Glutamate; T=Tesla, VOI=Voxel of interest.

2.8 METABOLITES MEASURED BY MRS IN GLAUCOMA

Published MRS glaucoma studies commonly discussed five metabolites which includes N-acetyl aspartate, Creatine, Choline, Myo-Inositol, and Glutamate-Glutamine (Aksoy et al., 2018; Boucard et al., 2007; Doganay et al., 2012; Guo et al., 2018; Sidek et al., 2016; Y. Zhang et al., 2013). As described in the preceding section, these metabolites were detected and measured by MRS in several brain regions associated with the visual pathway.

Aksoy et al., (2018) reported a significant decrease in NAA in the VC of glaucoma group as compared to healthy group. The study also found a lower NAA level in the corpus geniculatum laterale (CGL), also known as LGN and VC of subjects with glaucoma relative to controls (Aksoy et al., 2018). This finding in the CGL suggested that there is neuronal tissue loss in glaucoma. Their findings were in agreement with previous study that reported a reduction in the NAA/Cr ratio in geniculocalcarine tract and striate area (also known as primary VC) of glaucoma group (Y. Zhang et al., 2013).

Although glaucoma is one of neurodegenerative disease and lower NAA may mark the diseases, not all study found a lower NAA level in their glaucoma group (Doganay et al., 2012; Y. Zhang et al., 2013). Doganay et al., (2012) found no significant statistical difference although the levels of NAA/Cr ratio were lower in the LGN of glaucoma subjects compared to healthy individuals. However, they were confident that if a larger number of glaucoma patients could be recruited, the decrease in NAA indicating neuron loss would be demonstrated (Doganay et al., 2012). Additionally, (Boucard et al., 2007) also found no variation in NAA and claimed that the progression of necrosis or apoptosis was slow among their patient groups and thus the NAA level was not detectable.

The increase in Glx level in the area of VC in a study by (Guo et al., 2018) suggesting of cortical plasticity in patient with open angle glaucoma. The condition is believed due to a disrupted metabolism within the area of investigation (Vrabec & Levin, 2007). In addition, a pioneer study found a higher level of Glx in the vitreous and LGN in patient with glaucoma (Dogonay et al., 2012). Their findings were in favour with the apoptosis theory of the neurotoxic effect of Glx (Vrabec & Levin, 2007). The Glx neurotoxic effect may cause nerve damage in the vitreous and LGN thus leading to the increase of the Glx level in the area.

Cr is one of the primary metabolites in the brain, and it is measured by MRS in all glaucoma studies involving the brain regions. It is expected that there will be no significant differences in Cr between glaucoma studies, as Cr is typically constant throughout the brain. However, one study cautions against using absolute metabolite concentration rather than metabolite ratio to Cr (Boucard et al., 2007). This is due to the fact that, during tissue necrosis, Cr variation occurs as a general loss alongside other metabolites (Gujar et al., 2005). As a result, for instance, both metabolites' compounds will decrease, leading to unreliable evaluation results.

In cases of glaucoma, as discussed in section 2.2, the decrease in Cho concentration was interpreted as an indication of deteriorating cell integrity and apoptosis in neuronal tissue. Cho was significantly reduced in the LGN of glaucoma group compared to healthy group as reported by Aksoy et al., (2018) and Cho was also reported to decrease in the VC in glaucomatous group in a study by Zhang et al., (2013). Apoptosis, the process of programmed cell death that results in the degradation of intracellular organelles, has been identified in numerous neurodegenerative diseases (Zhang et al., 2013). Both studies concluded that the observation of reduction in Cho in their respective study regions was due to the neuron apoptosis of RGCs in those regions.

On the basis of investigating whether metabolism turbulence in a VC is associated with the brain's ability to reorganise and adapt in response to changes or damage (cortical plasticity), a recent study reported a lower level of mI in the early open angle glaucoma group compared to the healthy group (Guo et al., 2018). The reduction in mI level may be led by osmotic stress whereby the increase in Glx level in the extracellular space triggers a mechanism that results in more mI transport across the cell membrane into the intracellular cytoplasm, thus leading to a decrease in mI level in the extracellular space (Guo et al., 2018). Guo et al. (2018) concluded that the changes in metabolites might reflect adaptive changes in response to the disease, which indicate the brain's attempt to maintain visual function despite glaucoma-related damage.

Despite the fact that the reviewed studies offer valuable insights into the metabolic markers associated with glaucoma, it is essential to acknowledge the variability in findings regarding NAA levels. The discrepancy, particularly evident in the studies by Doganay et al. (2012) and Boucard et al. (2007), raises questions about the consistency of NAA as a reliable marker for neuronal loss in glaucoma. Doganay et al. (2012) precisely pointed out the potential influence of sample size on detecting such nuanced changes, implying that a larger cohort might yield more conclusive evidence. Moreover, the contrasting results on NAA levels may be attributed to the pace of necrosis or apoptosis, as speculated by Boucard et al. (2007). This underscores the need for a detail examination of how things would change over time in glaucoma progression.

Similarly, the increase in Glx levels observed in the study by Guo et al. (2018) prompts an intriguing discussion regarding cortical plasticity. While this finding indicates a potential compensatory mechanism, it also raises questions about the underlying metabolic disturbances within the visual cortex. Additionally, the consistent decrease in Cho levels across studies aligns with the notion of deteriorating cell integrity and apoptosis in glaucomatous neuronal tissue. However, the broader implications of this reduction in terms of functional outcomes and potential interventions warrant further investigation. These critical discussions highlight the complexity of metabolic changes in glaucoma and emphasize the need for methodological accuracy and larger sample sizes in future studies.

2.9 SELECTED RESEARCH APPROACH AND JUSTIFICATION

In conducting this research, the selection of SVS with STEAM technique played a pivotal role in uncovering possible subtle metabolite changes within the anatomical structures associated with the visual pathway. This method was chosen for its demonstrated effectiveness in giving higher SNR, allowing precise characterisation, and yielding detailed metabolite information from a specific region of interest (Dydak et al., 2001; Fayad et al., 2007). While considering alternative approaches, such as SVS with PRESS technique, it became evident that SVS with STEAM offered distinct advantages. Specifically, it can be applied with a shorter TE in conjunction with long TR, resulting in superior resolution and higher SNR, along with improved water suppression and lower SAR power deposition (Blüml, 2013; Mandal, 2007). However, it is essential to acknowledge its limitations, such as its lower sensitivity compared to the PRESS technique (Mandal, 2007). Despite these constraints, the judicious application of the STEAM technique provided a robust foundation for this study. Its utilization not only drew valuable findings for previous published studies on alterations in brain region metabolites, but also serves as a reference model for current and future investigations in this domain.

2.10 RESEARCH GAPS

When this study commenced, it was evident that only a limited number of investigations had addressed metabolite variations within the LGN, and merely a handful had extended their view to the VC, each employing distinct methodological parameters and yielding divergent outcomes, such as the variability of NAA findings as that critically acknowledged in section 2.8. Given the complex nature of glaucoma as a pathophysiological entity, these preliminary studies represent an initial step towards resolving its metabolic foundation via MRS. The complexity of the condition originates from its multifactorial etiology, encompassing not only elevated intraocular pressure but also intricate vascular, inflammatory, and neurodegenerative components. This intricate relationship makes it difficult to delineate the precise metabolic changes associated with the disease. This further emphasizes the need for larger cohort studies, possibly investigating temporal changes in glaucoma progression, to potentially contribute to more the conclusive findings.

Consequently, there is a compelling need for a more nuanced investigation. This requires a comprehensive evaluation of metabolite concentration changes, the intentional manipulation of parameters, and the inclusion of subjects with a range of glaucoma severity. Such a stratified approach has the potential to yield a more nuanced understanding of the metabolic signatures that correspond to the various stages of the disease, which could provide crucial insights for the development of targeted therapeutic interventions. Given the uncertain future within this methodological framework, it is evident that additional research is necessary and holds great promise for shedding light on previously obscure aspects of glaucoma's metabolic foundations. Moreover, given the increasing global prevalence of glaucoma and its potential for further expansion, a thorough investigation of its metabolic profile is of heightened importance. This research project not only marks an important advance in our understanding of glaucoma but also opens up fresh opportunities for the creation of diagnostic and therapeutic modalities that will improve patient care and outcomes over the long term.

2.11 CHAPTER SUMMARY

This chapter has reviewed on study of metabolites, the potential of the study of metabolite interaction in glaucoma studies, the modality and method that can be used for studying metabolite interaction in brain structures of people with glaucoma. It is concluded that SVS with STEAM technique through MRS method using MRI can be the best approach for the evaluation of metabolite changes in brain structures associated with visual pathway in people with glaucoma.

CHAPTER THREE

GENERAL METHODOLOGY

3.1 INTRODUCTION

This section outlines the methodology used in this study in detail.

3.2 RESEARCH METHOD FRAMEWORK

Every experiment in this current study used a cross-sectional study design. Generally, the study recruited four distinct groups to achieve all the outlined objectives. The groups include young healthy adults group, elderly healthy adults group, mild glaucoma group, and severe glaucoma group. The healthy elderly groups possessed a similar age to those subjects in the glaucoma groups. It should be noted that gender-matched criteria were not considered in this study following the findings in the literature (Grachev & Apkarian, 2000; Raininko & Mattsson, 2010) that reported no significant metabolites differences between sexes in various brain regions, with the exception in the orbitofrontal cortex and sensorimotor cortex. The primary focus of our investigation lies in examining metabolic trends across the LGN and VC, which do not encompass the areas of the orbitofrontal cortex and sensorimotor cortex. Therefore, it was deemed prudent to rationalize our analytical approach. It is crucial to acknowledge that while gender is undoubtedly a crucial variable in numerous biomedical investigations, its specific relevance to the metabolic trends examined in this study, as substantiated by the existing literature, led us to the conclusion that it was not a primary factor warranting consideration.

This data collection in the current study was conducted in two phases. The first phase comprised of subjects' recruitment and eye screening. In this initial phase, recruitment was conducted through various advertisements strategies, including the WhatsApp messenger and invitation calls. These methods especially were used in recruiting young healthy adults, mainly among the students in the International Islamic University Malaysia Kuantan Campus (IIUM), where they were then brought for measurement in Sungai Buloh. The elderly healthy subjects on the other hand were recruited from Kuala Lumpur and Selangor using the similar advertisement approach. Participants with glaucoma were recruited from the patients who attended the Ophthalmology Clinic in the Universiti Teknologi MARA (UiTM) Specialist Hospital Sungai Buloh. Following recruitment, subjects' eye conditions and medical histories were screened and evaluated. Eye screening was conducted at the Ophthalmology Department of the UiTM Specialist Hospital Sungai Buloh. All subjects were deemed acceptable following a list of inclusion and exclusion criteria which will be elaborated in the following section.

The second phase of the study involved acquisition and analysis of the magnetic resonance spectroscopy (MRS) spectrum data. In the second phase, all subjects who underwent eye screening and medical history evaluation undergone a MRI scan for the MRS acquisition. The MRS acquisitions for all subjects were performed at the radiology department of the same hospital. After the MRS acquisition, raw spectra obtained from the MRS were processed using the jMRUI software (version 6.0 beta)(Stefan et al., 2009) for metabolite quantification. The metabolite concentration values are in arbitrary units. The metabolite concentration values were then analysed using IBM SPSS software version 23 (SPSS Inc., Chicago, IL, USA). Figure 3.1 depicts the framework of the research method framework.

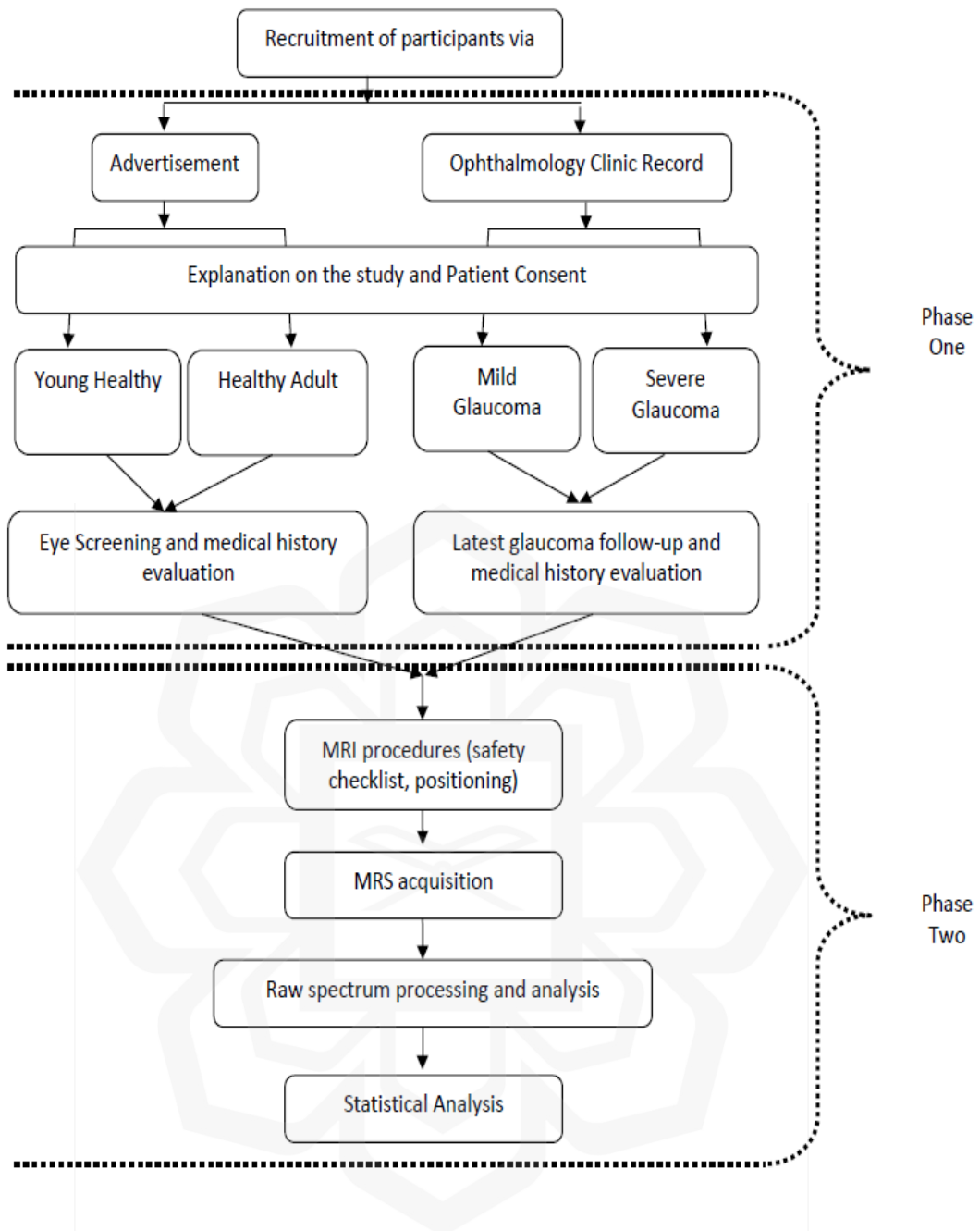


Figure 3.1 The research method framework.

3.3 ETHICS AND CONSENT FORM

The study protocol with reference code 600-IRMI (5/1/6) was reviewed and approved by the UiTM Research Ethics Committee in accordance with the International Council for Harmonisation of Technical Requirements for Pharmaceuticals for Human Use (ICH) Good Clinical Practice Guidelines, Malaysia's Good Clinical Practice Guidelines, and Declaration of Helsinki (Appendix E).

All subjects were ensured to fulfil the inclusion criteria. Participants were also informed of the study's protocols and procedures, benefits, safety measures, and possible risks. Participants were recruited on a voluntary basis only after they grasped the information provided. Following their agreement to participate in the study and prior to MRI acquisition, the participant was given a consent form to complete and sign. The subject information details (Appendix B) together with consent form (Appendix C) are attached in this thesis.

3.4 STUDY GROUP CATEGORY CRITERIA

Several criteria for inclusion, exclusion, and diagnosis were determined based on previous studies (Aksoy et al., 2018; Doganay et al., 2012; Sidek et al., 2016). These criteria were necessary to ensure that the sampling was of high quality. Participants were eligible to participate if they met the following inclusion criteria: no history of brain trauma, neurological diseases, schizophrenia, central nervous system infection, chronic metabolic disturbance, uncontrolled diabetes, and uncontrolled hypertension.

On the other hand, subjects who have any of the study's exclusion criteria were excluded to participate. The exclusion criteria were as follows: have presence of other retinal diseases besides glaucoma, having secondary glaucoma or history of central nervous system disorder, had previous ocular surgery, had laser therapy, have trauma history, having corneal and lens pathologies preventing ocular fundus examination, have uveitis and posterior segment pathologies, have uncontrolled systemic diseases such as diabetes and hypertension, on pregnancy, have claustrophobia, and have implanted electronic objects such as cardiac pacemakers, cochlear implants, or other ferromagnetic body implants.

Group-specific selection criteria were also applied. The histories and their most recent glaucoma follow-up reports received from the Ophthalmology Clinic of the UITM Specialist Hospital Sungai Buloh were evaluated. The Hodapp-Parrish-Anderson (Hodapp E, Parrish RK II, 1993) categorization method was used to divide the mild and severe glaucoma groups. Table 3.1 lists the group-specific characteristics that were considered.

Table 3.1 Specific criteria of each group

Group	Criteria
Healthy young	<ul style="list-style-type: none"> • Age of 19 to 20 years old • Intraocular pressure (IOP) of 21 mmHg or less • Normal visual field • Normal optic nerve head
Healthy elderly	<ul style="list-style-type: none"> • Over 40 years old • IOP of 21 mmHg or less • Normal visual field • Normal optic nerve head
Mild glaucoma	<ul style="list-style-type: none"> • Over 40 years old • Mean deviation score of Humphrey visual testing less than -6dB • loss of less than half of the visual field
Severe glaucoma	<ul style="list-style-type: none"> • Over 40 years old • Mean deviation score of Humphrey visual testing greater than -12dB • more than half of the visual field lost in either eye

3.5 EYE SCREENING

All healthy subjects underwent eye screening conducted by the same dedicated clinician consistently, prior to MRS acquisition. The screening comprehensively evaluated the IOP, the posterior segment of the eye, and the visual field.

The Goldman applanation tonometer was utilized to assess the IOP. For the healthy subjects, only those with IOP of less than 21mmHg were accepted into the study.

The posterior segment of the eye was examined using a digital retinal camera (model CR-2 AF, Canon Medical System Europe B.V.). The fundus camera allows examination of the retinal structures including the optic nerve head, and macula. Evaluation of the optic nerve head was especially important for glaucoma screening by scrutinizing of any glaucomatous cupping, neuroretinal rim appearance and retinal nerve fiber layer appearance. It should be noted that,

The frequency-doubling technology (FDT) perimeter was used to screen the visual field of the healthy subjects. Any abnormality indicated by FDT were assessed. The selected healthy subjects were considered into the study if their visual field is deemed normal by the test. To ensure that only healthy eyes were included in the healthy group, any eyes with a mean deviation (MD) score equal to or greater than -6.00 dB were considered ineligible for the study and were therefore removed from the list of eyes for MRS acquisition (Table 3.2). The Humphrey Visual Field Analyzer (HVFA) on the other hand was used to measure the visual field for subjects with glaucoma. The Hodapp-Parrish-Anderson (HPA) classification system was used to determine the severity of glaucoma (Table 3.2) and hence determined the grouping for the subjects. Upon ophthalmologist diagnosis, subjects with severe glaucoma were considered for subjects with MD score of greater than -12.00 dB, and mild glaucoma groups was when the MD was less than -6.00 dB.

Table 3.2 Hodapp-Parrish-Anderson (HPA) classification system

Stage	Humphrey MD score	Additional Criteria at least 1 of the listed criteria must apply)
Stage 0: No or Minimal Defect		
Stage 1: Early Defect	≥ -6.00 dB	- a cluster of ≥ 3 points on the pattern deviation plot in an expected location of the visual field depressed below the 5% level, at least one of which is depressed below the 1% level - CPSD/PSD significant at P<00.5 - GHT Outside Normal Limits™
Stage 2: Moderate Defect	≥ -6.00 to -12.00 dB	- ≥ 25% but <50% of points on the pattern deviation plot depressed below the 5% level, and ≥15% but <25% of points depressed below the 1% level - at least 1 point within the central 5° with sensitivity of <15 dB but no points in the central 5° with sensitivity of <0 dB - only 1 hemifield containing a point with sensitivity <15 dB within 5° of fixation
Stage 3: Advanced Defect	≥ -12.01 to -20.00 dB	- ≥ 50% but <75% of points on pattern deviation plot depressed below the 5% level and ≥25% but <50% of points depressed below the 1% level - any point within the central 5° with sensitivity <0 dB - both hemifields containing a point(s) with sensitivity <15 dB within 5° of fixation
Stage 4: Severe Defect	≥ -20.00 dB	- ≥ 75% of points on pattern deviation plot depressed below the 5% level and ≥50% but <50% of points depressed below the 1% level - at least 50% of points within the central 5° with sensitivity <0 dB - both hemifields containing >50% of points with sensitivity <15 dB within 5° of fixation
Stage 5: End-Stage Disease		Unable to perform HVFA in worst eye due to central scotoma or worst eye VA 6/60 or worse due to POAG. Fellow eye may be at any stage

MD: mean deviation; CPSD: Corrected pattern standard deviation; PSD: Pattern standard deviation; GHT: Glaucoma hemifield test; dB: decibel; POAG: primary open angle glaucoma; VA: visual acuity.

Note. Retrieved from. Clinical decisions in glaucoma, pp. 52–61 by Hodapp E, Parrish RK II, Anderson DR, 1993, St Louis: The CV Mosby Co.

3.6 SAMPLE SIZE

The sample size was calculated based on spectrums using data from (Doganyay et al., 2012). The choice to use spectra as the sample unit, rather than the number of subjects, stems from the nature of the data collection process. Given that multiple spectra were acquired from each individual subject, this approach allows for a more detail examination of metabolite variations within the constraints of available resources. The number of spectrum was calculated using the mean and standard deviation of the Glx/Cr ratio in the LGN from the glaucoma group (1.29 ± 1.21) and the healthy group (0.38 ± 0.35). The sample size calculation was performed using the Power and Sample Size Calculation software (version 3.9.1.4)(Faul, Erdfelder, Lang, & Buchner, 2007). The comprehensive breakdown of the calculations is attached in Appendix F.

From the calculation, the study required a sample size of ten ($n=10$) spectrums for each group (i.e., a total sample size of 20, assuming equal group sizes) to achieve a power of 80% and a level of significance of 5% (one-sided) to detect a true difference in means between the test (glaucoma) and the reference (healthy) groups. The number of spectrums that were successfully obtained and available for analysis in this study from healthy young adults was $n=26$, from healthy adults of similar age ($n = 17$), from those with mild glaucoma ($n = 14$), and from those with severe glaucoma ($n = 6$).

It is preferable to have an equally divided sample size between groups to ensure the highest statistical power in a study (Karen Grace-Martin, 2020). Nevertheless, the number of metabolites obtained in each group in this study showed an unequal sample size. Moreover, the severe glaucoma group sample size in this study did not meet the minimum required sample size. However, the unequal and the small sample size in the glaucoma group was deemed acceptable for analysis considering it was challenging and difficult to achieve a larger number, sufficient sample size and match the sample size. The rarity and severity of glaucoma cases, compounded by the stringent ethical considerations surrounding patient recruitment, significantly limited the available pool of subjects (Lakens, 2022). Consequently, despite the uneven distribution of spectra across groups, the small sample size in the glaucoma group was considered acceptable for analysis.

It's important to emphasize that this study battled the inherent challenges associated with the disease's prevalence and the availability of eligible subjects. While the sample size may be smaller than ideal, it is crucial to acknowledge that it reflects the contextual realities of conducting clinical research. Moreover, methodological detail, careful data analysis, and the adherence to ethical guidelines were maintained throughout the study to mitigate potential biases. Given these constraints, the inclusion of the available six spectra for severe glaucoma was a deliberate decision made to derive valuable insights within the limits of feasibility. This approach allows for an exploratory examination of metabolite variations in this subgroup, providing a foundation for future studies to build upon. It is essential to recognize that while the sample size may be modest, the findings may contribute to the evolving body of knowledge in this critical area of research.

3.7 MAGNETIC RESONANCE IMAGING (MRI) PROCEDURES

The following MRI procedures applies to every experiment carried out in this study. All subjects must complete the MRI safety checklist (Appendix D). All subjects were scanned using a 1.5 Tesla MRI scanner (Siemens Magnetom Aera 1.5T) with a magnet bore size of 70 cm. Prior to entering the MRI suite, the subjects were asked to remove all ferromagnetic materials from their bodies and provide an MRI technologist with their height and body weight. The height and weight of the subjects were required to allow the MRI pulse sequence to adhere to the specific absorption rate (SAR) limitation. The SAR, measured in watts per kilogram (W/kg), is the rate at which electromagnetic energy from the radio frequency pulse is absorbed by body tissues during the MRI scan (Murphy & Chang, 2019). The International Electrotechnical Commission and the Food and Drug Administration (in the United States) specifies that the electromagnetic energy absorbed by the head during a single examination must be less than 3.2 W/kg and that any pulse sequence must not cause a temperature rise of more than 1° C (Joseph P. Hornak, 2020). The SAR estimate is displayed on the scanner console prior to initiating any scanning to allow the MRI technologist to manage any SAR reduction approaches if needed. It is important to note here that in this study, SAR data and temperature rise were not collected, however, comprehensive steps which includes protocol adherence and real-time monitoring were implemented to ensure that both SAR levels and temperature rise remained well within established safety limits.

Participants were instructed to lie head-first on the MRI examination table. To make the subjects comfortable, a blanket was given to protect their bodies from the extreme cold in the MRI suite. In addition, a headphone was also provided to the subjects to protect their ears from loud noise. In addition, the subjects were given an emergency push button to alert the MRI technologist outside in the event of an emergency, such as shortness of breath. Each participant was assured of the MRI staff's concern for comfort and safety. A head coil with 20 receiver channels was then set around the participant's head. The subjects were also cautioned against moving their heads or eyeballs, as this could result in unwanted spectrum results that could compromise the quality of the spectrum produced for spectrum processing. The MRI examination table is positioned within the gantry of the scanner.

3.8 MAGNETIC RESONANCE SPECTROSCOPY (MRS) ACQUISITION

The following MRS acquisition procedures applies uniformly to every experiment conducted in this study. The MRS protocol started with the key-in of the subjects' details in the MRI control panel system. An automated positioning and alignment of slices using the anatomical landmark (AAHScout) sequence was used. This AAHScout sequence automatically generated three dimensional T1 weighted (3DT1W) images in a three-plane localizer display loaded into three windows to facilitate slice prescription. The parameters of this protocol were: TR = 4.52 ms, TE = 2.38 ms, field of view (FOV) = 260 mm x 260 mm, matrix = 160x160, slice thickness = 1.6 mm, flip angle (FA) = 8°, number of excitation (NEX) = 1 with slice overlap = 0. The images produced by this sequence served as anatomical references for the placement of the voxels in the region to be studied, which were performed during the spectroscopy sequence.

In this study, the SVS with stimulated echo acquisition mode (STEAM) technique was utilized as the MRS method. Because the installed spectroscopy technique in the MRI suite of the Radiology Department was the only SVS technique, it is important to note that only the SVS technique was used in this study and no MVS study was conducted. The parameters in the sequence were as follows: TR = 1500 ms, TE = 30 ms, voxel of interest (VOI) size = 13 mm × 13 mm × 13 mm, and slice thickness = 13 mm. The VOI placement was confirmed based on the axial, coronal, and sagittal anatomical 3DT1W images produced in the previous sequence. The VOI placement for the LGN was at the rear end of the thalamus (Figure 3.2), while the VOI placement for the VC was placed as close as possible to the posterior position of the VC, and each case was standardized along the calcarine sulcus, towards the midline of the brain (Figure 3.3). Any contact of the VOI placement with the bone, subcutaneous fat, vasculature, or any other tissue was also avoided. It is important to note here that, the steps taken for VOI placement were based on study by (Aksoy et al., 2018; Doganay et al., 2012) for reference as well as recommendations from publication by (Lin et al., 2021). It is also important to note that throughout the study, the VOI placement was consistently performed by a single dedicated radiographer with extensive expertise in neuroimaging techniques.

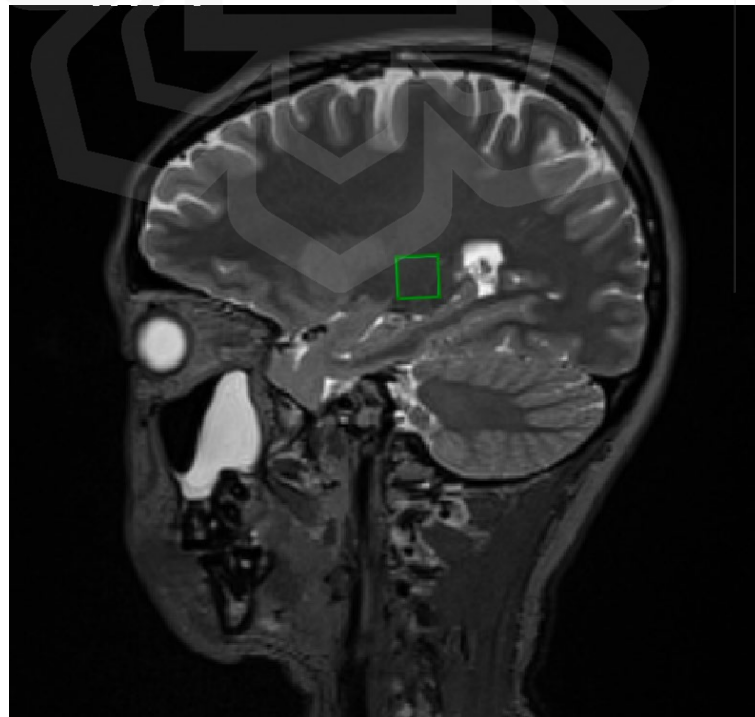


Figure 3.2 The VOI for LGN was placed at the rear end of the thalamus.

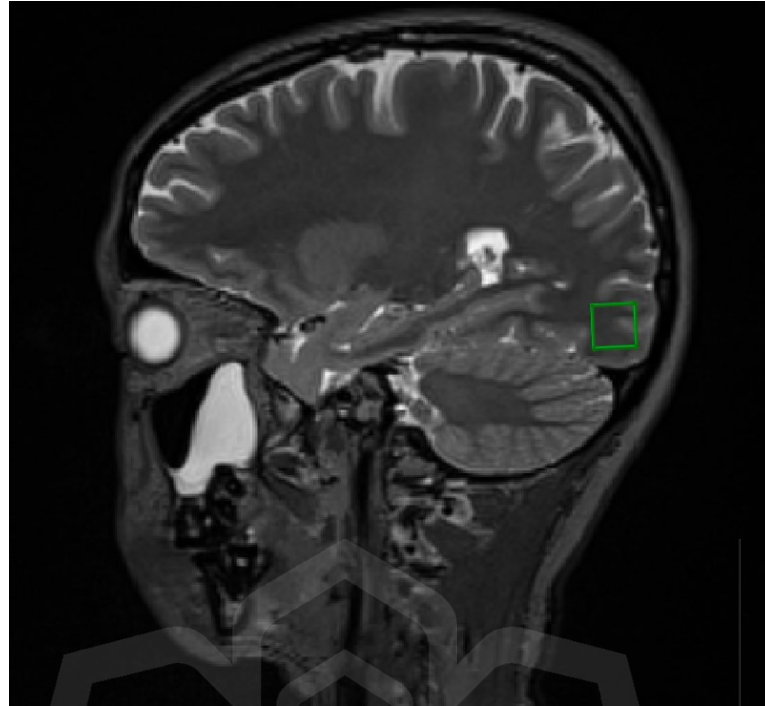


Figure 3.3 The VOI for VC was placed as close as possible to the posterior position of the VC.

Prior to the STEAM sequence, after proper placement of the VOI, shimming and water suppression were performed using an automated manufacturer's protocol. These two automated protocols were executed to guarantee that no field distortion occurred, to prevent the generation of spectral inhomogeneity, and to obtain an optimal metabolite signal that does not originate from protons in water (Aksoy et al., 2018; Brief, 2000; Doganay et al., 2012; Sidek et al., 2016).

3.9 MRS ANALYSIS

The jMRUI processing software was selected for each experiment's MRS analysis in this study. Compared to other software such as the LCModel software, jMRUI requires user interaction for data analysis in the time domain. jMRUI divides MRS data analysis into two stages, namely the pre-processing stage and analysis and quantification stage (Near et al., 2021).

As MRS acquisition generated spectra in this study, a radiologist visually examined each spectrum displayed on the MRI console. Any spectrum passed by the radiologist was regarded as raw spectral data and underwent MRS data analysis. The raw spectra from the MRS were then pre-processed to eliminate residual water signals in the spectrum and visually inspected a second time before spectral analysis and quantification. Subsequently, the chosen spectra were analysed using the Advanced Method for Accurate, Robust, and Efficient Spectral (AMARES) algorithm in the jMRUI software to provide a more unambiguous interpretation which is less prone to error (Jansen et al., 2006).

3.9.1 Spectral Data Pre-Processing

MRS data must be pre-processed to eliminate certain imperfections to the MRS data that could be due to receiver imperfection, physiologic motion, fast decaying signal, overlapping signals, truncation of data and presence of residual water peaks (Mandal, 2012). Before pre-processing, the raw spectroscopy data obtained from the MRI scanning system were stored on an external storage device and exported as IMA files to a personal computer. The raw data was then transferred into the jMRUI software for pre-processing. The pre-processing started with mounting the data into the jMRUI SpectrIm (a combined analysis of magnetic resonance spectroscopy and imaging) plugin. Conventionally, preprocessing involved noise filtering, residual water removal, peak extraction, and phase correction (Mandal, 2012). The steps were conducted manually based on the knowledge of the individual performing the process (Mandal, 2012; Pedrosa de Barros, McKinley, Knecht, Wiest, & Slotboom, 2016). This process is not only time-consuming but also has the potential to introduce variation between processes (Pedrosa de Barros et al., 2016).

In this study, however, the jMRUI SpectrIm plugin enables MR spectroscopy imaging data to automatically exclude residual water and set the spectrum phase directly. The evaluation of the spectral quality of raw spectroscopy could therefore be performed immediately prior to the analysis of the spectrum. At this stage, a spectrum is deemed suitable and would be selected for quantification if it has the desired shape of a narrow and upright spectral peak(Kreis, 2004). All pre-processed spectrum containing peaks with an abnormal phase or unusual line shape in this study was deemed unsuitable and would not be selected for quantification (Kreis, 2004). An example of a suitable and unsuitable spectrum is shown in Figure 3.4 and Figure 3.5.

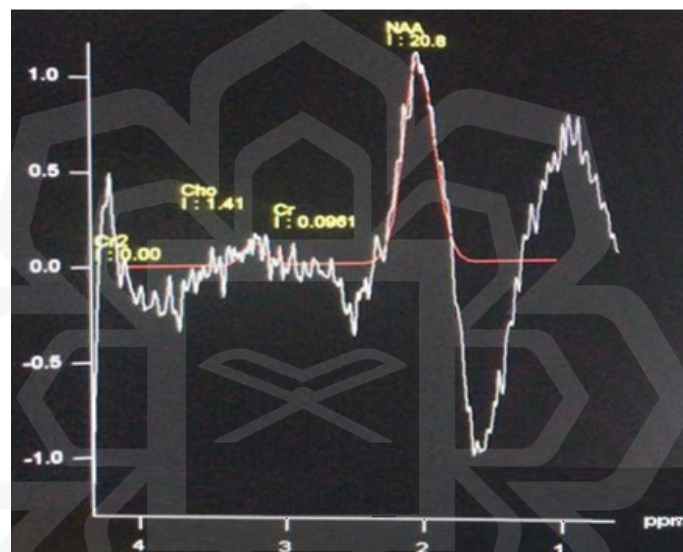


Figure 3.4 Example of unacceptable spectrum due to the undesirably biphasic waveform shown between 1.0 ppm and 2.0 ppm.

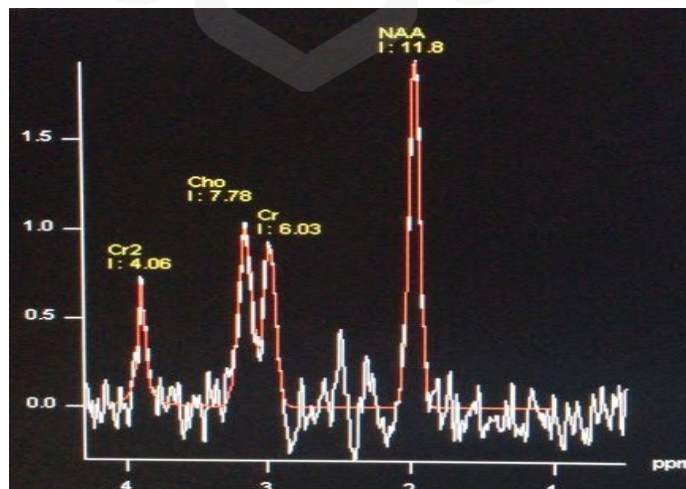


Figure 3.5 Example of acceptable narrow and upright spectrum.

3.9.2 Spectral Analysis and Quantification

Following the automatic process of the spectral pre-processing, the AMARES algorithm was used to quantify the selected quality spectra. The quantification started with the identification of metabolites, including the NAA, Glx, Cr, Cho, and MI, to fit the metabolite contribution in the water-suppressed spectrum. The top of each metabolite peak and line width (width of spectral line at half of the top height) were defined at the start of the quantification step (Graveron-demilly, 2016). In this study, all analyses peaks (NAA, Glx, Cr, Cho, and ml) positions were set at 2.05 ppm and 0.5 line width, 2.23 ppm and 0.5 line width, 3.05 ppm and 0.5 line width, 3.24 ppm and 0.5 line width and 3.58 ppm and 0.5 line width, respectively. The precise adjustment of peak positions at specified ppm values, along with setting the line width, was crucial for ensuring accurate spectral fitting (Ernst & Linda, 2006; Stefan et al., 2009). These steps guided the processing software in using the most appropriate basis set and fitting algorithm that align with the expected spectral pattern (Ernst & Linda, 2006; Stefan et al., 2009). Figure 3.6 shows the identification that was performed during the starting of the spectral analysis process.

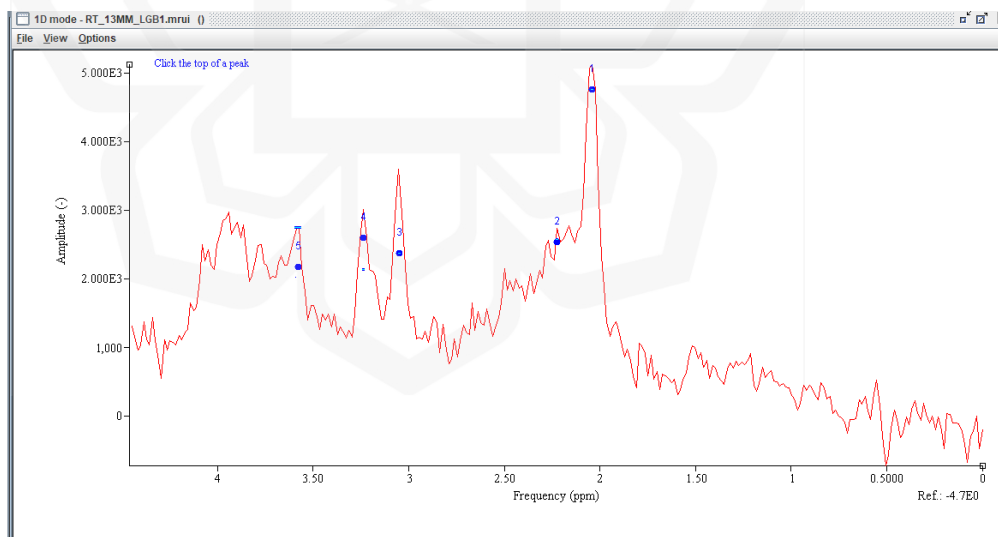


Figure 3.6 Identification of the top and line widths of a metabolite.

After identifying the metabolites and their values, the next step was to incorporate prior knowledge into the process to improve quantification (Graveron-demilly, 2016). Prior knowledge incorporated in this study defines the soft constraints of the selected metabolites, as shown in Figure 3.7. The respective peaks of the five metabolites were set with soft constraints at 2.02-2.04 ppm, 2.1-2.5 ppm, 3.02-3.08 ppm, 3.2-3.3 ppm and 3.5-3.65 ppm as shown in Figure 3.7. This step is required to account for the possibility of overlapping metabolite signals in quantitative analysis, as a combined or overlapping metabolite signal could result in unreliable quantification (Cudalbu, Cristina Ramona; Lanz, B.; Duarte, J. M.; Kunz, N.; Gruetter, 2011). This objective automated software analysis obviated the need for inter-observer comparisons. There are other parameters of metabolite peaks that can be imposed in prior knowledge, such as the line width and phase of the metabolite, as shown in Figure 3.7. However, for simplicity, the other parameters were left at their default values, as this step is optional and only recommended when the relationship between spectral parameters is known (Graveron-demilly, 2016).

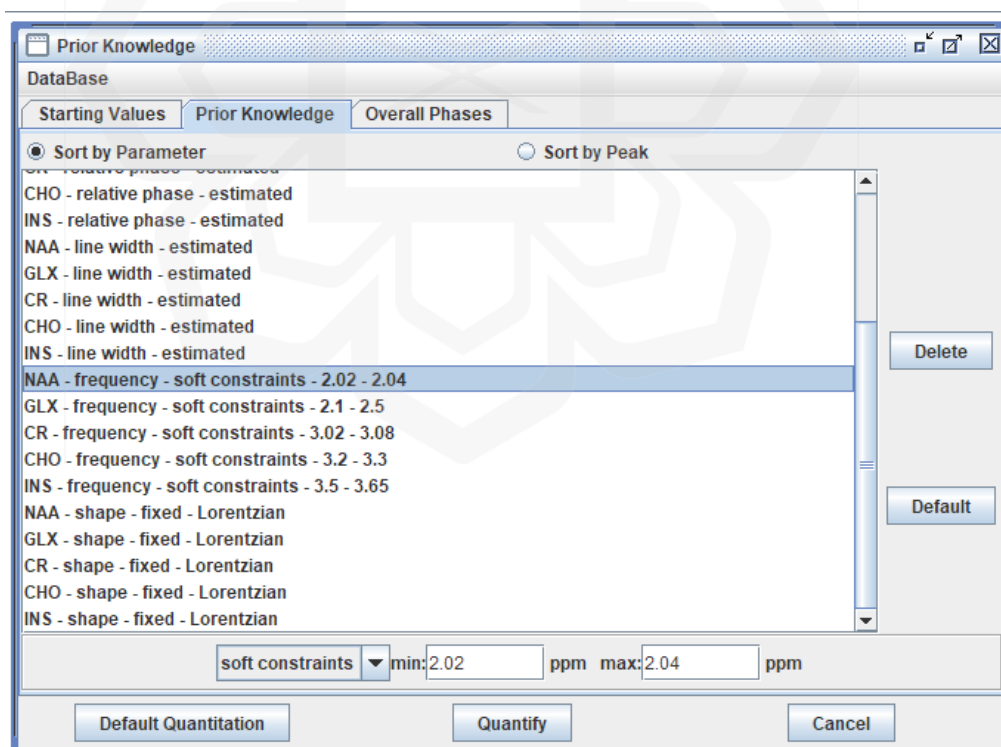


Figure 3.7 Soft constrains for each metabolite.

Phase definition is the third step prior to launching quantification (Graveron-demilly, 2016). This step is also optional; therefore, the 'Overall Phases' tab in the AMARES window (Figure 3.7) was left at its default value. The final step was to press the "Quantify" button to initiate calculation. The calculation then yielded the amplitude of each metabolite, which was defined in the first step of this quantification procedure.

In this study, based on the review of quantification approaches in Chapter Two, we decided to use the signal amplitude value, which is in the arbitrary unit generated by the AMARES for the statistical analysis. For statistical analysis, the amplitude values were also quantified further to obtain the metabolite ratio. The purpose of the statistical analysis based on metabolite ratio was to provide more opportunities for gaining additional insights regarding any changes in the balance of different metabolites (Kantarci et al., 2000). It is important to note that the amplitude was proportional to the concentration of the metabolite peaks; and therefore, the term 'concentration amplitude' of metabolite is used throughout experiment's chapters when discussing metabolite concentration. Metabolite concentration amplitudes were taken for use in statistical analysis.

3.10 PATIENT CARE

Patient care is an important part of health care that goes beyond undergoing medical procedures or treating symptoms. By putting patient care first, medical health practitioners can make sure that their patients feel valued, heard, and safe. Careful management of medications, medical advice, and assurance are important measures that can keep people from getting hurt and improve the quality of healthcare.

3.10.1 Eye Care

Since a dilation procedure was performed during the eye screening, it's crucial to take specific steps to care for the eyes. Firstly, protecting the eyes from the sun is essential. Dilation can lead to temporary blurry vision and increased sensitivity to light. Therefore, subjects were advised to wear sunglasses with full UV protection after the eye screening for several hours until their pupil come back normal again. This was to help prevent any eye discomfort or strain. Subjects were also advised to have someone else drive them home or to refrain from driving until their pupils returned to their normal size before driving themselves. This precaution ensures safety for both subjects and others on the road.

After the screening, subjects were also advised to give their eyes a break. They were encouraged to avoid prolonged screen time or tasks that require close focus. They should find a comfortable spot to relax, gently close their eyes, and allow them to recover. This simple step was recommended to enhance overall eye comfort and recovery. Lastly, subjects were reminded to observe anything unusual or experience significant pain, sudden vision changes, or prolonged discomfort after the screening. They should promptly contact an eye care professional, seeking advice or treatment when needed.

3.10.2 MRI Care

Throughout the MRI procedures, patient care was prioritized. As concurrently described in section 3.7, this involved paying close attention to their safety, comfort, and overall well-being. Strict protocols for aseptic techniques were also adhered to, ensuring all equipment was properly sterilized, and precautions were taken to confirm that everyone was free from ferromagnetic objects. This hands-on approach was pivotal in minimizing any potential infection risks and demonstrated a strong commitment to patient safety.

Additionally, clear, and easy-to-understand information about the MRI procedure was provided to subjects. This included explaining the purpose of the MRI, detailing the steps of the procedure, advising on preparations for the MRI, and giving subjects an idea of what to expect during and after the scan. This was complemented together with the completion of the MRI safety screening form, as illustrated in APPENDIX D. Such direct communication not only fostered a collaborative atmosphere but also empowered patients with a greater sense of control and confidence throughout the MRI procedures for the MRS acquisition.

3.11 STATISTICAL ANALYSIS

The data taken for analysis were the metabolite concentration in the context of its amplitude. All data in this study were analysed using IBM SPSS software version 23 (SPSS Inc., Chicago, IL, USA) licensed under the university.

3.11.1 Repeatability Test

Using a paired t-test, the variation between two consecutive measurements of the metabolite signal amplitude in the same young, healthy subjects under identical conditions and by the same examiner was analysed (Statistics, 2015). The normality of data was tested using the Shapiro-Wilk test. The data were considered to conform to the normality assumption if $p > 0.05$. The metabolite data that does not meet the normality assumption was analysed using Wilcoxon Signed-Rank Test. The Bland-Altman plot was also used to visually assess the repeatability of the two consecutive metabolite measurements using SVS technique. The repeatability coefficient (RC) and coefficient of variation (CV) were calculated.

3.11.2 Mean Metabolites Differences Test (Independent T-Test)

All data are presented as mean \pm SD. The normality of data was tested using the Shapiro-Wilk test. The data were considered to conform to the normality assumption if $p > 0.05$. Data homogeneity of variance was determined using Levene's test. All metabolite data that met the assumption of homogeneity of variances were compared (between young and elderly groups) using an independent sample t-test. However, the metabolite data that violated the homogeneity of variance assumption were interpreted using the Welch t-test. The mean metabolite amplitude was compared using the Mann-Whitney U test for data did not conform to the normality assumption. Statistical significance was set at $p \leq 0.05$.

3.11.3 Mean Metabolites Differences Test (One Way-ANOVA)

All data are presented as mean \pm SD. Normality of the data was tested using the Shapiro-Wilk test. The data were considered to conform to the normality assumption if $p > 0.05$. Data homogeneity of variance was determined using Levene's test. All metabolite data that met the assumption of homogeneity of variances were compared (healthy controls, mild glaucoma group and severe glaucoma group) using one-way Analysis of variance (ANOVA), whereas data with violated homogeneity of variance were compared using Welch ANOVA. Statistical significance was set at $p \leq 0.05$.

3.12 CHAPTER SUMMARY

This chapter elaborates on the methodology employed, from participant recruitment and data collection to spectroscopic data analysis. The sample size calculation was also explained. The specific methodologies pertaining to each objective is outlined in the subsequent chapters.

CHAPTER 4

REPEATABILITY OF METABOLITES MEASUREMENT IN LATERAL GENICULATE NUCLEUS AND VISUAL CORTEX USING MAGNETIC RESONANCE SPECTROSCOPY IN HEALTHY YOUNG ADULT

Abstract

Purpose

To assess the repeatability of measurement of N-Acetyl Aspartate (NAA), Creatine (Cr), Choline (Cho), Glutamate (Glx) and Myo-Inositol (mI) in the lateral geniculate nucleus (LGN) and visual cortex (VC) using proton magnetic resonance spectroscopy (MRS) among healthy subjects.

Materials and methods

Using 1.5 Tesla magnetic resonance imaging (MRI), two consecutive scans were performed on fifteen healthy young subjects (19.0 ± 0.2 years). On each occasion, the spectroscopy data were measured bilaterally in the LGN and VC using single voxel spectroscopy (SVS) technique. Using jMRUI (version 6.0 beta) Click or tap here to enter text. fitting software, the metabolites NAA, Glx, Cr, Cho, and mI were quantified as concentration amplitudes in arbitrary units for use in statistical analysis. The paired sample t-test, repeatability coefficient (RC), and coefficient of variation (CV) were utilised to evaluate the repeatability between the first and second consecutive measurements of metabolites. Normality of data were tested using the Shapiro-Wilk normality test. The Wilcoxon Signed-Rank test was used for data that did not conform to normality. The Bland-Altman plot was also conducted to visually assess the level of agreement between the two consecutive metabolite measurements.

Results

The NAA, Glx, Cr, Cho, and mI concentration values in the LGN and VC showed no significant differences ($p > 0.05$). The RC% ranges from 30.76% to 106.33% for all metabolites in the LGN and from 13.03% to 50.71% for all metabolites in the VC. The CV% ranges from 11.10% to 38.36% for all metabolites in the LGN and from 4.7% to 18.29% for metabolites in the VC. The Bland-Altman plots revealed small biases and narrow limits of agreement for NAA, Cr, and Cho in both the LGN and VC regions,

indicating good agreement and small variability between the consecutive measurements of these metabolites.

Conclusion

The MRS technique using the 1.5 tesla MRI is repeatable in determining the concentration of metabolites in the LGN and VC.

Keywords: proton magnetic resonance spectroscopy, repeatability, single voxel spectroscopy, N-Acetyl Aspartate, Creatine, Choline, Glutamate, Myo-Inositol



4.1 INTRODUCTION

MRI of the visual pathway and its related anatomy has become an important procedure that is utilized for diagnosis, follow-up, and treatment of many ocular diseases (H. D. H. Brown, Woodall, Kitching, Baseler, & Morland, 2016). The involved anatomy may include important brain structures, such as the LGN and VC, that are out of reach of the routine ophthalmological imaging tools such as the optical coherence tomography. Of late, there a few studies of the LGN and VC were conducted using the MRS, a subsidiary technique of the MRI.

MRS is a relatively new method for evaluating brain metabolite levels *in vivo*. MRS has increasingly gained attention and being used in research and clinical settings in investigating tissues various metabolites compounds (Barta et al., 2018; Boussida et al., 2022; Gujar et al., 2005; Haddadin et al., 2009; Maudsley et al., 2009). Albeit of a handful published studies on MRS, comparison and interpretation of findings of the literature is difficult as published studies may have different MRI protocols. There has yet a consensus on the metabolite's measurement unit. Most of the studies reported of their own unique measurement unit, or specifically termed as the 'institutional unit' (Schmitz et al., 2018). For instance, (Harris et al., 2009) reported their metabolite absolute concentration using the water signal normalization in arbitrary institutional unit while (Doganay et al., 2012) reported their metabolite concentration as integral value using the Cr signal normalization in arbitrary institutional unit. The variation of reported measurement units places a challenge to compare these studies. In addition, a different MRI machine may yield a different measurement outcome, albeit the used MRI machines may have the same brand but differs in their models and having different strengths and parameters. Given that each MRI machine uses a different set of proprietary algorithms for data acquisition, depiction, and quantification, it is becoming increasingly crucial to confirm that the MRS test procedures chosen are sufficiently reliable to be used in subsequent tests in this study.

The MRS also involves operator-dependent technicalities. The location of the region of interest (ROI) on the selected anatomy for metabolites measurement is conducted subjectively. This operator-dependent bias, need the operator to determine the ROI, and the placement of ROI may place a challenge with underlying biological variation (Bunting et al., 2019). Therefore, in this respect, MRS metabolite measurements may be prone to variable repeatability, dependent to the operator (Bunting et al., 2019).

Given that each researcher's machine or environment uses a different set of proprietary algorithms for data acquisition, depiction, and quantification, it is becoming crucial to confirm that the test procedures chosen are reliable enough to be used in subsequent tests in this study.

Variations in measurements can be attributed to measurement accuracy, with a smaller variation indicating a more reliable result (Bunting et al., 2019). Repeatability of measurement refers to the variation in repeated measurements taken on a same subject under identical conditions (Bartlett & Frost, 2008). In this chapter, the repeatability of the MRS in measuring the metabolites concentration in the LGN and VC was examined.

4.2 SPECIFIC METHODOLOGY

4.2.1 Subjects

The subjects were recruited among the first-year Medical Imaging students (19.0 ± 0.2 years) from the International Islamic University Malaysia (Kuantan Campus) using convenience sampling. All 15 subjects were ensured to be in good health and were able to follow safety procedures for the MRI scan procedures.

4.2.2 MRS Acquisition

Two consecutive MRS scans using the Single-Voxel Spectroscopy (SVS) technique were performed on both sides of the LGN and VC at a magnetic field strength of 1.5 Tesla. The SVS with stimulated echo acquisition mode (STEAM) technique as outlined in chapter three was performed on four locations: in the right and left regions of the LGN, located at the rear end of the thalamus, and in the right and left regions of the VC along the calcarine sulcus as close as possible to the posterior position. Each participant underwent two repeated spectroscopic measurements of the bilateral LGN and VC. The total spectroscopy examinations performed and accepted for raw spectral review were 60 for LGN and 60 for VC from the 15 young healthy adults.

4.2.3 MRS Analysis

Following the spectral review after removal of residual water, 52 out of 60 raw spectra in LGN and 52 out of 60 raw spectra in VC demonstrated a good and acceptable spectroscopic curve (Table 4.1).

Table 4.1 The raw spectrum scan number from healthy young group for analysis after the spectral evaluation

<i>Both right and left sides</i>	Young (n = 15)	Eliminated spectrum	Total spectrum evaluated
LGN spectrums	30	4	26
VC spectrums	30	4	26
Total	60	8	52

4.2.4 Statistical Analysis

Descriptive data are presented as mean \pm standard deviation (SD). All data were analyzed using the IBM SPSS software version 23.0 (SPSS Inc., Chicago, IL, USA) licensed under the International Islamic University Malaysia. Normality of data were analysed using the Shapiro-Wilk test, and data with a p value of more than 0.05 is considered as normally distributed. Using a paired t-test, the variation between repeated measurements of the metabolite signal amplitude in the same young, healthy subjects under identical conditions and by the same examiner was analysed (Statistics, 2015). The metabolite data that does not meet the normality assumption was analysed using Wilcoxon Signed-Rank Test. Statistical significance was set at $p < 0.05$.

The Bland-Altman plot was also conducted to visually assess the level of agreement between the two consecutive metabolite measurements. The RC and CV values were calculated to verify the accuracy of the repeatability study. RC (in concentration amplitude arbitrary unit) was calculated as below, where WSD is the within-subject standard deviation (Ross et al., 2023).

Equation 4.1 Repeatability coefficient (RC)

$$RC = \sqrt{2} \times 1.96 \times WSD \text{ (in arbitrary unit)}$$

WSD was calculated as following below, where WMS is the within mean square (Lexell & Downham, 2005).

Equation 4.2 Within standard deviation (WSD)

$$WSD = \sqrt{WMS}$$

For comparison with other published studies, the RC% and CV % were then calculated. The RC% was calculated by dividing the RC by the mean of the two sets of metabolite measurements, and then multiplying the result by 100 to obtain a percentage value (Lexell & Downham, 2005), the equation is as below.

Equation 4.3 Repeatability Coefficient percentage (RC%)

$$RC\% = \frac{RC}{MEAN(overall)} \times 100$$

The CV% was calculated by dividing the WSD by the mean of the two sets of metabolite measurements, and then multiplying the result by 100 to obtain a percentage value (Lexell & Downham, 2005), the equation is as below.

Equation 4.4 Coefficient Variation percentage (CV%)

$$CV\% = \frac{WSD}{MEAN(overall)} \times 100$$



4.3 RESULTS

Paired t-test revealed that there is no statistically significant mean difference between the metabolite concentration amplitude for NAA ($p=0.812$), Glx ($p=0.056$), Cr($p=0.399$) and Cho ($p=0.530$) when two consecutive measurements for each metabolite were conducted (Table 4.2). Wilcoxon Signed-Rank Test revealed that there is no statistically significant mean difference between the metabolite concentration amplitude for mI ($p=0.694$) at the two consecutive measurements (Table 4.2).

Table 4.2 Mean \pm SD metabolite concentration amplitude of the quantified metabolites in the LGN.

Metabolites (n=26)	LGN (Mean \pm SD)		p
	Session 1	Session 2	
Paired t-test			
NAA	61.41 \pm 6.44	60.95 \pm 8.82	0.812
Glx	340.54 \pm 142.69	416.88 \pm 150.86	0.056
Cr	30.97 \pm 7.97	32.14 \pm 7.95	0.399
Cho	18.10 \pm 6.45	18.84 \pm 5.19	0.530
Wilcoxon Signed-Rank Test			
mI ^a	448.22 \pm 178.83	419.00 \pm 181.13	0.694

^aThe Wilcoxon Signed-Rank Test was used to assess the mean difference as Shapiro-Wilk test indicated that the normality assumption was not met for this variable.

Paired t-test revealed that there is no statistically significant mean difference between the metabolite concentration amplitude for NAA ($p=0.428$), Glx ($p=0.940$), Cho ($p=0.421$) and mI ($p=0.851$) when two consecutive measurements for each metabolite were conducted (Table 4.3). Wilcoxon Signed-Rank Test revealed that there is no statistically significant mean difference between the metabolite concentration amplitude for Cr($p=0.238$) at the two consecutive measurements (Table 4.3).

Table 4.3 Mean \pm SD metabolite concentration amplitude of the quantified metabolites in the VC.

Metabolites (n=26)	VC (Mean \pm SD)		p
	Session 1	Session 2	
Paired t-test			
NAA	58.23 \pm 6.44	57.62 \pm 6.08	0.428
Glx	723.51 \pm 235.37	724.67 \pm 234.24	0.940
Cho	13.76 \pm 1.71	13.27 \pm 2.28	0.421
mI	240.40 \pm 59.32	238.05 \pm 56.17	0.851
Wilcoxon Signed-Rank Test			
Cr ^a	40.80 \pm 5.53	40.58 \pm 4.94	0.238

^aThe Wilcoxon Signed-Rank Test was used to assess the mean difference as Shapiro-Wilk test indicated that the normality assumption was not met for this variable.

In the LGN, the mean difference, or bias, in Glx, Cr, and Cho was positive, with values of 76.34, 1.17, and 0.75, respectively (Table 4.4). On the other hand, the bias for NAA and mI was negative, with values of -0.46 and -29.21, respectively (Table 4.4). The negative bias values for NAA and mI suggest a tendency for lower metabolite concentration in the second measurement. Among all the metabolites, NAA had the smallest bias value of -0.46, indicating that the two consecutive measurements were essentially equivalent. Cho and Cr had bias values of 0.75 and 1.17, respectively, suggesting a small difference between the measurements. Glx had the largest bias value of 76.34, while mI had a negative bias value of -29.21, indicating a larger difference between the consecutive measurements for these metabolites.

Moreover, the narrow limits of agreement (LOA) for NAA (-19.63 to 18.71), Cho (-10.99 to 12.49), and Cr (-12.42 to 14.76) indicate that the measurement variability was minimal, suggesting good agreement between the consecutive measurements for these metabolites (Table 4.4). In contrast, the wider LOA for Glx (-304.93 to 457.61) and mI (-452.16 to 393.73) suggest that the measurement variability for Glx and mI is larger, indicating less agreement between the consecutive measurements (Table 4.4).

Table 4.4 The Bland-Altman bias and limit of agreement in LGN.

Metabolites (n=26)	Bias	95% LOA (95% CI) LB	95% LOA (95% CI) UB
NAA	-0.46	-19.63 (-26.47 to -12.79)	18.71 (11.87 to 25.55)
Glx	76.34	-304.93 (-440.96 to -168.89)	457.61 (321.57 to 593.64)
Cr	1.17	-12.42 (-17.27 to -7.57)	14.76 (9.91 to 19.60)
Cho	0.75	-10.99 (-15.18 to -6.80)	12.49 (8.30 to 16.68)
mI	-29.21	-452.16 (-603.82 to 544.63)	393.73 (242.82 to 544.63)

The Bland-Altman plots are shown below for each pair of metabolites in the (Figure 4.1 to Figure 4.5). Most data points lie within the upper limit of agreement (LOA) and lower LOA for each metabolite.

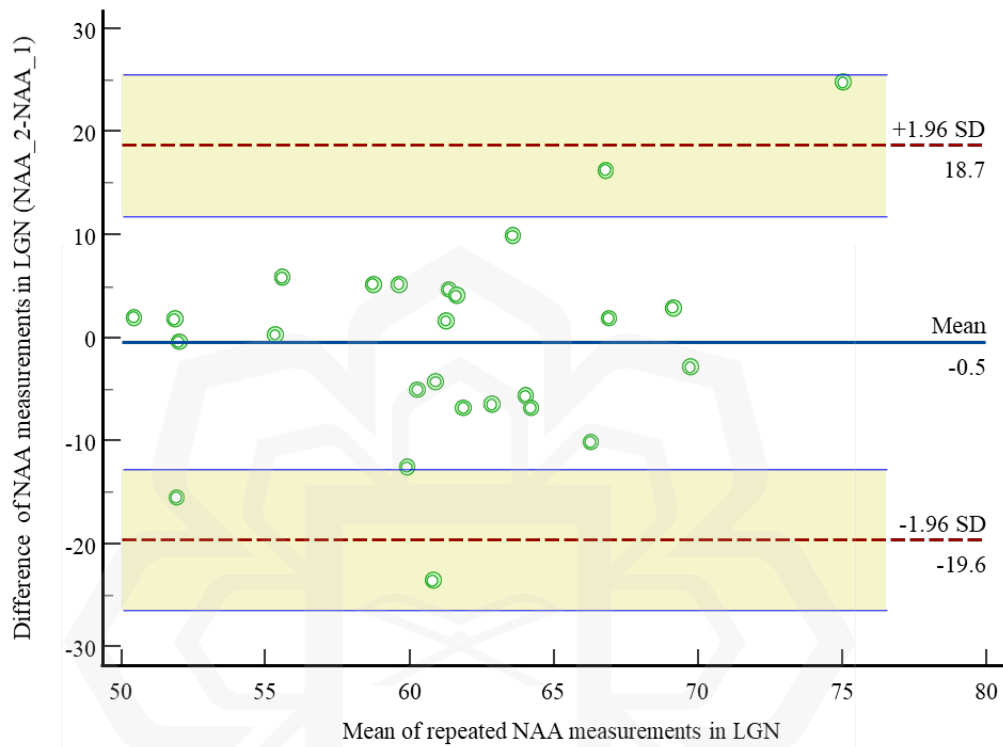


Figure 4.1 Bland and Altman difference plots using NAA concentration amplitude in the LGN in the first and second sessions of the MRS technique.

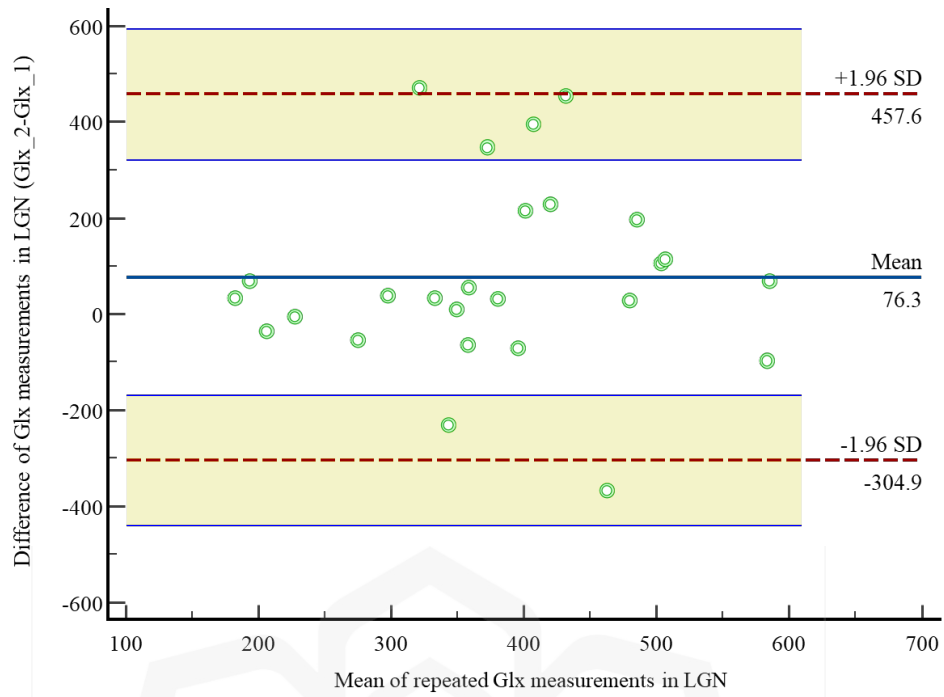


Figure 4.2 Bland and Altman difference plots using Glx concentration amplitude in the LGN in the first and second sessions of the MRS technique.

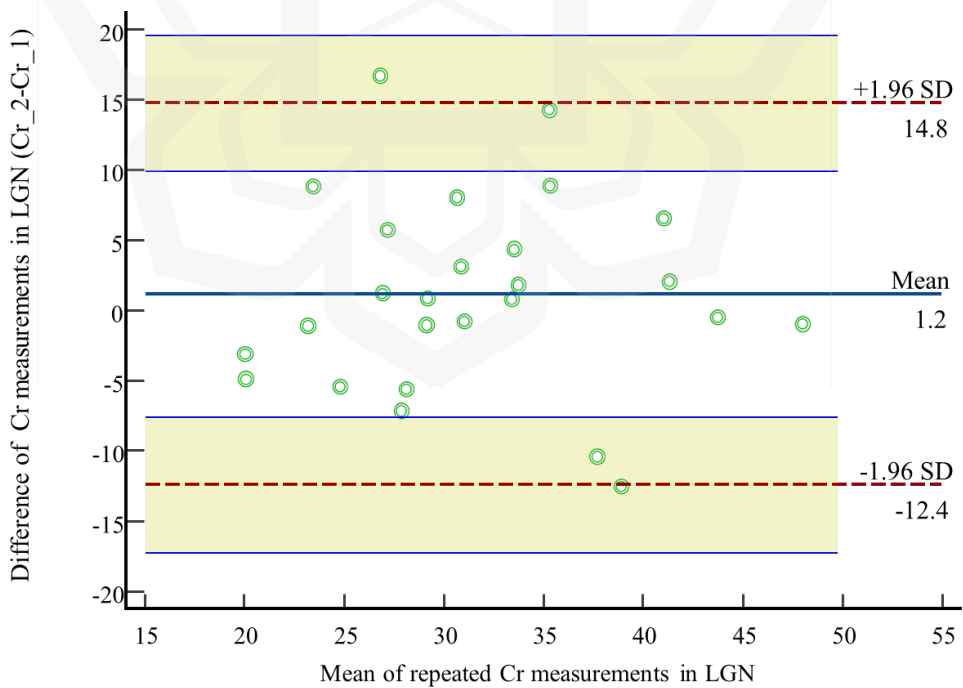


Figure 4.3 Bland and Altman difference plots using CR concentration amplitude in LGN in the first and second sessions of the MRS technique.

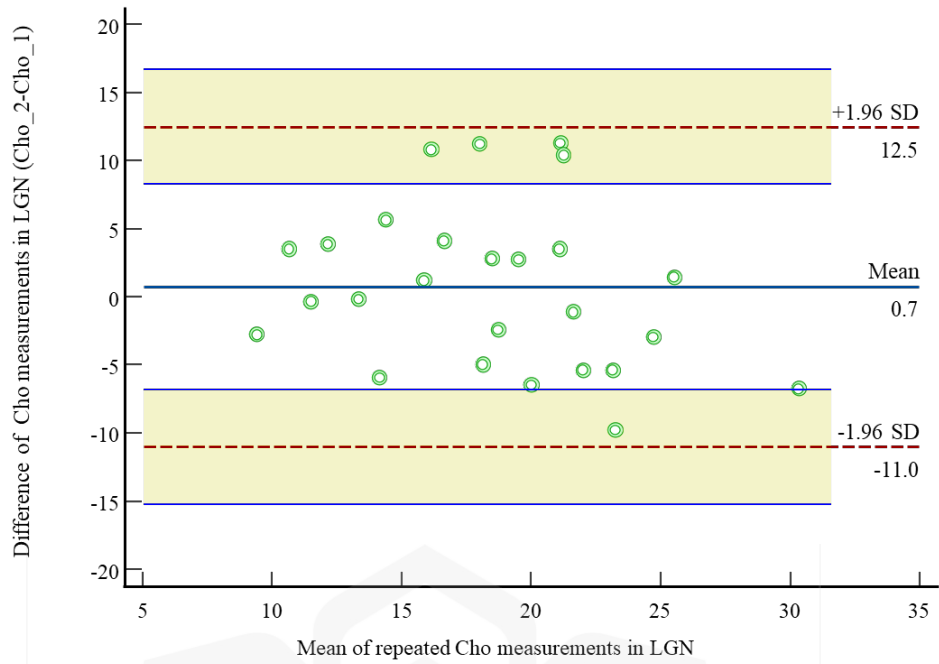


Figure 4.4 Bland and Altman difference plots using Cho concentration amplitude in the LGN in the first and second sessions of the MRS technique.

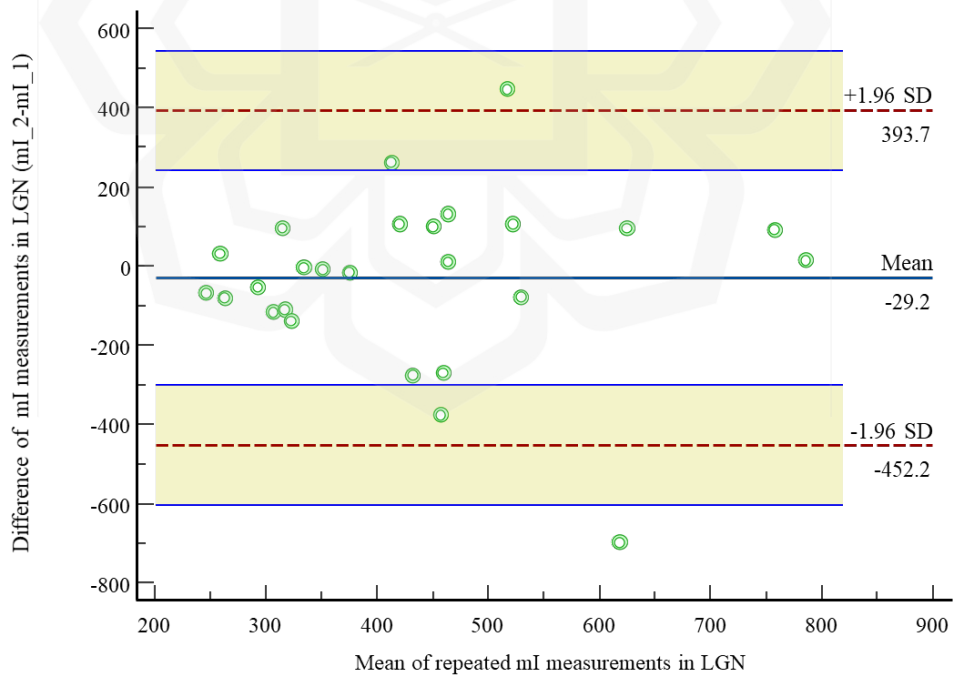


Figure 4.5 Bland and Altman difference plots using mI concentration amplitude in the LGN in the first and second sessions of the MRS technique.

Table 4.5 shows that in the VC region, the mean difference (bias) for Glx was positive, with a value of 1.16. Conversely, NAA, Cr, Cho, and mI had negative bias values of -0.61, -0.22, -0.49, and -2.35, respectively, indicating a tendency for lower metabolite concentration in the second measurement. Of all the metabolites, Cr had the smallest bias value of -0.22, with a narrow LOA range of (-8.90 to 8.46), indicating that the two consecutive measurements of Cr were essentially equivalent, with minimal measurement variability (Table 4.5). Cho and NAA had bias values of -0.49 and -0.61, respectively, with narrow LOA ranges (Cho: -6.49 to 5.50 and NAA: -8.21 to 6.99), suggesting a small difference and good agreement between the consecutive measurements for these metabolites (Table 4.5). In contrast, mI had the largest negative bias value of -2.35, while Glx had a positive bias value of 1.16, with wider LOA ranges (mI: -125.96 to 121.26 and Glx: -149.82 to 152.14), indicating a larger difference and less agreement between the consecutive measurements for these metabolites (Table 4.5).

Table 4.5 The Bland-Altman bias and limit of agreement in VC.

Metabolites (n=26)	Bias	95% LOA (95% CI) LB	95% LOA (95% CI) UB
NAA	-0.61	-8.21 (-10.92 to -5.50)	6.99 (4.27 to 9.70)
Glx	1.16	-149.82 (-203.69 to -95.95)	152.14 (98.27 to 206.00)
Cr	-0.22	-8.90 (-11.99 to -5.80)	8.46 (5.36 to 11.56)
Cho	-0.49	-6.49 (-8.62 to -4.35)	5.50 (3.34 to 7.64)
mI	-2.35	-125.96 (-170.06 to -81.85)	121.26 (77.16 to 165.34)

The Bland-Altman plots are shown below for each pair of metabolites in the VC (Figure 4.6 to Figure 4.10). Most data points lie within the upper limit of agreement (LOA) and lower LOA for each metabolite.

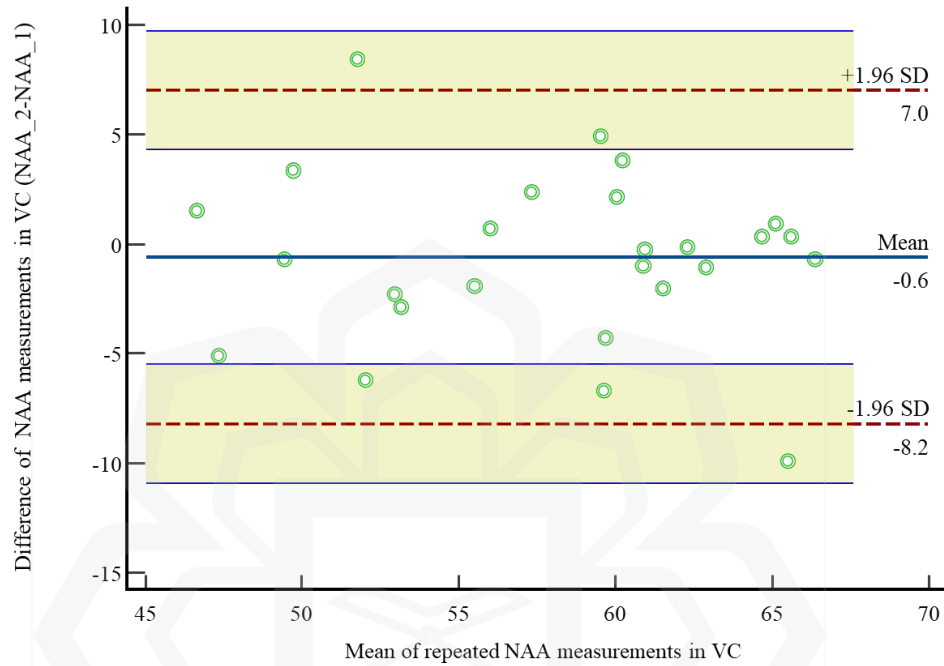


Figure 4.6 Bland and Altman difference plots using NAA concentration amplitude in the VC in the first and second sessions of the MRS technique.

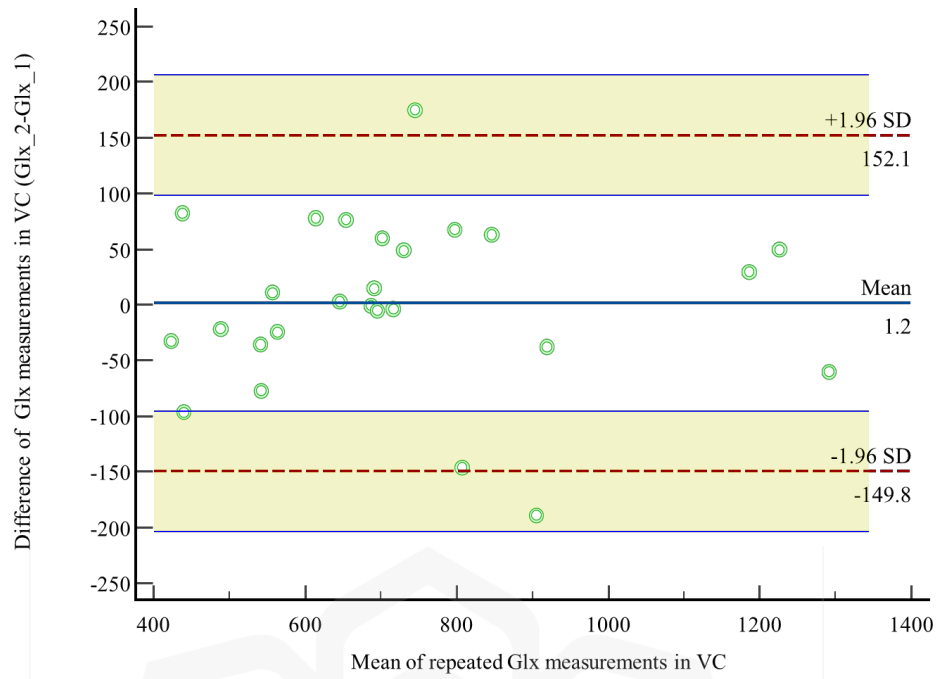


Figure 4.7 Bland and Altman difference plots using Glx concentration amplitude in the VC in the first and second sessions of the MRS technique.

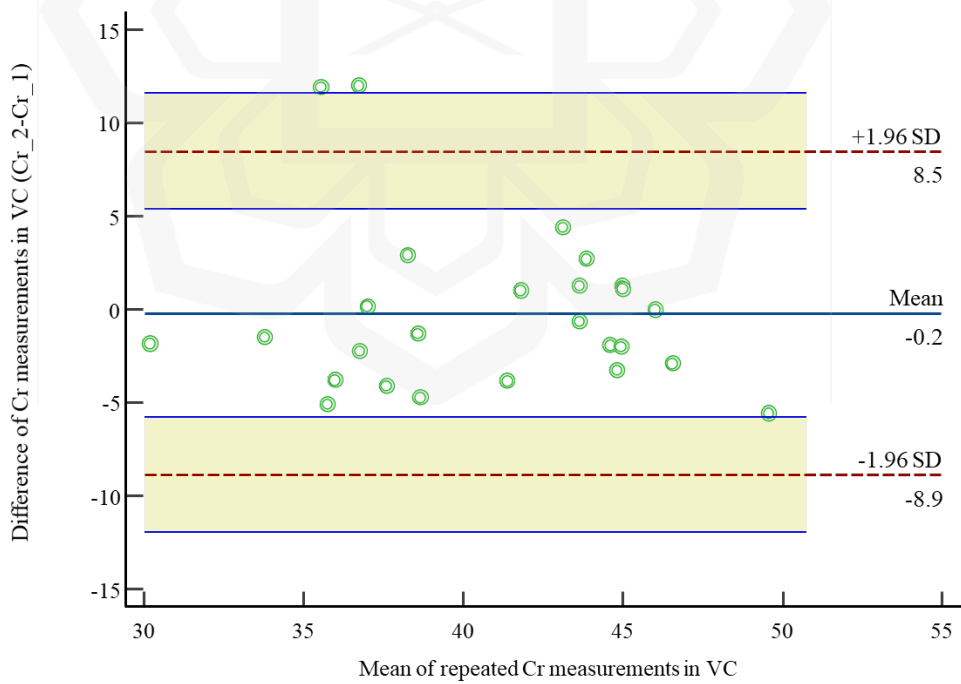


Figure 4.8 Bland and Altman difference plots using Cr concentration amplitude in VC in the first and second sessions of the MRS technique.

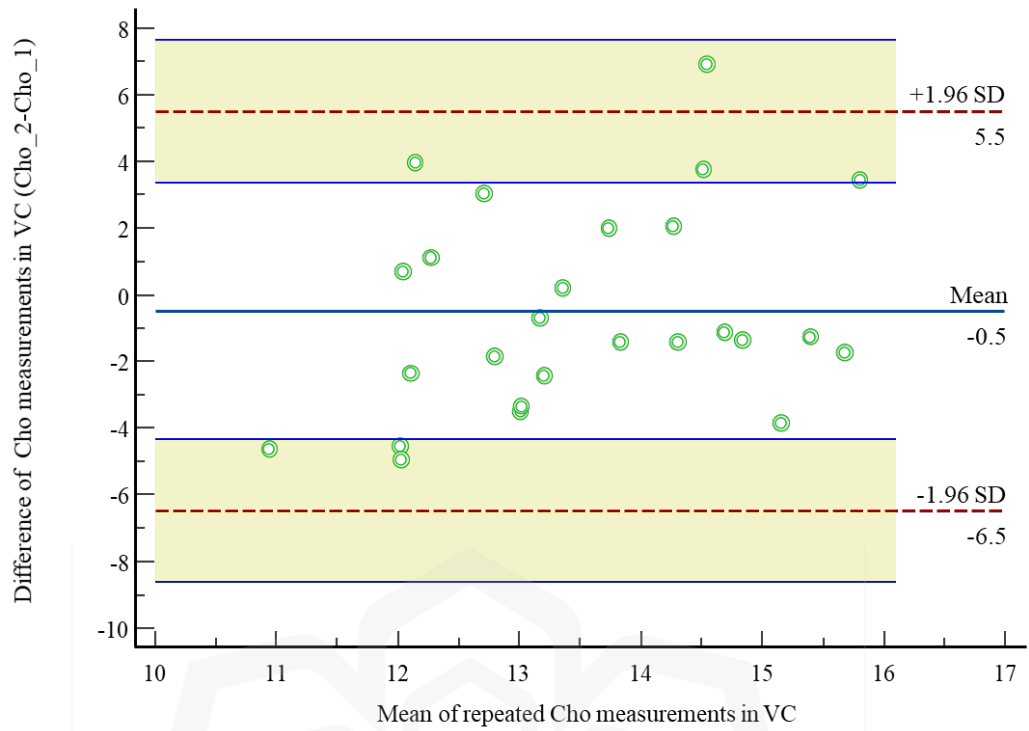


Figure 4.9 Bland and Altman difference plots using Cho concentration amplitude in VC in the first and second sessions of the MRS technique.

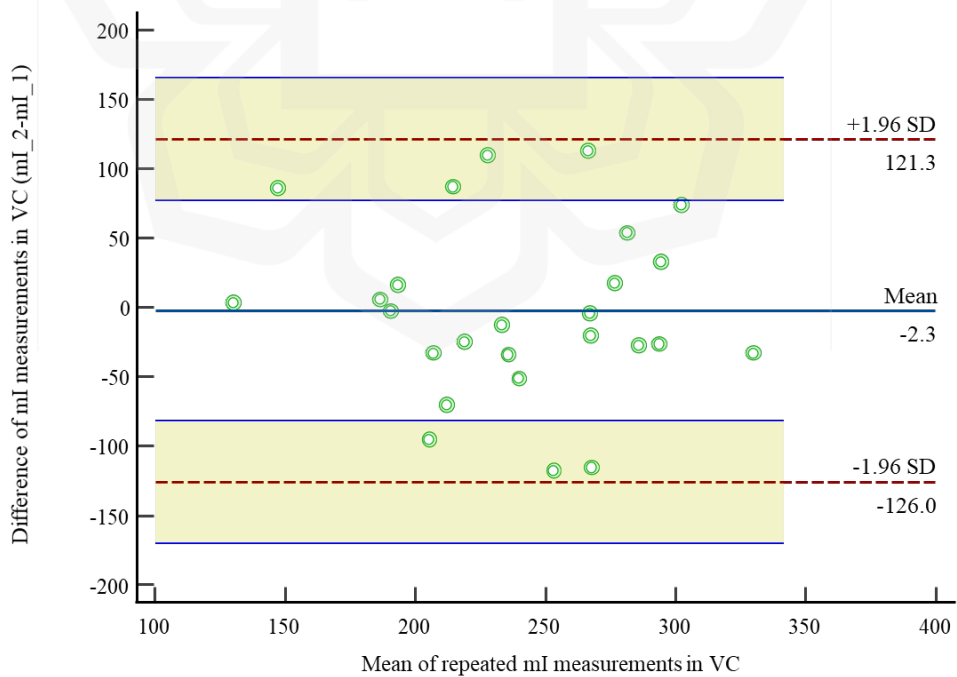


Figure 4.10 Bland and Altman difference plots using mI concentration amplitude in the VC in the first and second sessions of the MRS technique.

In the LGN, the mI concentration amplitude is the highest RC=418.66 (RC%=96.55%), followed by the concentration amplitude of Glx (RC=402.69) (RC%=106.33%), NAA (RC=18.82) (RC%=30.96%), Cr (RC=13.52) (RC%=42.84%), and Cho (RC=11.60) (RC%=62.83%) (Table 4.6). The highest CV% were 38.36% for Glx, followed by mI (CV=34.83%), Cho (CV=22.67%), Cr (CV=15.45%) and NAA (CV=11.10%) (Table 4.6).

Table 4.6 Repeatability statistics for metabolites measurement in LGN.

Metabolites (n=26)	Overall mean	WSD	RC	RC 95% CI	RC (%)	CV (%)
NAA	61.18	6.79	18.82	14.82 to 25.79	30.76	11.10
Glx	378.71	145.28	402.69	317.13 to 551.86	106.33	38.36
Cr	31.55	4.88	13.52	10.644 to 18.52	42.84	15.45
Cho	18.47	4.19	11.60	9.14 to 15.90	62.83	22.67
mI	433.61	151.04	418.66	329.70 to 573.75	96.55	34.83

In VC, the measurement of Glx concentration amplitude had the highest RC=148.06 (RC%=20.42%), followed by concentration amplitude of mI (RC=121.30) (RC%=50.71%), Cr (RC=8.52) (RC%=20.74%), NAA (RC=7.55) (RC%=13.03%), and Cho (RC=5.96) (RC%=44.08%) (Table 4.7). The highest CV were 18.29% for mI, followed by Cho (CV=15.90%), Cr (CV=7.55%), Glx (CV=7.38%) and NAA (CV=4.70%) (Table 4.7).

Table 4.7 Repeatability statistics for metabolites measurement in VC.

Metabolites (n=26)	Overall mean	WSD	RC	RC 95% CI	RC (%)	CV (%)
NAA	57.93	2.72	7.55	5.94 to 10.34	13.03	4.70
Glx	724.09	53.42	148.06	116.60 to 202.91	20.45	7.38
Cr	40.69	3.07	8.52	6.71 to 11.68	20.74	7.55
Cho	13.51	2.15	5.96	4.69 to 8.16	44.08	15.90
mI	239.22	43.76	121.30	95.52 to 166.23	50.71	18.29

4.4 DISCUSSION

This experiment was conducted to determine whether the MRS is repeatable and reliable method to measure metabolites. From the results, the metabolite measurements in two sessions on a same subjects yield no significant difference. The data suggest the SVS technique is a reliable method that provide repeatable measurements. It is crucial to emphasize that this repeatability study was conducted using only two consecutive measurements. This approach aligns with the study by Ross et al., (2023), which also employed just two consecutive measurements of other MRI parameters and has evidently considered sufficient for evaluating the consistency and reliability of a given measurement. While a larger number of measurements may provide more data points, the utilization of two consecutive measurements has been established as a valid and efficient method in assessing repeatability. This is particularly relevant in situations where acquiring a large number of measurements may be logistically challenging or impractical due to constraints in time or resources.

From the paired t-test and Wilcoxon signed-ranked test, there were no systematic differences in the metabolite measurements between the first and second sessions. The results also showed that all the 95 percent confidence intervals (CIs) in the paired sample t-test contained zero, indicating that the true mean differences between all pairs of metabolites in LGN and VC may indeed be zero. This indicated a non-statistically significant increase or decrease in the mean difference ($p > 0.05$) between all pairs of metabolites in the LGN and VC. However, the tests did not provide information on individual differences but rather on systematic differences between the means of two different sets of data. As a result, (Bruton, Conway, & Holgate, 2000) emphasized that this test alone was insufficient to determine the reliability of a study, and it cannot be used in isolation to make such an estimation. Therefore, the Bland-Altman agreement test was implemented to augment the results obtained by this parametric test.

Each Bland-Altman plot in the results section provides graphical displays of the difference between the two sets of quantified metabolite measurements (Y-axis) against the average of the two sets of quantified metabolite measurements (X-axis). Each plot also presented 95% limits of agreement together with its confidence interval. According to (Kalra, 2017), 95% of the data points should lie within ± 1.96 SD of the mean difference to indicate that there is agreement between the two measurements. However, it was also emphasized that it is important to set a priori the acceptable limit of the data before interpreting the related results (Kalra, 2017). This is due to the fact that different techniques or methods of application may have a different limit of any measurement that they can accept, depending on whether the measurement is appropriate for the subject's biological or clinical goals that were set.

The results indicated that most data points for all measured metabolites in the LGN and VC region fell within the limits of agreement, suggesting good agreement between the consecutive measurements. The Bland-Altman plots (Figure 4.1 to Figure 4.10) showed only a few outliers and no systematic trends in measurement error, indicating that the measurements were precise and reliable. However, it is important to note that while all measured metabolites showed good agreement between the consecutive measurements, the bias and LOA of each paired measurement differed, indicating variability in the range of difference between the consecutive measurements for each metabolite (Bland & Altman, 1999; Giavarina, 2015; Kalra, 2017). Therefore, while the overall agreement between the measurements was good, the specific characteristics of each paired measurement should be considered when interpreting the results.

In this current study, the consecutive measurements of NAA, Cho, and Cr in the LGN and VC regions showed a small bias with narrow LOA indicating strong agreement between the measurements. These results suggest that there is good consistency and minimal variability between the consecutive measurements of NAA, Cho, and Cr in both regions. The narrow LOA indicates that the range of differences between the consecutive measurements is small, suggesting that the measurements are precise and reliable (Bland & Altman, 1999; Giavarina, 2015).

This level of agreement underscores the reliability of the measurement technique used in this experiment. It provides confidence in the accuracy of the data collected, laying a robust foundation for the subsequent experiment in this current study and conclusions drawn from this experiment. Additionally, it aligns with previous studies that have demonstrated the effectiveness of similar measurement methods (Ross et al., 2023). It is important to note that the assessment of repeatability is a critical aspect of any measurement technique. Confirming the consistency of the measurements instills greater confidence in the validity of the findings, ultimately enhancing the overall robustness of this study.

In contrast, the consecutive measurements of Glx and mI in the LGN and VC regions showed a larger bias with wider limits of agreement (LOA), indicating less agreement between the measurements. These results suggest that there is greater variability and less precision between the consecutive measurements of Glx and mI in both regions. The wider LOA indicates that the range of differences between the consecutive measurements is larger, suggesting that the measurements may be less reliable (Bland & Altman, 1999; Giavarina, 2015). These findings and interpretations underscore the importance of understanding the potential variability in measuring Glx and mI.

Although, the larger bias values may indicate that there is a significant difference between the consecutive measurements of these metabolites, which may affect the accuracy of the results, it is crucial to note that there was actually no significant mean difference in the consecutive measurements proven by paired t-test and Wilcoxon signed rank test conducted in this current study. Moreover, the CIs around the bias of paired metabolite measurements did include zero as explained in the earlier paragraph, indicating that the difference between the two measurement is not statistically significant. This is a critical finding as it suggests that the consecutive measurements for Glx and mI in LGN and VC, despite their larger bias, still exhibited good agreement and were measuring the same underlying quantity. These results shed light on the nuances of measuring Glx and mI and highlight the need for a nuanced interpretation of bias and LOA. They also serve as a valuable contribution to the broader understanding of metabolite measurements in these regions and provide important insights for future studies examining Glx and mI in the context of glaucoma.

The reliability of a study can be evaluated using many forms of measurement indices. (Duda et al., 2021) discussed their result for repeatability and reliability with more than one variation index using CV for repeatability and ICC for reliability. (Gu et al., 2008) and (Marshall, Wardlaw, Cannon, Slattery, & Sellar, 1996) in their reproducibility study that was conducted to evaluate reliability used only CV to describe the variation in their findings. Meanwhile, studies such as (Puri, Egan, Wallis, & Jakeman, 2018), which show repeatability studies employing RC in addition to CV and ICC, were quite uncommon. Given the types of measurement indices discussed above, this condition contributes to the claim made by (Bruton et al., 2000) that evaluating reliability is a challenging task.

In this study, the reliability of the implemented MRS acquisition and associated quantified data were systematically evaluated from the repeatability study. To the best of our knowledge, there have been no studies on the repeatability of MRS single voxel in the in vivo measurement of NAA, Glx, Cr, Cho, and mI levels in the LGN and VC at a magnetic field strength of 1.5T.

The reproducibility of in vivo MRS utilizing single voxel methods has been widely studied, as reported by (Gu et al., 2008), (Marshall et al., 1996), and (Schirmer & Auer, 2000). However, there have been relatively few studies on the repeatability of MRS measurements. Two recent studies by (Duda et al., 2021) and (Puri et al., 2018) specifically examined repeatability, demonstrating the reliability of the MRS method for measuring metabolite concentrations. The findings of Duda et al. (2021) cannot be compared to those of this study because they focused on gamma-aminobutyric acid metabolites.

Marshall et al. (1996) conducted a repeatability test as part of their reproducibility study; they took six consecutive measurements from the voxel of interest in the parietal white matter. The repeated measurements were then analyzed, giving the CV of metabolite peak areas and area ratios from the spectroscopic data that were quantified by the two software programs. The CV of the repeated measurements using the manufacturer's software were 6.7% for NAA, 11.1 % for Cho and 9.3 % for Cr through successive metabolite measurements in parieto-occipital cortex region. Meanwhile, the CV for the repeated measurements from the data point that was quantified using external software were 4.4% for NAA, 8.2 % for Cho and 17.2 % for Cr.

Puri et al., (2018) reported CV and RC index for their repeatability study of human cerebral choline-containing compounds measurement using multi voxel spectroscopy technique. They discovered that the CV for Cho measurement ranged from 2.75% to 33.99%, while the RC index ranged from 5.68 % to 600 % (based on the ratio of Cho to Cr for each of the 64 voxels). They implied that their findings were found to be acceptable and produced an outstanding reproducibility.

The CV% data for the metabolite concentrations in this study were found to vary widely. Despite this variability, the CV values for NAA, Cho, and Cr, especially in the VC, were found to be comparable to those reported by Marshall et al. (1996) and Puri et al. (2018), as discussed in the previous paragraph. Specifically, the CV values for NAA, Cr, and Cho in the VC in the current study were found to be within the ranges reported by Marshall et al. (1996). Additionally, the CV value for Cho in the VC and LGN in the current study was found to be within the range reported for cerebral Cho by Puri et al. (2018). Notably, the VC area used in this study is included in the regions studied by Marshall et al. (1996) and Puri et al. (2018), indicating that the CV values in this study are comparable. Thus, despite the wide range of CV values observed in this study, the results suggest that the protocol used in this study is reliable for measuring metabolite concentrations in the brain.

The observation of comparable CV values to established studies indicates the robustness and reliability of the measurement protocol employed in this research. This finding underscores the validity of the methodology and instills confidence in the accuracy of the metabolite concentration measurements. It also provides a valuable reference point for future studies employing similar protocols, contributing to the advancement of research in this field.

The current study also found that there was a wide range of RC% data for the metabolite concentrations in both the LGN and VC regions. This variability in RC% values highlight the complexity of metabolite measurements. Despite this variability, it is noteworthy that the RC% values for Cho, especially in the VC, were found to be comparable to those reported by Puri et al. (2018), as discussed in the previous paragraph. Specifically, the RC% value for Cho in both LGN and VC in this current study fell within the range reported for cerebral Cho by Puri et al. (2018). This observation suggests that the RC% values for Cho in this study are in line with established research in the field. Moreover, it is worth noting that the LGN and VC areas studied in this research overlap with those studied by Puri et al. (2018), suggesting that the RC% values in this study are comparable to previous research.

The wide range of RC% values observed in this study underscores the need for careful consideration when interpreting metabolite concentration data. It highlights the importance of understanding the potential variability in these measurements and emphasizes the need for robust measurement protocols. This finding contributes to the broader understanding of metabolite measurements in the LGN and VC regions, providing valuable insights for future studies in this area.

4.5 CONCLUSION

The MRS appears repeatable enough to provide longitudinal measurement of metabolites. The results agree for the utilization of MRS in a 1.5 Tesla MRI as a scientific technique to investigate metabolites concentration in vivo, at least in the LGN and VC.

CHAPTER FIVE

METABOLITE COMPARISON IN THE LATERAL GENICULATE NUCLEUS AND VISUAL CORTEX OF HEALTHY YOUNG AND HEALTHY ELDERLY SUBJECTS

Abstract

Purpose

The aim of this chapter is to compare the metabolites, particularly the N-acetyl aspartate (NAA), creatine (Cr), choline (Cho), glutamate glutamine (Glx), and myo-inositol (mI) levels in the lateral geniculate nucleus (LGN) and visual cortex (VC) using magnetic resonance spectroscopy (MRS) between healthy young and healthy elderly subjects.

Materials and methods

An MRS acquisition using single-voxel spectroscopy (SVS) technique was performed using 1.5 Tesla MRI on 15 healthy young subjects (19.0 ± 0.2 years) and nine healthy elderly subjects (50.8 ± 7.6 years). All related metabolites were measured bilaterally in the LGN and VC. A standardized volume of interest (VOI) of $13 \times 13 \times 13$ mm was used for measurement. Spectral editing for metabolites was conducted for each scan. Using jMRUI fitting software, metabolites were quantified as concentration amplitudes in arbitrary units and then quantified further to obtain metabolite ratios for use in statistical analysis. Normality of data were tested using the Shapiro-Wilk normality test. Data homogeneity of variance was determined using Levene's test. An independent sample t-test was used to compare metabolite concentration between the young and the elderly groups. The Mann-Whitney U test was used for data that did not conform to normality.

Results

In the LGN, the NAA concentration was 61.41 ± 6.44 in the young and 53.33 ± 6.83 in the elderly group ($p < 0.001$). The Glx was 340.54 ± 142.69 in the healthy young and 439.92 ± 134.06 in the elderly ($p = 0.027$). The Cr concentrations were 30.97 ± 7.97 and 38.03 ± 10.90 in healthy young and healthy elderly respectively ($p = 0.018$). The concentrations of Cho were 18.09 ± 6.45 and 23.91 ± 7.02 in healthy young and healthy elderly respectively ($p = 0.008$). The mI concentrations were not significantly different ($p = 0.143$) in healthy young (419.00 ± 181.13) and healthy elderly (458.26 ± 104.14).

In the VC, the NAA concentration was 58.23 ± 6.44 in the young and 56.17 ± 9.50 in the elderly group ($p=0.441$). The Glx was 724.67 ± 234.24 in the healthy young and 745.00 ± 109.27 in the elderly ($p=0.398$). The Cr concentrations were 40.70 ± 5.53 and 45.90 ± 5.91 in healthy young and healthy elderly respectively ($p=0.006$). The concentrations of Cho were 13.76 ± 1.71 and 16.41 ± 3.24 in healthy young and healthy elderly respectively ($p=0.005$). The mI concentrations were 240.39 ± 59.32 in healthy young and 239.03 ± 46.55 in healthy elderly ($p=0.004$).

Conclusion

Age affects certain concentration of metabolites in the LGN and VC, as measured by MRS. Metabolites reading in a certain disease or condition should be coupled with metabolites concentration reading of the healthy in the respective age.

Keywords: proton magnetic resonance spectroscopy, glaucoma, lateral geniculate nucleus, single voxel spectroscopy, N-Acetyl Aspartate, Creatine, Choline, Glutamate, Myo-Inositol

5.1 INTRODUCTION

The non-invasive investigation of brain metabolites has been facilitated by the development of MRS. Various human body parts, both pathologically and in a healthy state, have been studied using this technology. The potential of MRS to identify pertinent metabolites in the brain has been extensively employed, particularly in neurodegenerative studies in numerous regions of the brain (Graff-Radford & Kantarci, 2013; Jones & Waldman, 2004; Öz et al., 2014).

The effect of age on metabolite concentrations in a healthy brain is a topic of ongoing research and is not yet fully understood. While some studies have reported age-related changes in metabolite concentrations, others have found no significant differences (Bracken et al., 2011; Duda et al., 2021; Haga, Khor, Farrall, & Wardlaw, 2009; Raininko & Mattsson, 2010; Rigotti et al., 2007, 2011; Wiebenga et al., 2014; Wijtenburg et al., 2019). For instance, (Raininko & Mattsson, 2010) conducted a study on the effect of aging on metabolite concentrations in the supraventricular white matter using magnetic resonance spectroscopy (MRS) with a short TE (22 ms) and long TR (6000 ms). The study aimed to investigate how age affects the levels of different metabolites in the brain. The authors recruited 57 healthy subjects aged 13 to 72 years and measured the concentrations of several metabolites, including N-acetyl aspartate (NAA), creatine (Cr), lactate, glutamate glutamine (Glx), and myo-inositol (mI). The results showed that mI levels increased, and NAA levels decreased with age in the supraventricular white matter. These findings suggest that changes in metabolite concentrations may be indicative of age-related changes in brain function or structure.

In this study, the LGN and VC have been chosen as the locations of measurement. It is purposive to measure the metabolite concentrations in healthy young and elderly subjects, where differences may be read as due to aging effects. This study is also important in establishing the normative value of metabolites concentrations in both LGN and VC, in both young and elderly age groups. Using the data in this study, valid and safe conclusions can be made later for latter chapters of this thesis upon analysis of subjects with glaucoma. The main metabolites including the NAA, Glx, Cho, Cr, and mI, were selected for quantification in this study.

5.2 SPECIFIC METHODOLOGY

5.2.1 Subjects

Fifteen healthy young subjects (19.0 ± 0.2 years) were recruited consisting of undergraduate students from the International Islamic University Malaysia (Kuantan Campus) via purposive sampling. Nine elderly subjects (50.8 ± 7.6 years) were recruited through advertisement in Kuala Lumpur and Selangor.

5.2.2 MRS Acquisition

Single-Voxel Spectroscopy (SVS) technique was performed on LGN and VC from both hemispheres of each subject's brain. The SVS with stimulated echo acquisition mode (STEAM) technique as outlined in chapter three was performed on four locations in each subject; in the right and left regions of the LGN, located at the rear end of the thalamus (Figure 5.1), and VC, as close as possible to the posterior VC position and along the calcarine sulcus in each case (Figure 5.2). The total spectroscopy examinations performed and accepted for raw spectral review were from 30 exams in the LGN and VC of healthy young group and 18 exams in the LGN and VC of healthy elderly group.

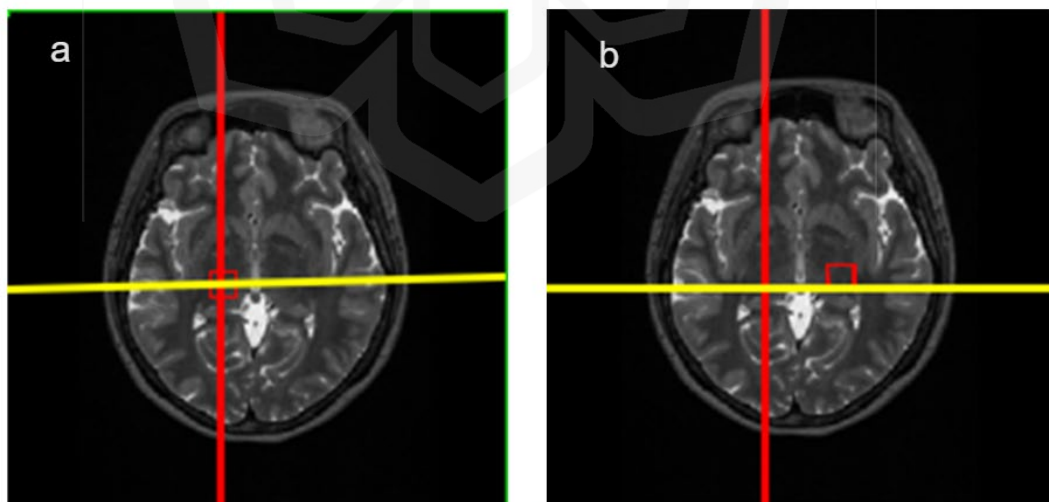


Figure 5.1 The VOI (red box) location in the right (a) and left (b) regions of the LGN.

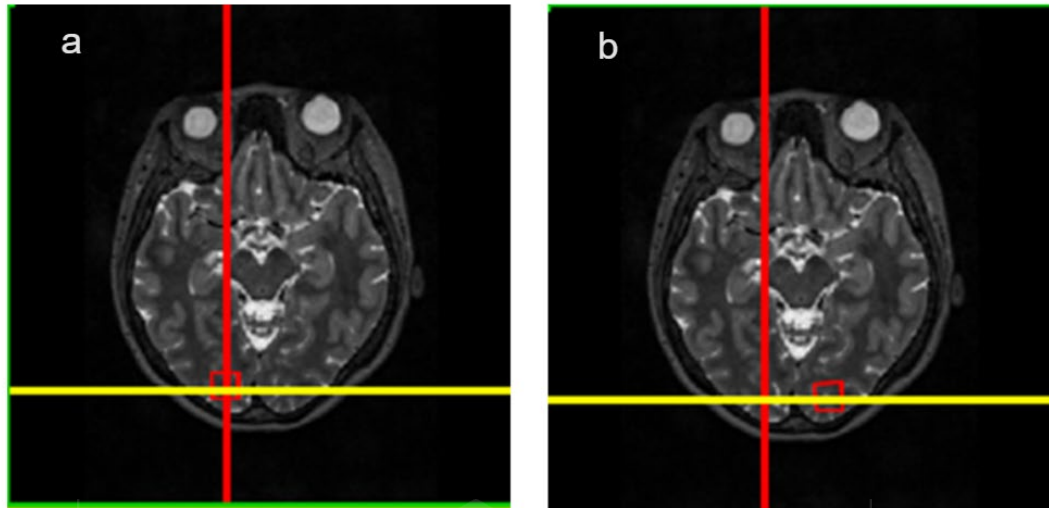


Figure 5.2 The VOI (red box) location in the right (a) and left (b) regions of the VC.

5.2.3 MRS Analysis

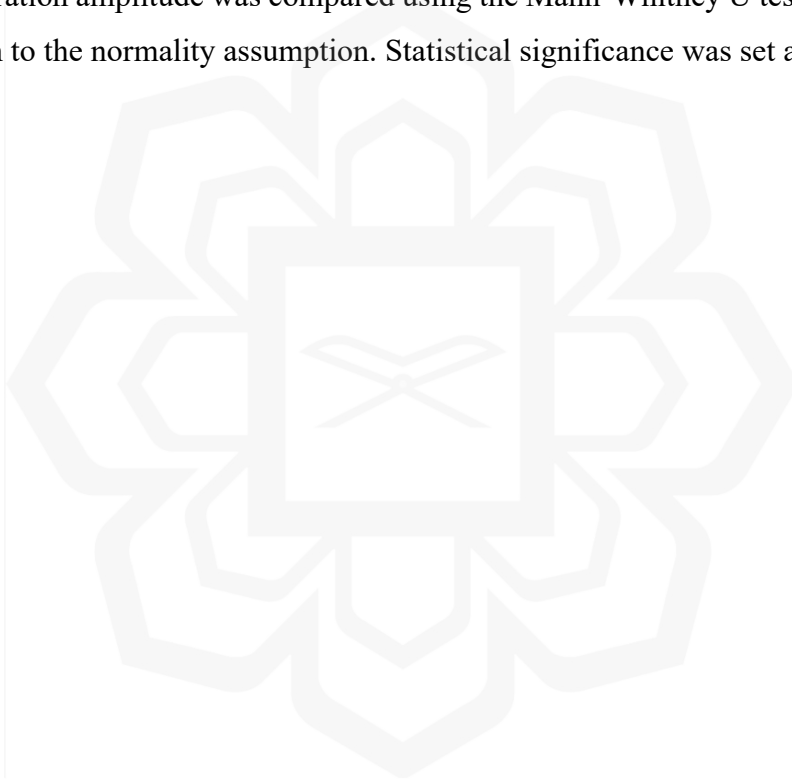
Following the spectral review, 86 out of 96 raw spectra demonstrated a good and acceptable spectroscopic curve (Table 5.1).

Table 5.1 The raw spectrum scan number in healthy young and elderly groups after the spectral evaluation

<i>Both right and left sides</i>	Young (n = 15)	Eliminated spectrum	Elderly (n = 9)	Eliminated spectrum	Total spectrum evaluated
LGN spectrums	30	4	18	1	43
VC spectrums	30	4	18	1	43
Total	60	8	36	2	86

5.2.4 Statistical Analysis

Descriptive data are presented as mean \pm standard deviation (SD). All data in this study were analyzed using IBM SPSS software version 23 (SPSS Inc., Chicago, IL, USA) licensed under the International Islamic University Malaysia (IIUM). The normality of data was tested using the Shapiro-Wilk test. The data were considered to conform to the normality assumption if $p > 0.05$. All metabolite data that met the assumption of homogeneity of variances were compared (between young and elderly groups) using an independent sample t-test. However, the metabolite data that violated the homogeneity of variance assumption were interpreted using the Welch t-test. The mean metabolite concentration amplitude was compared using the Mann-Whitney U test for data did not conform to the normality assumption. Statistical significance was set at $p \leq 0.05$.



5.3 RESULTS

In the LGN, healthy young subjects recorded a mean concentration of 61.41 ± 6.44 for NAA, while the elderly show a significantly lesser value of 53.31 ± 6.83 ($p < 0.01$). The Glx concentration is 340.54 ± 142.69 in healthy young while recorded a significantly higher 439.92 ± 134.06 concentration value in the elderly group ($p = 0.027$). The Cr concentrations are 30.97 ± 7.97 and 38.03 ± 10.93 for young and elderly groups, respectively, showing a significant increasing trend ($p = 0.018$). The Cho concentrations are recorded as 18.09 ± 6.44 and 23.91 ± 7.02 in healthy young and healthy elderly respectively, also showing a significant increasing trend ($p = 0.008$). In the LGN, the healthy young ml concentration which is recorded as $419.00 \pm 1.81.13$ is not significantly different to the concentration in healthy elderly subjects ($p = 0.143$). Table 5.2 summarizes the data recorded in the LGN for both age groups.

Table 5.2 Comparison of metabolite concentration amplitude between healthy young group and healthy elderly group in LGN.

	Healthy young (n=26)		Healthy elderly (n=17)		<i>p</i>
	M	sd	M	sd	
Independent sample t-test result					
NAA	61.41	6.44	53.31	6.83	<0.01*
Glx	340.54	142.69	439.92	134.06	0.027*
Cr	30.97	7.97	38.03	10.90	0.018*
Cho	18.09	6.45	23.91	7.02	0.008*
Man-Whitney U test					
ml^b	419.00	181.13	458.26	104.14	0.441

M: mean, sd: standard deviation.

^bThe Man-Whitney U test was used to compare the data as Shapiro-Wilk test indicated that the normality assumption was not met for this variable.

In the VC, healthy young and elderly subjects recorded a nonsignificant difference in concentration of NAA at 58.23 ± 6.44 and 56.17 ± 9.50 respectively ($p=0.441$). The mean Cr concentration is 40.70 ± 5.53 in the healthy young subjects while recorded a significantly higher 45.90 ± 5.91 concentration value in the elderly subjects ($p=0.006$). The Cho concentrations are recorded as 13.76 ± 1.71 and 16.41 ± 3.24 in healthy young and healthy elderly respectively, also showing an increasing trend with age ($p=0.005$). The mI concentration shows a significantly higher value in the healthy elderly subjects with 293.03 ± 46.55 relative to the 240.39 ± 59.32 of the healthy young subjects ($p = 0.004$). The Glx concentration in the VC recorded at 724.67 ± 104.14 in the healthy young group is not significantly different to the value in the elderly subjects of 745 ± 3.24 ($p=0.398$). Table 5.3 summarizes the data recorded in the VC for both age groups.

Table 5.3 Comparison of metabolite concentration amplitude between healthy young group and healthy elderly group in VC.

	Healthy young (n=26)		Healthy elderly (n=17)		<i>p</i>
	M	sd	M	sd	
Independent sample t-test result					
NAA^a	58.23	6.44	56.17	9.50	0.441
Cr	40.70	5.53	45.90	5.91	0.006*
Cho^a	13.76	1.71	16.41	3.24	0.005*
mI	240.39	59.32	293.03	46.55	0.004*
Man-Whitney U test					
Glx^b	724.67	234.24	745.00	109.27	0.398

M: mean, sd: standard deviation.

^aThe Welch test is reported because Levene's test indicated that the homogeneity of variances assumption was not met for this variable.

^bThe Man-Whitney U test was used to compare the data as Shapiro-Wilk test indicated that the normality assumption was not met for this variable.

5.4 DISCUSSION

This study provides evidence that aging causes metabolic concentration changes in the LGN and VC. Specifically, in the LGN, it was observed that there is a notable decrease in NAA concentration with advancing age, suggesting a potential decline in neuronal density or integrity (Currie et al., 2013; Hajek & Dezortova, 2008). It was also observed that Glx was concurrently increase, that may be indicative of alterations in glutamatergic neurotransmission (Ramadan et al., 2013; Zhou & Danbolt, 2014). Furthermore, Cr and Cho increase in concentrations may indicate alterations in energy metabolism and membrane turnover, respectively (Cecil, 2014). Collectively, these alterations suggest a subtle metabolic reconfiguration occurring in the LGN with aging, potentially reflecting a complex interaction of neuronal and glial activities. In contrast, a different observation was pointed out in the VC where Cr, Cho, and mI exhibited a significant increase with age. This could be attributed to various biochemical processes. For instance, the rise in Cr may point towards alterations in energy metabolism or cellular stress responses (Faghihi et al., 2017). The elevated Cho levels could be indicative of increased membrane turnover or inflammation, while the higher mI concentrations might suggest glial activation or osmoregulatory changes (Grover et al., 2015).

A direct comparison of the findings in this study to the existing literature body may be challenging considering the different anatomy of interests. Raininko and Mattsson (2010) in their study on supraventricular white matter using the MRS reported a decrease level of NAA and an uptake of mI levels following age, somehow in line with the current study. Supraventricular white matter is a region of white matter located above the lateral ventricles that is composed primarily of axons that serve to connect various regions of the brain, including the cortex, thalamus, and other white matter tracts (Azevedo et al., 2009; Tournier, Calamante, & Connelly, 2012). The supraventricular white matter is not directly adjacent to the LGN and VC, but the white matter tract, such as optic radiation within the supraventricular white matter, may be involved in the connectivity between the visual pathway's anatomical structures (Gennatas et al., 2017; Toosy, Mason, & Miller, 2014).

Interestingly, Raininko and Mattsson (2010) reported a U-shaped age dependence of Glx concentrations that peaks in their youngest and oldest age group. In their study, the subjects were binned into seven unequal age categories, with the most subjects landed in the 41-50 years age bin (14 subjects) and the least in 71-72 years age bin (two subjects). Concurrently with their objectives, linear regression analysis generated a relationship between age and metabolite concentrations. They concluded that some metabolite concentrations are slightly age-dependent, and that age dependency can be nonlinear. Furthermore, their warning about the inapplicability of their results as reference values for other techniques or regions underscores the importance of contextualizing findings within the specific experimental parameters.

To note, with 1.5 Tesla MRI, they used the SVS technique using a point resolved spectroscopy (PRESS) sequence with a TR of 6000 ms and a TE of 22 ms, while in this current study, the SVS technique using a STEAM sequence with a TR of 1500 ms and a TE of 30 ms was used. The selection of TE and TR in MRS can influence the obtained spectral data and the accuracy of metabolite concentration (Choi et al., 2013; Govindaraju et al., 2000). The findings in this current study, together with the findings by Raininko and Mattsson (2010) emphasizes the need for meticulous consideration of acquisition parameters in MRS studies, especially when exploring age-related effects.

Pouwels and Frahm (1998) reported metabolite concentrations in different areas of healthy human brain. They reported a higher concentration of NAA in the white matter compared to the grey matter, and an increasing concentration caudally. They also reported that a lesser concentration of Cr, mI, and Glx in the white matter, relative to the grey matter. In their study, 34 healthy volunteers of 27 ± 4 years of age were scanned using a 2.0 Tesla MRI with different VOI sizes. It is interesting to note that their experiment involves measurement of metabolite concentrations in the occipital brain where the VC is located, and in the thalamus where the LGN is located. It may not entirely accurate to compare their study to the current findings considering the difference in the MRS acquisition parameters (VOI size, scan region), however the findings from Pouwels and Frahm (1998) indirectly, but not exclusively, may support that NAA in the LGN of the healthy young group is consistently higher than that of the NAA in the healthy elderly group.

Study by Grachev & Apkarian (2000) revealed significant differences in the level of NAA, Cr, Cho, and mI across six different brain regions, including thalamus and cingulate, insula, sensorimotor, dorsolateral prefrontal, and orbital frontal cortices. In their study, nineteen healthy volunteers of 19 to 31 years of age were scanned using a 1.5 Tesla MRI with different VOI sizes for each region. It is interesting to note that their experiment showed significant increase of NAA and Glx in subjects 25 to 31 years of age compared to those in 19 to 20 years of age in the orbital frontal cortices and sensorimotor cortex. Their subsequent experiment comparing the nineteen healthy young subjects to sixteen middle-aged healthy subjects of 46.6 ± 3.4 years of age then revealed a significant decrease in NAA and Glx in the middle-aged group (Grachev & Apkarian, 2001). Grachev and Apkarian's (2000, 2001) research sheds light on metabolite variations across various brain regions and age groups. Notably, the significant changes in NAA and Glx levels observed in the orbital frontal cortices and sensorimotor cortex with age underscore the dynamic nature of metabolite concentrations in the brain.

In this current study, there were significant differences in the concentrations of several metabolites between the healthy young group and the healthy elderly group. These findings show that the chemical composition of the healthy human brain varies depending on age and brain area, which is in agreement with previous studies (Grachev & Apkarian, 2000; Pouwels & Frahm, 1998). In other words, the metabolites in the LGN and VC are age dependent, similar to metabolites in other brain regions, as evident in many studies (Grachev & Apkarian, 2000; Pouwels & Frahm, 1998; Raininko & Mattsson, 2010). However, it is essential to acknowledge the challenges of direct comparison with existing literature due to anatomical differences. The findings emphasize the complicated interplay of age, metabolite concentrations, and regional specificity. Understanding these nuances not only enriches our comprehension of glaucoma pathophysiology but also highlights the critical importance of meticulous methodology in MRS studies.

The discussion rightly emphasizes the significant variability inherent in spectroscopic studies of the brain, largely stemming from the specific techniques employed. There are several factors that can affect the results of this current study, which vary from other findings as discussed above. One of the main factors that can affect the results of MRS studies is the choice of spectroscopic technique (SVS or MVS). Each technique has its own strengths and limitations.

For example, SVS, which was chosen as the technique used in this current study, is a commonly used technique that allows for the acquisition of spectra from a single voxel within the brain. While SVS can provide high spectral resolution and sensitivity, it is limited in its ability to accurately target small structures and may be subject to contamination from extraneous tissues (Buonocore & Maddock, 2015; Grover et al., 2015; Tognarelli et al., 2015). In this current study, however, optimum measures were taken by localising the voxel with care by avoiding any contact with bone, vessels, air, or fat.

In contrast, MVS allows for the acquisition of spectra from multiple voxels within the brain, providing a more comprehensive picture of metabolic changes (Blüml, 2013). However, MVS may have lower spectral resolution and sensitivity compared to SVS (Anith Alfred J, Abubacker Sulaiman F, Divya Shree, Ashraf Ahmed & Prabhu, 2018; Buonocore & Maddock, 2015). The mention of these factors highlights the critical importance of methodological choices in spectroscopic studies.

Another factor that can cause variation in metabolite concentration is the combination of TE and TR parameters, which can have a significant impact on the sensitivity and specificity of metabolite measurements in spectroscopic studies (Kreis, Slotboom, Hofmann, & Boesch, 2005). TE determines the degree of spectral resolution, while TR determines the time between consecutive excitations of protons in the brain, and it plays a key role in determining the signal-to-noise ratio (SNR) of the spectroscopic measurement (Blüml, 2013). A combination of short TE and long TR, which was applied in the study by Raininko and Mattsson (2010) and in this current study, could result in more accurate metabolite measurement because short TE provides better resolution while long TR can result in higher SNR (Blüml, 2013).

However, it is imperative to acknowledge the potential trade-offs associated with TE and TR selection. For instance, a very short TE may result in reduced sensitivity to certain metabolites that take more time to decay over time, while a very long TR may lead to an increase in the acquisition time of the measurement (Blüml, 2013; Choi et al., 2013). This understanding of TE and TR implications highlights the meticulous approach required in spectroscopic studies.

It is important to note that, with similar combinations, but different values of TE and TR used in spectroscopic studies, such as those conducted by Raininko and Mattsson (2010) and in this current study, draws attention to the potential variations in the measured metabolite concentrations, even these studies involved similarly healthy subjects. This is because different TE and TR values affect how the signals from the brain molecules decay over time (Blüml, 2013). Therefore, changes in TE and TR can affect the signal intensity of the brain molecules, which can impact the accuracy of the measurements. This observation not only highlights the importance of consistent methodology but also underscores the need for careful consideration of acquisition parameters across studies.

In conclusion, this discussion elucidates the critical impact of methodological choices, particularly with respect to spectroscopic techniques and TE/TR parameters, in the present study. The current study's meticulous methodology and comparisons to previous research highlight the significance of these considerations. Such attention to detail not only improves the accuracy and reliability of findings, but also contributes to the field of spectroscopic studies as a whole.

5.5 CONCLUSION

The differences of metabolite concentrations in the LGN and VC between young and elderly healthy subjects were shown in this study. Comparing metabolite concentration in a human brain should be done cautiously with consideration of the aging effects and the impact of MRI protocols on measurements.

CHAPTER SIX

METABOLITES CONCENTRATION IN THE LATERAL GENICULATE NUCLEUS OF GLAUCOMA PATIENTS

Abstract

Purpose

The aim of this chapter is to determine the metabolite concentrations, particularly the N-acetyl aspartate (NAA), creatine (Cr), choline (Ch), glutamate (Glx), and myo-inositol (mI) in the lateral geniculate nucleus (LGN) in subjects with glaucoma using the magnetic resonance spectroscopy (MRS). The study also aimed to compare the metabolite concentrations between groups of healthy subjects, subjects with mild glaucoma, and subjects with severe glaucoma.

Materials and methods

An MRS acquisition using a single-voxel spectroscopy (SVS) technique was performed using 1.5 Tesla MRI on nine healthy subjects (50.8 ± 7.6 years), seven subjects with mild glaucoma (59.4 ± 10.2 years), and three subjects with severe glaucoma (52.0 ± 11.8 years). Glaucoma severities were categorized based on the Hodapp-Parrish-Anderson (HPA) classification. A standardized volume of interest (VOI) of $13 \times 13 \times 13$ mm was placed in the region of the lateral geniculate nucleus in both brain hemispheres. Spectral editing for metabolites was conducted for each scan. Using jMRUI fitting software, metabolites were quantified as concentration amplitudes in arbitrary units and then quantified further to obtain metabolite ratios for use in statistical analysis. Normality of data were tested using the Shapiro-Wilk normality test. Data homogeneity of variance was determined using Levene's test. Metabolites concentrations and ratios were compared between groups using one-way ANOVA and Welch ANOVA. Post-hoc test was conducted to test all possible group comparisons.

Results

The metabolites concentration amplitude in the LGN in group with mild glaucoma are 60.71 ± 9.15 , 439.54 ± 110.08 , 33.55 ± 6.61 , 377.07 ± 103.72 and 22.63 ± 4.23 for NAA, Glx, Cr, mI and Cho, respectively. Group with severe glaucoma recorded metabolite concentrations amplitude of 65.03 ± 14.66 (NAA), 433.30 ± 122.80 (Glx), 31.13 ± 12.47 (Cr), 424.01 ± 99.41 (mI) and 14.09 ± 5.07 (Cho). Healthy controls recorded metabolite concentrations amplitude of 53.31 ± 6.83 (NAA), 439.92 ± 134.06 (Glx), 38.03 ± 10.90 (Cr), 458.26 ± 104.14 (mI), 23.91 ± 7.02 (Cho). A significant increase in the NAA concentration amplitude (Tukey HSD, $p=0.03$) and a significant decrease in the Cho concentration amplitude (Games-Howell, $p=0.016$) are found in group with severe glaucoma compared to the same area in healthy control group. No significant mean differences are found for Glx, Cr and mI concentration amplitude between the groups (one-way ANOVA $p>0.05$). The NAA/Cr ratio is significantly higher in the mild glaucoma group relative to the healthy group (Games-Howell, $p=0.038$) while the Cho/Cr ratio is significantly lower in the severe glaucoma group relative to the group of mild glaucoma (Tukey HSD, $p=0.023$). No significant mean differences are found for Glx/Cr and mI/Cr ratios between the groups ($p>0.05$).

Conclusion

Glaucoma may cause shift in the metabolite concentration amplitudes and ratio in the LGN. Severe glaucoma subjects showed higher NAA concentrations and lower Cho concentrations in the LGN than in healthy eyes, while mild glaucoma subjects show higher NAA/Cr ratio relative to healthy subjects, and higher Cho/Cr ratio relative to severe glaucoma subjects.

Keywords: proton magnetic resonance spectroscopy, glaucoma, lateral geniculate nucleus, single voxel spectroscopy, N-Acetyl Aspartate, Creatine, Choline, Glutamate, Myo-Inositol

6.1 INTRODUCTION

Glaucoma is a disease that is chronic in nature and indistinctive at an early stage, leading to late detection. It has become a major public health problem and a leading cause of irreversible blindness worldwide (Kapetanakis et al., 2016; Nduaguba & Lee, 2006). Among the main pathological characteristics of glaucoma is apoptosis of the retinal ganglion cell (RGC) (Christopher Bowd; Linda M. Zangwill; Charles C. Berry; Eytan Z. Blumenthal; Cristiana Vasile; Cesar Sanchez-Galeana; Charles F. Bosworth; Pamela A. Sample; Robert N. Weinreb et al., 2001) Ninety percent of the RGCs terminate at the lateral geniculate nucleus (LGN), a major relay station between the retina and visual cortex (Bressloff, 2005). Injury to the RGC due to glaucoma may result in atrophy of the optic nerve and optic tract, which in turn results in degeneration and atrophy of the LGN (You et al., 2021).

Magnetic resonance spectroscopy (MRS) has been used to evaluate common neurologic disorders, including brain tumours, inherited metabolic disorders, demyelinating disorders, and infectious brain lesions (Öz et al., 2014). As previously discussed in the literature review chapter regarding the atrophy of anatomical structures associated with the visual pathway, which results in neurodegeneration of the involved anatomy in glaucoma brain, it seems necessary to conduct additional research on metabolite interactions in related anatomy. As a non-invasive spectroscopic technique, MRS may yield the ability to detect early onset metabolic changes in the brain, which may be indicative of diseases such as glaucoma. The aim of this study was to investigate the metabolite concentrations and any metabolites difference in the LGN which may be stemmed from glaucoma.

6.2 SPECIFIC METHODOLOGY

6.2.1 Subjects

Subjects were recruited to form three study groups namely the healthy controls, mild glaucoma group and severe glaucoma group. Ophthalmological data that included IOP, visual field, and cup disc ratio (CDR) for glaucoma subjects were obtained from the most recent ophthalmology routine checkup. Glaucoma severity is based on Hodapp-Parrish-Anderson (HPA) classification system as described in Chapter 3. All subjects were determined based on the inclusion and exclusion criteria as described in Chapter 3. Nine healthy subjects (50.8 ± 7.6), seven subjects with mild glaucoma (59.4 ± 10.2), and three subjects with severe glaucoma (52.0 ± 11.8), were recruited (Table 6.1).

Table 6.1 The demographics of all subjects following the respective groups.

	Healthy	Mild glaucoma	Severe glaucoma
Number of scanned LGN	17	14	6
Age (mean \pm SD in years)	50.8 ± 7.6	59.4 ± 10.2	52.0 ± 11.8
Visual field MD (mean \pm SD in dB)	-1.07 ± 1.5	-2.85 ± 1.4	-18.06 ± 3.3
IOP (mean \pm SD in mmHg)	14.12 ± 1.5	13.79 ± 0.6	19.33 ± 1.6
CDR (mean \pm SD)	N/A	0.65 ± 0.1	0.87 ± 0.1

LGN lateral geniculate nucleus, SD standard deviation, MD mean deviation, dB decibel, IOP intraocular pressure, CDR cup disc ratio, N/A not applicable

6.2.2 MRS Acquisition

Single-Voxel Spectroscopy (SVS) with stimulated echo acquisition mode (STEAM) technique was performed on LGNs from both hemispheres of each subject's brain. The total spectroscopy examinations performed and accepted for raw spectral review were from 18 from the healthy group, 14 from the mild glaucomatous group, and six from the severe glaucomatous group.

6.2.3 MRS Analysis

Following the spectral review after removal of residual water, 37 out of 38 raw spectra demonstrated a good and acceptable spectroscopic curve.

6.2.4 Statistical Analysis

Descriptive data are presented as mean \pm standard deviation (SD). All data in this study were analysed using IBM SPSS software version 23 (SPSS Inc., Chicago, IL, USA) licensed under the International Islamic University Malaysia. Normality of data were tested using the Shapiro-Wilk normality test. The data were considered to conform to the normality assumption if $p > 0.05$. Data homogeneity of variance was determined using Levene's test. Metabolites concentrations and ratios data with homogeneity of variance were compared using one-way Analysis of variance (ANOVA), whereas data with violated homogeneity of variance were compared using Welch ANOVA. Statistical significance was set at $p < 0.05$.

6.3 RESULTS

The NAA concentration amplitude values are 53.31 ± 6.83 , 60.71 ± 9.15 , and 65.03 ± 14.66 for healthy group, mild glaucoma group, and severe glaucoma group respectively. One-way ANOVA revealed that there is a significant mean difference ($p=0.018$) between the groups (Table 6.2). Tukey post-hoc test revealed the NAA concentration amplitude is significantly higher in the severe glaucoma group relative to the healthy group (adjusted $p=0.03$) (Figure 6.1). No significant differences in the metabolite concentration amplitudes are recorded for Glx ($p=0.993$), Cr ($p=0.253$), and ml ($p=0.108$) (Table 6.2).

The Cho concentration amplitude values are 23.91 ± 7.02 , 22.63 ± 4.23 , and 14.09 ± 5.07 for healthy group, mild glaucoma group, and severe glaucoma group respectively. Welch ANOVA revealed significant mean difference ($p = 0.006$) between the groups (Table 6.2). The Games-Howell post-hoc test revealed the Cho concentration amplitude is significantly lower in the severe glaucoma group compared to mild glaucoma group (adjusted $p=0.016$) and healthy group (adjusted $p = 0.008$) (Figure 6.2).

Table 6.2 Comparison of metabolites concentration amplitude in the LGN between groups.

Metabolites	Scanned LGN (mean \pm SD)			P value
	Healthy (n=17)	Mild glaucoma (n=14)	Severe glaucoma (n=6)	
One-way ANOVA				
NAA	53.31 ± 6.83	60.71 ± 9.15	65.03 ± 14.66	0.018*
Glx	439.92 ± 134.06	439.54 ± 110.08	433.30 ± 122.80	0.993
Cr	38.03 ± 10.90	33.55 ± 6.61	31.13 ± 12.47	0.253
ml	458.26 ± 104.14	377.07 ± 103.72	424.01 ± 99.41	0.108
Welch ANOVA				
Cho ^a	23.91 ± 7.02	22.63 ± 4.23	14.09 ± 5.07	0.006*

*The mean difference is significant at the 0.05 level

^aThe Welch ANOVA test was used to compare means as Levene's test indicated that the homogeneity of variances assumption was not met for this variable.

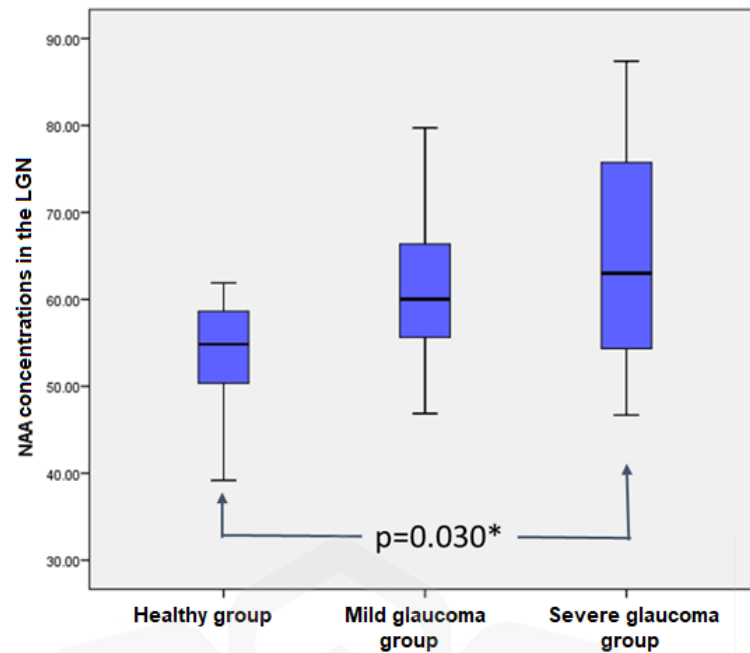


Figure 6.1 The box and whiskers plot illustrating a significantly higher NAA amplitude in the LGN of severe glaucoma group compared to the healthy group. There is an increase in NAA amplitudes from 53.31 ± 6.83 in the healthy group to 65.03 ± 14.66 in the severe glaucoma group, an increase of 11.72 (95% CI, 0.95 to 22.49) ($p=0.03$).

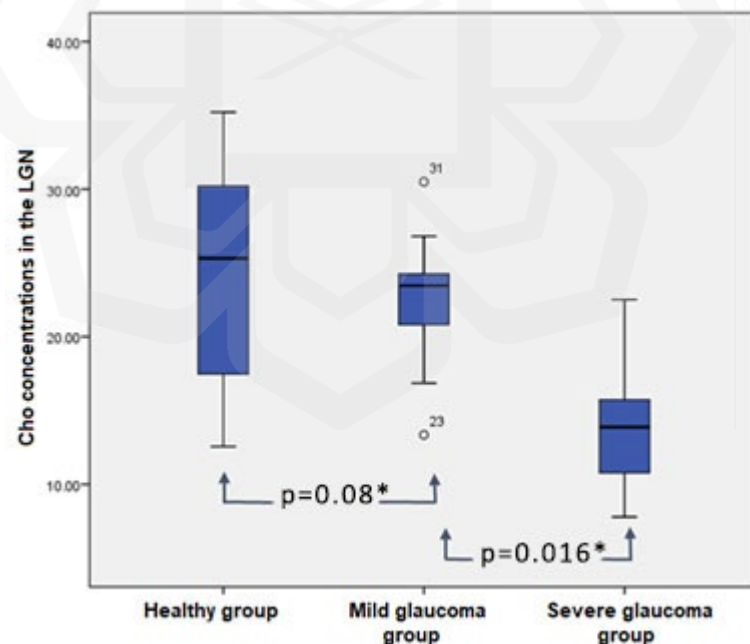


Figure 6.2 The box and whiskers plot illustrating the significant difference in mean of Cho between groups. There is a decrease in Cho amplitudes from 23.91 ± 7.02 in the healthy group to 14.09 ± 5.07 in the severe glaucoma group, a decrease of 9.82 (95% CI, 2.68 to 16.95) ($p=0.008$). There is also a significant decrease in Cho amplitudes from 22.63 ± 4.23 in the mild glaucoma group to 14.09 ± 5.07 in the severe glaucoma group, a decrease of 8.54 (95% CI, 1.82 to 15.26) ($p=0.016$).

The NAA/Cr ratio values are 1.49 ± 0.37 , 1.86 ± 0.41 , and 2.43 ± 1.25 for healthy group, mild glaucoma group, and severe glaucoma group, respectively. Welch ANOVA revealed that there is a significant mean difference ($p = 0.04$) between the groups (Table 6.3). Games-Howell post-hoc test revealed the NAA/Cr ratio is significantly higher in the mild glaucoma group relative to the healthy group (adjusted $p = 0.038$) (Figure 6.3). No significant difference in the metabolite ratio is recorded for Glx/Cr ($p=0.255$) (Table 6.3).

The Cho/Cr ratio values are 0.64 ± 0.15 , 0.70 ± 0.18 , and 0.48 ± 0.14 for healthy group, mild glaucoma group, and severe glaucoma group, respectively. One-way ANOVA revealed significant mean difference ($p = 0.029$) between the groups (Table 6.2). The Tukey post-hoc test revealed the Cho/Cr ratio is significantly higher in the mild glaucoma group compared to severe glaucoma group (adjusted $p = 0.023$) (Figure 6.4). No significant difference in the metabolite ratio is recorded for mI/Cr ($p=0.346$) (Table 6.3).

Table 6.3 Comparison of metabolites ratio in the LGN between groups.

Metabolites	Scanned LGN (mean \pm SD)			p value
	Healthy (n=17)	Mild glaucoma (n=14)	Severe glaucoma (n=6)	
Welch ANOVA				
NAA/Cr ^a	1.49 ± 0.37	1.86 ± 0.41	2.43 ± 1.25	0.040*
Glx/Cr ^a	11.80 ± 2.72	13.15 ± 2.47	15.20 ± 6.09	0.255
One-Way ANOVA				
Cho/Cr	0.64 ± 0.15	0.70 ± 0.18	0.48 ± 0.14	0.029*
mI/Cr	13.52 ± 6.16	11.99 ± 4.86	16.47 ± 8.97	0.346

*The mean difference is significant at the 0.05 level

^aThe Welch ANOVA test was used to compare means as Levene's test indicated that the homogeneity of variances assumption were not met for these variables.

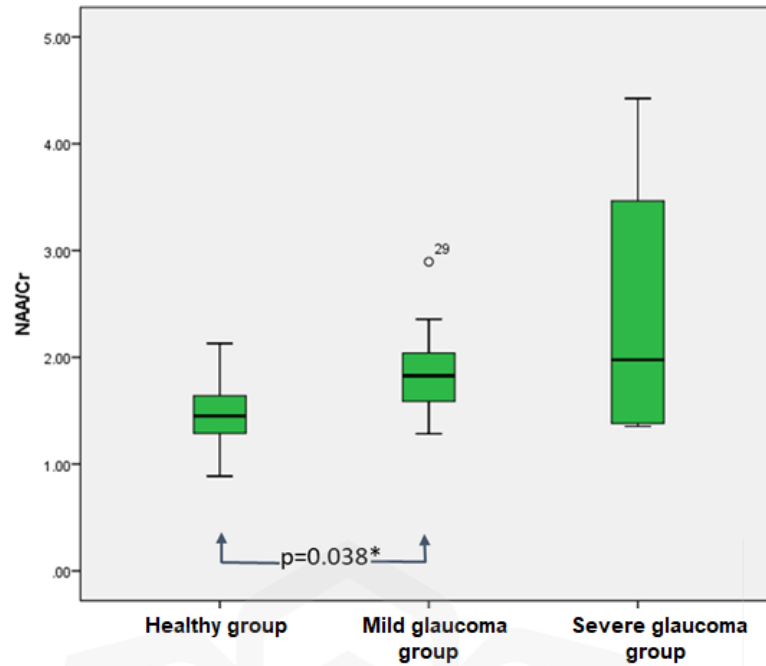


Figure 6.3 The box and whiskers plot show a lower NAA/Cr ratio in healthy group compared to the mild glaucoma group. There is an increase in NAA/Cr ratio in LGN from 1.49 ± 0.37 in the healthy group to 1.86 ± 0.41 in the mild glaucoma group, an increase of 0.37 (95% CI, 0.02 to 0.73) ($p=0.038$).

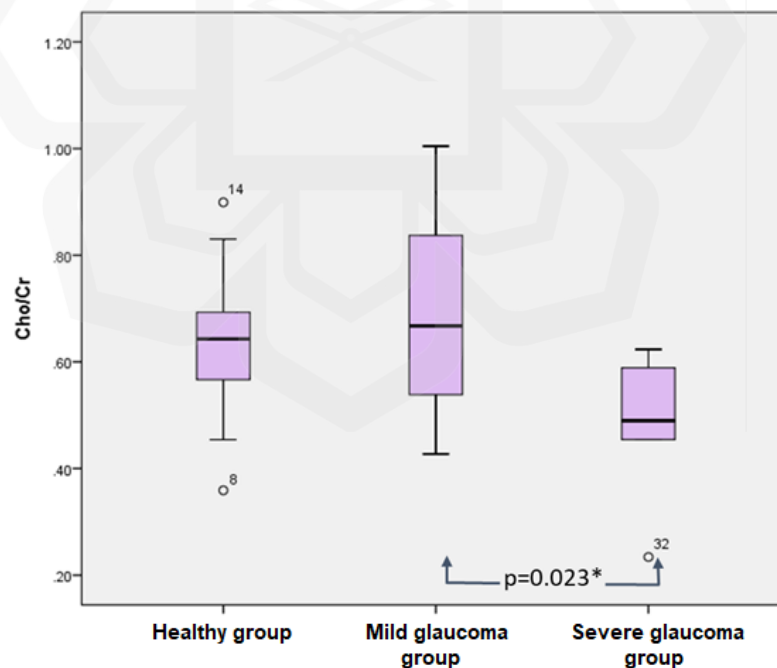


Figure 6.4 The box and whiskers plot show a decrease in Cho/Cr in the severe glaucoma group compared to the mild glaucoma group. There is a decrease in the Cho/Cr ratio in the LGN from 0.70 ± 0.18 in the mild glaucoma group to 0.48 ± 0.14 in the severe glaucoma group, a decrease of 0.22 (95% CI, 0.03 to 0.41), ($p=0.023$).

6.4 DISCUSSION

This current study adapted two approaches for quantitation of the metabolite concentrations in the LGN. The first method involves calculating the concentration amplitudes of metabolites using a method that matches spectrum integral value with a mathematically defined spectrum. The second method for metabolite concentration quantification was taken as the metabolite ratio, which data style is presented in the works of (Aksoy et al., 2018; Doganay et al., 2012). This metabolite concentration data value is similar to that reported by Aksoy et al. (2018).

The current study has established that glaucoma may yield different metabolite concentrations, by means of different metabolite concentration amplitude values or different metabolite ratio values, relative to the healthy controls. It was observed that the NAA concentration amplitude in the LGN of severe glaucoma group was significantly higher (65.03 ± 14.66) than the healthy subjects (53.31 ± 6.83) ($p=0.03$). In addition, it was found that the NAA/Cr ratio was recorded higher in the LGN of mild glaucoma group (1.86 ± 0.41) compared to the NAA/Cr ratio of the healthy group (1.49 ± 0.37) ($p=0.038$).

Different to the current findings, Aksoy et al. (2018) reported a lower NAA value in their glaucoma and suspected glaucoma groups, relative to the healthy control. To note, Aksoy et al. (2018) uses VOI size of $13 \times 13 \times 13$ mm on a 1.5 Tesla MRI, similar to the current study. However, it's worth noting that the mean ages of the healthy control and glaucoma groups in Aksoy et al.'s study were different from those in the current study. Specifically, Aksoy et al.'s healthy controls had a mean age of 49.27 ± 13.17 years, while the glaucoma group had a mean age of 53.80 ± 12.0 years. In contrast, the current study used healthy controls with a mean age of 50.8 ± 7.6 years and subjects with severe glaucoma with a mean age of 52.0 ± 11.8 years. These differences in age distribution may contribute to the discrepancies in NAA values observed between the two studies. Thus, the differing age distributions in the study populations should be taken into account when comparing NAA values. Moreover, other factors such as differences in the severity or duration of glaucoma and spectral analysis methods may also affect the results. To note, Aksoy et al. (2018) used software in their workstation to generate the MRS spectra and automatically quantify metabolite values.

On the other hand, Doganay et al. (2012) found no significant difference in the NAA/Cr ratio between glaucomatous group and the healthy group. They reported 1.15 ± 0.56 NAA/Cr ratio in glaucoma group and 1.44 ± 0.57 in healthy controls, a value not far to those in the current study. They placed the region of interest (ROI) size of $12 \times 12 \text{ mm}$ in the LGN using point resolved spectroscopy technique on a group of older subjects with a mean age of 65.8 ± 5.4 in glaucoma subjects and 62.8 ± 4.2 in healthy controls. With the MRI capability used in the current study, the smallest VOI size that could be applied was $13 \times 13 \times 13 \text{ mm}^3$, which is slightly larger than the $12 \times 12 \times 12 \text{ mm}^3$ VOI size used in the study by (Doganay et al., 2012).

It's worth noting that the specific VOI size that can be used in an MRS study depends on several factors. Differences in variables such as VOI size, MRI field strength, voxel localization method, and acquisition parameters (including TE and TR) can all contribute to variations in MRS results. For instance, the MRS acquisition parameters used in Doganay et al.'s study was different from this current study. Specifically, the TE and TR used in MRS acquisition can affect the spectral quality and signal-to-noise ratio of the data. The different in TE (136 ms) values in (Doganay et al., 2012) compared to the current study (TE =30 ms) could have allowed (Doganay et al., 2012) to use a smaller VOI size without sacrificing spectral quality or signal-to-noise ratio. Another factor that could affect the ability to use a smaller VOI size is the voxel localization method used. Different localization methods, such as point-resolved spectroscopy (PRESS) or STEAM have different sensitivities to voxel placement and geometry, which can affect the optimal VOI size that can be used. To note (Doganay et al., 2012) used PRESS localisation method, which is different from the STEAM used in the current study. Therefore, it is essential to acknowledge these potential sources of variability when contextualizing the findings.

It is uncertain what may be causes of the current study's observation on the increased NAA concentration in glaucoma subjects. But one may postulate the followings; (i) brain tissue being heterogeneous may lead to different metabolite concentrations findings (Grachev & Apkarian, 2000; Minati et al., 2010; Pouwels & Frahm, 1998), (ii) it is typical for the thalamus to have a very high concentration of NAA (Moffett et al., 2007), (iii) glaucoma is associated with reduction of the LGN's volume and size ((Kosior-Jarecka et al., 2020; J. Y. Lee et al., 2014), (iv) increase in NAA concentration may reflect a compensatory mechanism in response to the damage caused by glaucoma (Reichardt et al., 2022).

Taking all the postulations together, there is a possibility of the current study's VOI of $13 \times 13 \times 13 \text{mm}^3$ may be occupying more than the LGN area within the thalamus. This in turn may increase the likelihood of observing a stronger NAA concentration signal in the spectroscopy technique. Albeit a great care has been taken in placing the VOI at the desired LGN tissue area, the reduced LGN size due to glaucoma may overestimates the NAA concentration findings. Applying the multi-voxel spectroscopy (MVS) technique may improve measurement as MVS may be better suited for measuring heterogeneous, diffuse, and extensive areas of pathological changes in the brain (Jansen et al., 2006). With its large field of view, which can reflect the spatial distribution of metabolites, the MVS technique can increase signals while reducing the number of other tissues that are unintentionally included in the voxel (partial volume effect).

In some cases, the LGN may not be clearly visible on standard T1-weighted contrast imaging. Previous studies have suggested that in order to obtain a more distinct LGN image, a proton density-weighted image should be obtained (N. Gupta et al., 2009; Horton, Landau, Maeder, & Hoyt, 1990; M. Li et al., 2012). For example, (Fujita et al., 2001) highlighted that the LGN was not well defined by standard T1-weighted contrast imaging and suggested the use of a double-echo turbo spin echo sequence for proton density-weighted imaging, which provides better contrast between the LGN and surrounding white matter.

In this current study, only a three-dimensional T1-weighted (3DT1W) image was obtained for anatomical reference prior to the examination. While subjective bias of volume of interest (VOI) placement is always a possibility, particularly for small structures such as the LGN, extensive care was taken in this study to ensure the VOI placement in the LGN excluded any bones, subcutaneous tissues, vasculatures, or other tissues that could have potentially interfered with the measurements. Although proton density-weighted images were not obtained in this study, the careful VOI placement reduces the likelihood of any potential bias in the results due to imperfect imaging.

The NAA has been suggested as a marker of neuronal integrity (Moffett et al., 2007). Considering NAA has the greatest peak in the adult brain spectrum, it was suggested that its reduction may be indicative of neuronal and axonal damage. On a different note, there are reports of NAA levels elevation in the brain corresponding to certain pathologies. As elaborated earlier in the second chapter of this thesis, increased NAA concentration may be associated to disease such as the sickle cell illness or Canavan disease (Moffett et al., 2007; Steen & Ogg, 2005). In addition, there was also report of an animal study of spiking NAA concentrations upon administration of haloperidol, an anti-psychotic drug (Harte, Bachus, & Reynolds, 2005).

The observed increase in NAA concentrations in the LGN of glaucoma subjects may be indicative of a compensatory response to the ongoing damage caused by the condition. The grounding of these findings was made based on a previous study that suggested that increased NAA levels in the brain may be a compensatory response to improve brain function (Reichardt et al., 2022). Reichardt et al., (2022) found a significant increase of NAA concentration in frontal white matter in patients with neuropsychiatric symptoms in hepatitis C (7.05 ± 1.11), autoimmune hepatitis (7.06 ± 1.00), and primary biliary cholangitis (7.30 ± 0.83) compared to healthy control (6.16 ± 0.89). In this current study, the higher NAA levels observed in the LGN of glaucoma groups may reflect an attempt by the brain to maintain neuronal integrity or function in the face of ongoing damage from glaucoma. Further research is needed to clarify the mechanisms underlying the observed differences in NAA levels in the LGN between healthy controls and glaucoma groups.

In this current study, a noteworthy finding emerged regarding Cho concentration amplitude within the LGN among subjects with varying degrees of glaucoma severity. Cho concentration amplitude demonstrated a statistically significant reduction in the LGN of subjects with severe glaucoma compared to those with mild glaucoma ($p=0.016$) and is lower in the mild glaucoma group relative to the healthy controls ($p=0.008$). Similarly, the Cho/Cr ratio shows significant decrease in the LGN of subjects with severe glaucoma compared to the mild glaucoma group ($p=0.023$). These reduction in Cho may be interpreted as a sign of deteriorating cell integrity due to apoptosis in neuronal tissues in the LGN of the glaucoma patients. These findings are consistent with those of Aksoy et al. (2018), where they reported of a decreased Cho levels in the LGN of their glaucoma group.

Doganay et al., (2012) on the other hand reported no significant changes in the Cho levels in their glaucoma group. Reduction of Cho in glaucoma patients may suggest of a neuronal loss in the LGN region (Y. Zhang et al., 2013). Cho plays an important role in the synthesis and degradation of cell membranes and is one of the key substances that regulate cell apoptosis (Y. Zhang et al., 2013). In contrast to necrosis, apoptosis is a process of programmed cell death that results in destruction of intracellular organelles. Therefore, a decline in Cho levels may indicate neuronal apoptosis. Y. Zhang et al., (2013) concluded in their study that the decrease in Cho in the geniculocalcarine tract of glaucoma patients is the cause of neuronal apoptosis in this region.

There have been several reports of decreased Cho levels in various regions of the brain. For example, a study by Cecil, Lenkinski, Gur, & Gur, (1999) found significantly lower Cho/Cr ($p=0.0059$) levels in the temporal lobes of patients with schizophrenia disorder compared to healthy controls. Similarly, a study by (Kumar et al., 2021) reported decreased Cho/Cr levels in the dorsolateral prefrontal cortex in hyperthyroid patients (0.249 ± 0.036) compared to healthy controls (0.290 ± 0.047). These findings suggest that measuring Cho levels using magnetic resonance spectroscopy has the potential to provide valuable insights into the pathophysiology of different brain disorders.

In summary, the observed reduction in Cho levels bears significant implications for understanding the underlying pathological processes associated with glaucoma. Cho is a pivotal component involved in the synthesis and degradation of cell membranes, exerting a crucial role in regulating cellular apoptosis. The decline in Cho levels may serve as a sensitive marker indicative of neuronal loss in the LGN region. It is noteworthy to acknowledge the discrepancies in findings across different studies. This discrepancy underscores the importance of considering various methodological factors, including VOI size, field strength, and acquisition parameters, which may contribute to variations in MRS results. Additionally, the potential impact of age-related changes on metabolite concentrations should not be overlooked, as it may account for some of the observed differences. By considering methodological variations and potential confounding factors, future studies can further elucidate the role of Cho in glaucoma pathogenesis, potentially opening new avenues for therapeutic intervention and early detection strategies.

6.5 CONCLUSION

This current study demonstrated alterations in the LGN metabolites of subjects with glaucoma. The data from this current study adds evidence to the molecular changes that takes place in the LGN of glaucomatous subjects. Further improvement to the MRS technique may aid a non-invasive analysis of the metabolites in the LGN, which in turn may add clinical value for glaucoma detection and management.

CHAPTER SEVEN

METABOLITES CONCENTRATION IN THE VISUAL CORTEX OF GLAUCOMA PATIENTS

Abstract

Purpose

This study aimed to determine the metabolite concentrations of N-acetyl aspartate (NAA), creatine (Cr), choline (Ch), glutamate (Glx), and myo-inositol (mI) in the visual cortex (VC) in subjects with glaucoma using magnetic resonance spectroscopy (MRS). The study also aimed to compare the metabolite concentrations between groups of healthy subjects, subjects with mild glaucoma, and subjects with severe glaucoma.

Material and methods

MRS acquisition using a single-voxel spectroscopy (SVS) technique was performed using 1.5 Tesla MRI on nine healthy subjects (50.8 ± 7.6 years), seven subjects with mild glaucoma (59.4 ± 10.2 years), and three subjects with severe glaucoma (52.0 ± 11.8 years). Glaucoma severities were categorized based on the Hodapp-Parrish-Anderson (HPA) classification. A standardized volume of interest (VOI) of $13 \times 13 \times 13$ mm was placed in both (bilateral) VCs of each subject. Spectral editing for metabolites was conducted for each scan. Using jMRUI fitting software, metabolites were quantified as concentration amplitudes in arbitrary units and then quantified further to obtain metabolite ratios for use in statistical analysis. Normality of data were tested using the Shapiro-Wilk normality test. Data homogeneity of variance was determined using Levene's test. Metabolites concentrations and ratios were compared between groups using one-way ANOVA and Welch ANOVA. The Kruskal–Wallis test was used for comparing data that did not conform to normality. Post-hoc test was conducted to test all possible group comparisons.

Results

The metabolites concentration amplitude in the VC in group with mild glaucoma are 57.93 ± 7.44 , 713.21 ± 216.61 , 41.34 ± 6.05 , 17.12 ± 4.81 and 296.85 ± 93.74 for NAA, Glx, Cr, Cho, and mI, respectively. Group with severe glaucoma recorded metabolite concentrations amplitude of 54.78 ± 7.78 (NAA), 604.93 ± 93.55 (Glx), 43.37 ± 6.84 (Cr), 12.92 ± 2.92 (Cho), and 424.01 ± 99.41 (mI). Healthy controls recorded metabolite concentrations amplitude of 56.17 ± 9.50 (NAA), 745.00 ± 109.27 (Glx), 45.90 ± 5.91 (Cr), 16.41 ± 3.24 (Cho), and 293.03 ± 46.55 (mI). A significant decrease in the Glx concentration amplitude (Games-Howell, $p=0.031$) is recorded in the severe glaucoma group relative to the healthy control group. No significant mean differences are found for NAA, Cr, Cho, and mI concentration amplitudes between the groups (one-way ANOVA $p>0.05$). The Cho/Cr ratio shows a significant decrease in the severe glaucoma group relative to the mild glaucoma group (Tukey HSD, $p=0.031$). No significant mean differences are found for Glx/Cr and mI/Cr ratios between the groups ($p>0.05$).

Conclusion

Glaucoma causes shift in the metabolite concentration amplitudes and ratio in the VC. Severe glaucoma subjects showed lower Glx concentrations and lower Cho/Cr ratio in the VC relative to the healthy groups and mild glaucoma groups respectively.

Keywords: proton magnetic resonance spectroscopy, glaucoma, visual cortex, single voxel spectroscopy, N-Acetyl Aspartate, Creatine, Choline, Glutamate, Myo-Inositol

7.1 INTRODUCTION

The VC is located along the superior and inferior sides of the calcarine fissure in the occipital lobe, which is located in the posterior region of the brain (Huff et al., 2022; Sheffield, 2022). Visual information from the retina is conveyed to the VC through the LGN where it is received, integrated, and processed (Huff et al. 2022). Glaucoma is a disease that causes a progressive visual field defect that may prevent normal stimulation of the VC (Boucard et al., 2007). The degeneration and atrophy of the VC may be the direct result from glaucomatous related atrophy of the optic nerve and visual tract, caused by the apoptosis of retinal ganglion cells (RGC) (You, Rong, Zeng, Xia, & Ji, 2021). Apoptosis of the RGCs is a hallmark for glaucoma pathological characteristics (H. A. Quigley, 1999).

Glaucomatous damage on the VC may be primarily due to trans neuronal degeneration, evidenced with the decline of neuronal activity in the retinal-lateral geniculate nucleus (LGN)-VC pathway (You et al., 2021). A significant loss of LGN relay neurons terminating in the VC was reported in glaucoma induced-affected monkeys which resulted in VC damage (Yücel, Zhang, Gupta, Kaufman, & Weinreb, 2000; Yücel et al., 2003). Animal study involving glaucomatous marmosets reported a reduction in the VC volume using the magnetic resonance imaging (MRI), matches the degeneration of the LGN and VC that they found using histological analyses (Noro et al., 2019). The depression of brain-derived neurotrophic factor (BDNF) and tropomyosin receptor kinase B (TrkB), which play important roles in neuroprotection for RGCs, was evident in glaucomatous marmosets. These findings reinforce the claims made by You et al. (2021) that atrophy of the central visual system occurs in glaucoma animal models, and that trans neuronal degeneration in the visual pathway appears to be one of the sources of damage to the VC.

Human studies reported the similar observations on glaucoma patients. Studies have reported of reduced VC thickness and volume, functional abnormalities, and connectivity disruption among glaucoma patients (Giorgio, Zhang, Costantino, De Stefano, & Frezzotti, 2018; T. Li et al., 2020; Nuzzi et al., 2018b). Murphy et al. (2016) reported a compromised integrity in the optic radiation of subjects with severe glaucoma, together with compromised anatomical findings at the retinal level. They also reported changes at the VC level that matches the peculiarities at the LGN and retina. Gupta et al. (2006) evaluated the VC area under the sulcus calcarine using Nissle staining on cadaver brain of patients with severe glaucoma. They reported a significant thinning of the VC relative to control brain that was correlated with visual field loss, retinal optic nerve head damage and functional visual field defect. These findings suggest that glaucoma causes structural, and functional changes to both ocular and brain particularly the VC, which may as well cause metabolic changes in the area.

It appears necessary to conduct further research on metabolite interactions in VC, as atrophy of anatomical structures associated with the visual pathway results in neurodegeneration of the involved anatomy in glaucoma brain, as discussed in the literature review chapter. Early onset metabolic changes in the brain may be indicative of diseases like glaucoma, and MRS, as a non-invasive spectroscopic technique, may make this possible. The aim of this study was to determine the characteristics of metabolites in the VC on glaucoma subjects. The results of this study may contribute to a better understanding of glaucoma pathogenesis involving the VC.

7.2 SPECIFIC METHODOLOGY

7.2.1 Methodological Variation

In this experiment, the subjects, the methodology for conducting spectroscopy acquisition, and the approach to analysing spectroscopy data closely mirror those outlined in Chapter Six. The primary deviation in this experiment pertains to the specific location of the Single-Voxel Spectroscopy (SVS) technique with stimulated echo acquisition mode (STEAM) technique, which was conducted within the VC from both hemispheres of each subject's brain.

7.2.2 Statistical Analysis

Descriptive data are presented as mean \pm standard deviation (SD). All data in this study were analysed using IBM SPSS software version 23 (SPSS Inc., Chicago, IL, USA) licensed under the International Islamic University Malaysia. Normality of data were tested using the Shapiro-Wilk normality test. Data homogeneity of variance was determined using Levene's test. Metabolites concentrations and ratios data with homogeneity of variance were compared using one-way Analysis of variance (ANOVA), whereas data with violated homogeneity of variance were compared using Welch ANOVA. The Kruskal–Wallis test was used for comparing metabolite concentrations that did not conform to normality. Statistical significance was set at $p < 0.05$.

7.3 RESULTS

The Glx amplitude values are 745.00 ± 109.27 , 713.21 ± 216.61 , and 604.93 ± 93.55 for healthy group, mild glaucoma group, and severe glaucoma group respectively. Welch ANOVA revealed that there is a significant mean difference ($p = 0.031$) between the groups (Table 7.1). Games-Howell post-hoc test revealed the Glx amplitude is significantly lower in the severe glaucoma group relative to the healthy group (adjusted $p = 0.031$) (Figure 7.1). No significant differences in the metabolite amplitudes are recorded for NAA ($p=0.721$), Cr ($p=0.131$), Cho (0.092) and mI ($p=0.843$) (Table 7.1).

Table 7.1 Comparison of metabolites concentration amplitude in the VC between groups.

Metabolites	Scanned VC (mean \pm SD)			P value
	Healthy (n=17)	Mild glaucoma (n=14)	Severe glaucoma (n=6)	
One-way ANOVA				
NAA	56.17 ± 9.50	57.93 ± 7.44	54.78 ± 7.78	0.721
Cr	45.90 ± 5.91	41.34 ± 6.05	43.37 ± 6.84	0.131
Cho	16.41 ± 3.24	17.12 ± 4.81	12.92 ± 2.92	0.092
mI	293.03 ± 46.55	296.85 ± 93.74	312.56 ± 63.32	0.843
Welch ANOVA				
Glx ^a	745.00 ± 109.27	713.21 ± 216.61	604.93 ± 93.55	0.031*

*The mean difference is significant at the 0.05 level

^aThe Welch ANOVA test was used to compare means as Levene's test indicated that the homogeneity of variances assumption was not met for this variable.

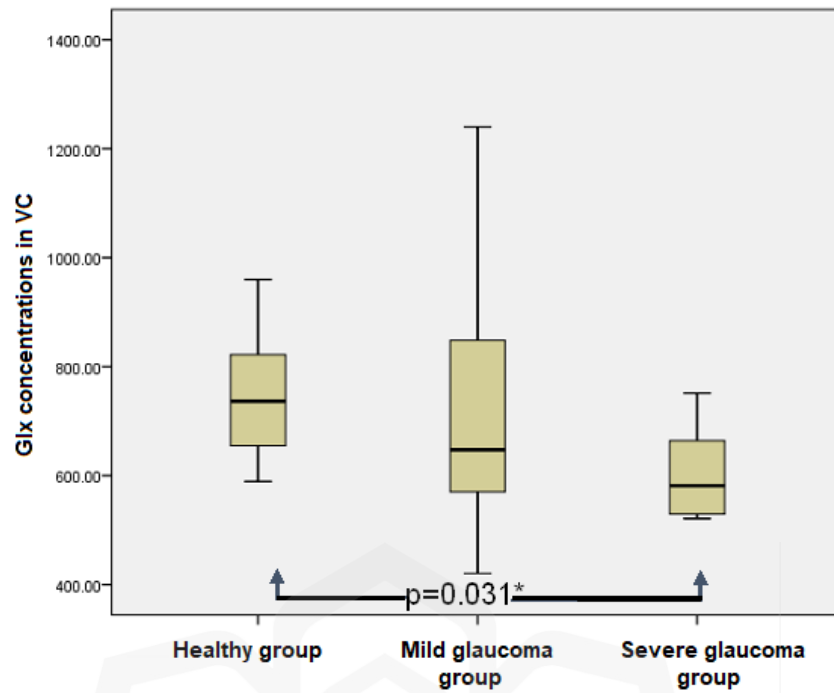


Figure 7.1 The box and whiskers plot illustrate a significantly lower Glx amplitude in the severe glaucoma group compared to the healthy group. There is a decrease in Glx amplitudes in VC from 745.00 ± 109.27 in the healthy group to 604.93 ± 93.55 in the subjects with severe glaucoma group, a decrease of 140.07 (95% CI, 13.13 to 267.03) ($p=0.031$).

The Cho/Cr ratio values are 0.36 ± 0.08 , 0.42 ± 0.11 , and 0.30 ± 0.06 for healthy group, mild glaucoma group, and severe glaucoma group, respectively. One-way ANOVA revealed that there is a significant mean difference ($p = 0.034$) between the groups (Table 7.2). Tukey HSD post-hoc test revealed the Cho/Cr ratio is significantly higher in the mild glaucoma group relative to the severe glaucoma group (adjusted $p = 0.031$) (Figure 7.2). No significant differences in the metabolite ratios are recorded for NAA/Cr ($p=0.138$), Glx/Cr ($p=0.086$) and ml/Cr ($p=0.329$) (Table 7.2).

Table 7.2 Comparison of metabolites ratio in the VC between groups.

Metabolites	Scanned VC (mean \pm SD)			p value
	Healthy (n=17)	Mild glaucoma (n=14)	Severe glaucoma (n=6)	
Kruskal Wallis				
NAA/Cr ^a	1.23 \pm 0.21	1.44 \pm 0.35	1.30 \pm 0.31	0.152
Welch ANOVA				
Glx/Cr ^b	16.45 \pm 3.00	17.40 \pm 5.14	14.11 \pm 2.14	0.086
One-Way ANOVA				
Cho/Cr	0.36 \pm 0.08	0.42 \pm 0.11	0.30 \pm 0.06	0.034*
ml/Cr	6.45 \pm 1.12	7.22 \pm 1.96	7.30 \pm 1.79	0.329

*The mean difference is significant at the 0.05 level

^aThe Kruskal-Wallis test was used to compare means as data did not conform to normality.

^bThe Welch ANOVA test was used to compare means as Levene's test indicated that the homogeneity of variances assumption was not met for this variable.

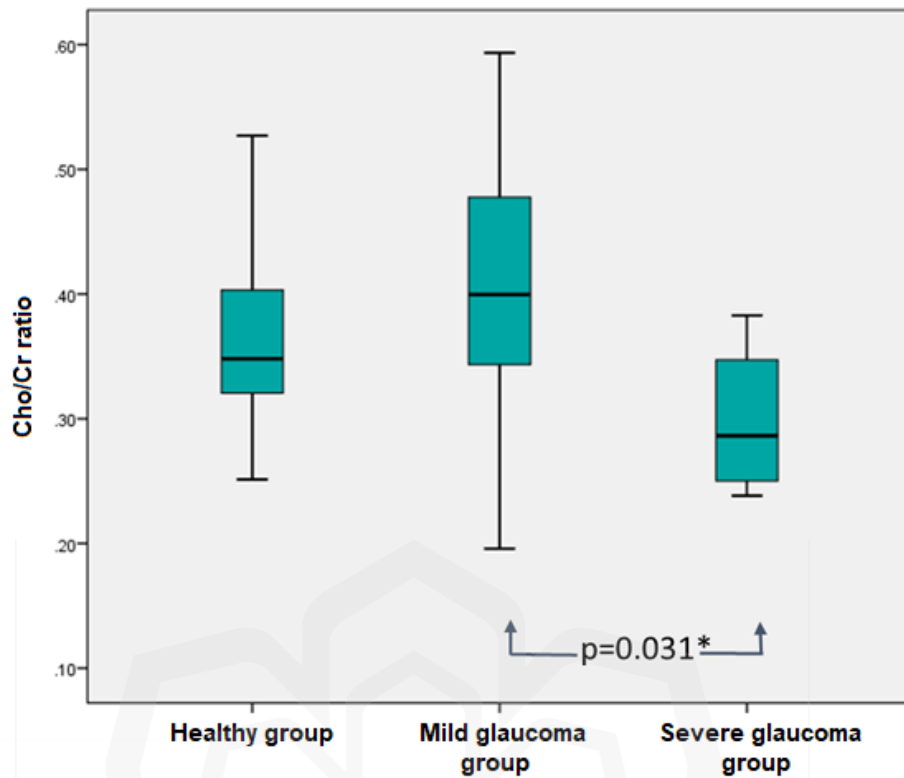


Figure 7.2 This box and whiskers plot illustrates the significant reduction in the mean Cho/Cr in the severe glaucoma group compared to the mild glaucoma group. There was a decrease in the Cho/Cr ratio in the VC from 0.42 ± 0.11 in the mild glaucoma group to 0.30 ± 0.06 in the severe glaucoma group, a decrease of 0.12 (95% CI, 0.01 to 0.23) ($p=0.031$).

7.4 DISCUSSION

The current study observes a significant reduction in the Glx concentrations amplitude in the VC of subjects with severe glaucoma (604.93 ± 93.55), as compared to the healthy subjects (745.00 ± 109.27). Using data based on the metabolite ratio, Guo et al. (2018) reported a higher Glx/Cr ratio, and a lower ml/Cr ratio in the VC of their early open angle glaucoma group relative to the controls. To support their findings, Guo et al. (2018) argued that the spike in Glx concentration is due to the extended exposure of glutamate, a neurotransmitter, to the neuronal receptors. The extended exposure in turn results in neuronal death, closely relate to the apoptosis that occur in glaucoma pathophysiology. They further argued that observation in the VC was consistent with the other studies that observed brain's Glx spike such that from Doganay et al. (2012), and Okuno et al. (2006). However, it is important to iterate that Doganay et al. (2012), and Okuno et al. (2006) saw the increment of Glx concentration not in the VC, but rather at the optic nerve and LGN, respectively.

The possible explanation of the contradicting observation in this current study to that of Guo et al. (2018) may be stemmed from the recruited glaucoma subjects. Specifically, the pathological process in severe glaucoma patients, as recruited in this study, may not be as active compared to early glaucoma patients as recruited in Guo et al. (2018) study. This difference in disease stage could have led to a greater degree of neuronal death in early glaucoma patients, which may result in a higher Glx/Cr ratio, as observed in the Guo et al.'s study. Specifically, the current study recruited patients with severe glaucoma, whose disease may be at a more advanced stage and therefore characterized by a lower degree of active pathological changes compared to early glaucoma patients. This could result in a lower degree of excitotoxicity and glutamate release in the LGN in severe glaucoma patients, which may explain the observed reduction in Glx levels. In a different take, other MRS study on the VC which includes Boucard et al. (2007), Zhang et al. (2013), Murphy et al. (2016) and Aksoy et al. (2018) did not observed any changes in the Glx concentrations in the VC of their glaucoma subjects. Given to the inconsistent observations in the body of literature, it should be noted that the exact mechanisms underlying the changes in Glx/Cr ratio in different stages of glaucoma are still not fully understood, and further research is needed to elucidate these mechanisms.

To further reiterate, metabolite concentrations value disagreement among the literature could also be attributed to the site of measurement (Grachev & Apkarian, 2000; Minati et al., 2010; Pouwels & Frahm, 1998). Metabolic concentration values across a typical brain structure may be reported differently as a direct result of heterogeneity of human brain tissue (Govindaraju et al., 2000). Other factors that may affect metabolite quantitation include MRS technique from different scanners employed, partial volume effect, and low signal-to-noise ratio, despite the fact that measures have been taken to ensure homogeneous magnetic field and suppression of water signal from tissue (Barker, 2001; Kreis, 2004). For instance, the current study used MRS technique with a small VOI measured at $13 \times 13 \times 13$ mm. Comparatively, Guo et al. (2018) used $20 \times 30 \times 20$ mm VOI, Zhang et al. (2013) used $18 \times 18 \times 10$ mm VOI, Murphy et al. uses $20 \times 25 \times 30$ mm VOI, and Aksoy et al. (2018) used $20 \times 20 \times 20$ mm VOI. The use of different VOI sizes may yield different observations on the metabolite concentrations.

Cho is one of the most abundant metabolites in the brain and essential for cell membrane synthesis and degradation (Blusztajn, 1998; Zeisel & Da Costa, 2009) In this current study, it was observed that the Cho/Cr ratio was lower in the VC of severe glaucoma group than those in with mild glaucoma group. The group with severe glaucoma recorded Cho/Cr concentration ratio of 0.30 ± 0.06 while the group with mild glaucoma recorded 0.42 ± 0.11 . The healthy controls recorded a higher mean of 0.36 ± 0.08 , higher than the severe glaucoma albeit statistical analysis revealed no significance between the two.

On the same note of the current study, Y. Zhang et al., (2013) reported a decreased in Cho/Cr ratio in the VC, using a multiple voxel technique MRS. Y. Zhang et al., (2013) noted a reduction in the NAA/Cr in the glaucoma group. They concluded that Cho reduction in the VC as a sign of active neurodegenerative processes due to glaucoma. Murphy et al. (2016) also recorded a lower level of Cho in the VC following the severity of glaucoma in their recruited subjects. They argued glaucoma leads to a reduced cortical cholinergic function, a similar observation in other neurodegenerative diseases such as Alzheimer's (Miettinen et al., 2015; Rombouts, Barkhof, Van Meel, & Scheltens, 2002). Studies have shown that functional brain responses were improved with cholinergic stimulation in neurodegenerative diseases (Bentley, Driver, & Dolan, 2008; Miettinen et al., 2015).

Taking in a similar context (glaucoma is a neurodegenerative disease), a reduction in Cho concentration in the VC may indicate cholinergic neurotransmission involvement in the visual deterioration in the VC of subjects with glaucoma. Therefore, reduction in Cho may indicate that apoptosis, neuronal damage, and a slowing in cellular metabolism are already occurring. Boucard et al. (2007), Guo et al. (2018) and Aksoy et al., (2018) on the other hand, reported no significant change in the Cho concentration in the VC.

In this current study, no significant changes between groups were recorded for NAA, Cr, and mI in the VC. The mean difference in NAA in the VC of the severe glaucoma groups (54.78 ± 7.78) was, however, lower than that in the healthy group (56.17 ± 9.50), despite of being not statistically significant, is noteworthy. A similar observation was reported by Zhang et al. (2013) and Aksoy et al. (2018), which noted a reduced NAA level in the glaucoma group relative to the healthy group. They advocated that the reduction in the NAA concentration in their glaucoma group may indicate functional or structural damages to neurons and axons, emphasizing the NAA as an important biomarker for evaluating the survival of both neurons and axons in the brain.

In summary, the present study provides valuable insights into the metabolic alterations occurring in the VC of subjects with severe glaucoma. While the observed changes in Glx and Cho concentrations suggest potential indicators of glaucoma pathophysiology, it is essential to consider disease severity and stage when interpreting MRS results. The discrepancies across studies underscore the need for further research to elucidate the precise mechanisms underlying these metabolic changes in glaucoma.

7.5 CONCLUSION

This current study shows evidence of metabolite changes in the VC of glaucoma patients, particularly the Glx and Cho. The information obtained in this study on the metabolites alteration in the VC may suggest that the VC of glaucomatous subjects are experiencing continuing neurodegenerative processes. The MRS technique may be utilized as a non-invasive methodology for analysing molecular changes in the VC, which in turn may add clinical value for glaucoma detection and management.



CHAPTER 8

CONCLUSION

8.1 GENERAL DISCUSSION

The MRS technique being non-invasive have the potential as a clinical tool in aiding diagnosis and management of diseases. The MRS enables an in vivo measurement allowing sensitive tissues, such as the brain, to be measured. The MRS has a potential to be an important clinical application in the future. The current study has demonstrated that the MRS is a repeatable and reliable technique in measuring the LGN and VC metabolites concentrations. Chapter 4 findings have indicated that the measurements of the NAA, Glx, Cr, Cho and mI metabolites were repeatable using the single voxel spectroscopy of a 1.5 Tesla MRI system in the LGN and the VC. It was shown that the range of repeatability coefficient (RC) percentage for Cho in LGN and VC and coefficient variation (CV) percentage for NAA, Cho and Cr in VC were comparable to previous published studies.

Chapter 5 of this thesis details the experiment comparing metabolites concentrations in the LGN and the VC between young and elderly. It was shown that in the LGN, all metabolites except the mI having significantly different values between the two age groups, with NAA shows reduction with age and the others reported the opposite. While in the VC, the Cr, Cho and mI were observed to be significantly higher in the elderly group. The significant difference between elderly's concentrations to that of the younger group may indicate the healthy aging effect on metabolite concentrations. These data are important in this study as they serve as a baseline of metabolite concentration for both age groups. The data also served as a baseline upon comparison to metabolic data of patients with glaucoma, the disease of interest in this study.

Chapter 6 of this thesis details the metabolic concentration comparison in the LGN between healthy controls to groups with mild glaucoma and severe glaucoma. It was found that the NAA concentration is significantly higher than those of healthy controls. One possible explanation for this observation is that the increased NAA concentration may reflect a compensatory mechanism in response to the damage caused by glaucoma. The Cho reduction following the severity of glaucoma was also observed. These reduction in Cho may be interpreted as a sign of deteriorating cell integrity due to apoptosis in neuronal tissues in the LGN of the glaucoma patients.

Chapter 7 of this thesis details the metabolic concentration comparison in the VC between healthy controls to groups with mild glaucoma and severe glaucoma. The current study observed a reduction in Glx concentration in the severe glaucoma group relative to the healthy controls, which may be explained by advanced stage glaucoma is characterized by a lower degree of active pathological changes compared to early glaucoma patients, hence result in a lower degree of excitotoxicity and glutamate release in the LGN. The current study also saw reduction of Cho in the severe glaucoma group, indicating apoptosis, neuronal damage, and a slowing in cellular metabolism are occurring.

Based on the findings, it appears that there are neurochemical changes associated with both healthy aging and severe glaucoma, but the specific patterns differ between the two conditions. The metabolite changes of healthy aging, as mentioned above, suggest alterations in neuronal health and metabolism. Meanwhile, the metabolite changes of severe glaucoma in LGN and VC, as mentioned above, may reflect the impact of glaucoma on the neurochemical environment in these brain areas involved in visual processing. Additionally, the variation in metabolite concentration observed in LGN and VC in this study means that the biochemical makeup and processes occurring in these two regions exhibit unique metabolite profiles. These indicate that the metabolite profiles obtained are actually based on specific functions or responses to various physiological or pathological conditions. These findings also suggest that metabolite changes associated with healthy aging may overlap with some of the metabolic changes seen in severe glaucoma. This implies that age-related metabolic shifts and brain regional differences should be considered when studying glaucoma. These aspects are crucial in contextualising a study's findings, as they may confound or influence the interpretation of metabolic changes specific to the disease.

In a general perspective, there is lacking in consensus of the exact metabolite concentrations in the LGN and VC of patients with glaucoma. With only handful literatures available, different observations were reported which may be stemmed to different MRS setting, anatomy of interest, and the imaging system the study applied. This current study adds to the body of knowledge on metabolite concentrations in glaucoma, especially involving the LGN and VC. The findings in this current study, whether or not in line with the earlier research, open for new avenues of understanding the pathophysiological details of glaucoma, which may be beneficial in aiding its diagnosis and management.

8.2 CONTRIBUTION AND BENEFITS OF THE RESEARCH

This comprehensive study makes notable contributions to both the field of neurobiology and clinical practice. By demonstrating the potential of MRS as a non-invasive clinical tool, it paves the way for improved disease diagnosis and management, with implications for enhanced healthcare outcomes globally. The research has established a standardised approach to conducting MRS acquisition that can serve as a resource for both clinicians and researchers alike. This research not only advances scientific knowledge but also has extensive societal benefits, potentially reducing the burden of visual impairments associated with glaucoma, thereby positively impacting public health and contributing to the overall well-being of the population. Additionally, the study's rigorous methodology and significant findings make it a noteworthy addition to the body of scientific literature, enhancing the national and international research landscape.

The study's findings also hold significant applications and implications across various domains. In clinical medicine, the insights of metabolite concentration change provide a crucial foundation for healthcare professionals. Understanding the subtle changes in metabolite concentrations associated with healthy aging and glaucoma equips clinicians with invaluable information to refine diagnoses and tailor treatment approaches for their patients. In addition, this research is poised to play a pivotal role in the field of geriatric medicine. By shedding light on the complexities of age-related metabolic shifts, it offers a deeper understanding of the healthcare needs specific to older individuals. Furthermore, this work has direct relevance within the field of ophthalmology. The identification of metabolite alterations in severe glaucoma represents a potential breakthrough in the understanding and management of this condition, potentially leading to more effective therapeutic strategies for patients affected by glaucoma.

8.3 THE LIMITATION OF THE STUDY RESULTING FROM THE IMPACT OF COVID-19

This study was heavily affected by the pandemic Corona virus disease (COVID-19). During the data collection stage, the Malaysian government implemented the movement control order (MCO) on March 18, 2020, which severely restricted the movement of all civilians. To a greater difficulty, the data collection was conducted in the vicinity of Sungai Buloh, near the COVID-19 designated Sungai Buloh Hospital, which created pessimistic perceptions for subject recruitment. This significantly disrupted the data collection and limited the study's sample size, as both the researcher and subjects were unable to travel to the study site. The original aims of the study were restructured, and the study design was amended yet fitting a doctoral study workload and scope. Due to COVID-19, some amendments were made digressing from the intentional study plan.

1. The initial plan of the study was to include different classes of glaucoma, apart of the current severe and mild glaucoma group. It was thought to include suspected glaucoma, and normal tension glaucoma as well into the study. The inclusion of these glaucoma subgroups may yield a deeper information of metabolite concentration in this disease. Future studies could employ all glaucoma subgroups for a more holistic research coverage.
2. It was also originally planned for the study to include the 3.0 Tesla MRI system as a method of measurement. Nevertheless, due to logistical and sampling issues, exaggerated by the situation posed by the MCO, a 1.5 Tesla MRI system was deemed the best at the point of data collection. It would be interesting to obtain MRS reading from a powerful MRI system, such that can be obtained from a 3.0 Tesla MRI system, yet this expedient could be conducted in the future studies.
3. The original objective of the study was to recruit at least 15 subjects per group; however, due to the restrictions imposed by the pandemic, full recruitment was not possible, and the study had to proceed with a smaller sample size. Despite this setback, it was determined that the study's final sample size was sufficient for analysing the objectives of the study. However, future studies with larger sample sizes are highly recommended to expand these results.

The amendments made to the original study plan do not by any intention, reduce the academic prestige of the current study. As per the elaborations, any limitations in the current study shall be justified for an opportunity for future experiments.

8.4 STUDY LIMITATION AND FUTURE STUDIES

This study has several limitations. First, the sample size was relatively small. There were only mild glaucoma group and severe glaucoma group included in the study. The small sample may miss important observations such that that may be occurring in other glaucoma groups such as moderate glaucoma, suspected glaucoma, normal tension glaucoma, and ocular hypertensives. Future studies may incorporate these other glaucoma groups for a greater investigation on glaucoma.

Second, this current study used metabolite concentration amplitude that was obtained from the amplitude magnitude of the acquired spectra using jMRUI software for use in statistical analysis. Future research should consider using techniques that enable the computation of more accurate absolute metabolite concentrations, as it allows for a more precise quantification of metabolite concentrations, can provide a better understanding of the underlying biochemical changes and it can be useful in comparing metabolic changes between different studies.

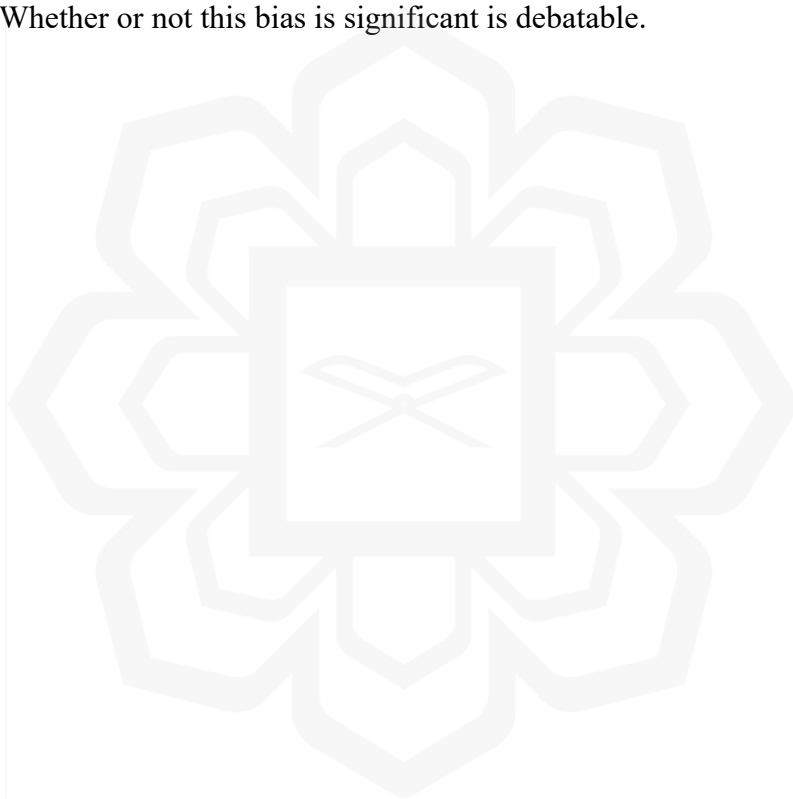
Third, it should be emphasized that single-voxel spectroscopy makes it impossible to choose an identical VOI that fits the geometry of the LGN and VC while also preventing extraneous tissue contamination, which could affect the metabolic concentration and may not exactly reflect degeneration or atrophic field. Future studies should investigate the performances of single- and multi-voxel spectroscopy.

Fourth, one radiographer and one spectral reviewer were assigned to locate the VOI and measure the amount of each metabolite. Inter-operator repeatability of the spectral analysis was not investigated. A study with different radiographers and spectral reviewers under the same conditions need to be established in the future studies.

Fifth, the measurements were taken only on the LGN and VC. Considering there are more areas involved in the visual pathway, metabolites measurements may be warranted in areas such as the vitreous, mid brain, or optic radiation. Such experiments may yield a deeper coverage on the effect of glaucoma on different areas of the brain.

Sixth, the MRS employed in this study was using 1.5 Tesla MRI scanner. While this is a widely used field strength for clinical MRI, higher field strengths, such as 3 Tesla or 7 Tesla, may provide greater information on the metabolite concentrations in the brain.

One general caveat to keep in mind regarding the overall elements of this work has to do with the selection process for healthy controls. The glaucoma patients were recruited from the Ophthalmology Clinic of the UiTM Specialist Hospital, whereas healthy controls were recruited by leaflet and poster exposure. As a result, glaucoma patients are driven by health issues, but healthy controls may be motivated by other factors. Whether or not this bias is significant is debatable.



REFERENCES

- Abdull, M. M., Chandler, C., & Gilbert, C. (2016). Glaucoma, ‘the silent thief of sight’: Patients’ perspectives and health seeking behaviour in Bauchi, northern Nigeria. *BMC Ophthalmology*, 16(1), 1–10. Retrieved from <https://doi.org/10.1186/s12886-016-0220-6>
- Aizen, R., Tao, K., Rencus-Lazar, S., & Gazit, E. (2018). Functional metabolite assemblies—a review. *Journal of Nanoparticle Research*, 20(5). Retrieved from <https://doi.org/10.1007/s11051-018-4217-3>
- Aksoy, D. Ö., Umurhan Akkan, J. C., Alkan, A., Aralaşmak, A., Otçu Temur, H., & Yurtsever, İ. (2018). Magnetic Resonance Spectroscopy Features of the Visual Pathways in Patients with Glaucoma. *Clinical Neuroradiology*, 29(4), 615–621.
- Allen D. Elster. (2023a). PRESS. Retrieved 29 September 2023, from <https://mriquestions.com/press.html>
- Allen D. Elster. (2023b). STEAM. Retrieved 29 September 2023, from <https://mriquestions.com/steam.html>
- Altaf-Ul-Amin, M., Kanaya, S., & Mohamed-Hussein, Z. A. (2019). Investigating metabolic pathways and networks. *Encyclopedia of Bioinformatics and Computational Biology: ABC of Bioinformatics*, 489–503. Retrieved from <https://doi.org/10.1016/B978-0-12-809633-8.20140-4>
- Anatomy of the Eye | Biology for Majors II. (n.d.). Retrieved 9 January 2023, from <https://courses.lumenlearning.com/wm-biology2/chapter/anatomy-of-the-eye/>
- Anith Alfred J, Abubacker Sulaiman F, Divya Shree, Ashraf Ahmed, S. K., & Prabhu, V. (2018). Comparison of Single Voxel and Multi Voxel Magnetic Resonance Spectroscopy in Evaluation of Brain Tumors. *International Journal of Contemporary Medicine, Surgery and Radiology*, 3(2), 36–40. Retrieved from <https://doi.org/10.21276/ijcmsr.2018.3.2.9>

- Antimo Buonocore. (2010). *Remote distractor effects in saccadic , manual and covert attention tasks*. The University of Edinburgh & The University of Trieste.
- Armstrong, R. A., & Cubbidge, R. C. (2019). *The Eye and Vision: An Overview. Handbook of Nutrition, Diet, and the Eye* (2nd ed.). Elsevier Inc. Retrieved from <https://doi.org/10.1016/b978-0-12-815245-4.00001-6>
- Arrigo, A., Aragona, E., Saladino, A., Arrigo, D., Fantaguzzi, F., Battaglia Parodi, M., & Bandello, F. (2021). Cognitive Dysfunctions in Glaucoma: An Overview of Morpho-Functional Mechanisms and the Impact on Higher-Order Visual Function. *Frontiers in Aging Neuroscience*, 13(747050), 1–13.
- Azevedo, F. A. C., Carvalho, L. R. B., Grinberg, L. T., Farfel, J. M., Ferretti, R. E. L., Leite, R. E. P., Filho, W. J., Lent, R. & Herculano-Houzel, S. (2009). Equal numbers of neuronal and nonneuronal cells make the human brain an isometrically scaled-up primate brain. *Journal of Comparative Neurology*, 513(5), 532–541. Retrieved from <https://doi.org/10.1002/cne.21974>
- Babourina-Brooks, B., Wilson, M., Arvanitis, T. N., Peet, A. C., & Davies, N. (2014). MRS water resonance frequency in childhood brain tumours a novel potential.pdf. *NMR Biomed.*, 10(27), 1222–1229. Retrieved from <https://doi.org/https://doi.org/10.1002/nbm.3177>
- Bairwa, D., Kumar, V., Vyas, S., Das, B. K., Srivastava, A. K., Pandey, R. M., Sharma, S. K., Jagannathan, N. R & Sinha, S. (2016). Case control study: Magnetic resonance spectroscopy of brain in HIV infected patients. *BMC Neurology*, 16(1), 1–10. Retrieved from <https://doi.org/10.1186/s12883-016-0628-x>
- Bang, J. W., Parra, C., Yu, K., Wollstein, G., Schuman, J. S., & Chan, K. C. (2023). GABA decrease is associated with degraded neural specificity in the visual cortex of glaucoma patients. *Communications Biology*, 6(679), 1–11. Retrieved from <https://doi.org/10.1038/s42003-023-04918-8>

- Barbosa-Breda, J., Himmelreich, U., Ghesquière, B., Rocha-Sousa, A., & Stalmans, I. (2018). Clinical Metabolomics and Glaucoma. *Ophthalmic Research*, 59(1), 1–6. Retrieved from <https://doi.org/10.1159/000479158>
- Barker, P. B. (2001). N -Acetyl Aspartate — A Neuronal Marker ? *Annals of Neurology*, 49(4), 423–424. Retrieved from <https://doi.org/https://doi.org/10.1002/ana.90>
- Barta, H., Jermendy, A., Kolossvary, M., Kozak, L. R., Lakatos, A., Meder, U., Szabo, M. & Rudas, G. (2018). Prognostic value of early, conventional proton magnetic resonance spectroscopy in cooled asphyxiated infants. *BMC Pediatrics*, 18(1), 1–11.
- Bartlett, J. W., & Frost, C. (2008). Reliability, repeatability and reproducibility: Analysis of measurement errors in continuous variables. *Ultrasound in Obstetrics and Gynecology*, 31(4), 466–475. Retrieved from <https://doi.org/10.1002/uog.5256>
- Bentley, P., Driver, J., & Dolan, R. J. (2008). Cholinergic modulation of visual and attentional brain responses in Alzheimer ' s disease and in health. *Brain*, 131(Pt 2), 409–424. Retrieved from <https://doi.org/10.1093/brain/awm299.Cholinergic>
- Bland, J. M., & Altman, D. G. (1999). Measuring agreement in method comparison studies. *Statistical Methods in Medical Research*, 8(2), 135–160. Retrieved from <https://doi.org/10.1177/096228029900800204>
- Blüml, S. (2013). Magnetic Resonance Spectroscopy: Basic. In S. Blüml & A. Panigraphy (Eds.), *MR Spectroscopy of Pediatric Brain Disorders* (pp. 11–23). Springer New York. Retrieved from <https://doi.org/10.1007/978-1-4419-5864-8>
- Bluml, S., Zuckerman, E., Tan, J., & Ross, B. D. (1998). Proton-decoupled 31P magnetic resonance spectroscopy reveals osmotic and metabolic disturbances in human hepatic encephalopathy. *Journal of Neurochemistry*, 71(4), 1564–1576. Retrieved from <https://doi.org/10.1046/j.1471-4159.1998.71041564.x>

- Blusztajn, J. K. (1998). Choline, a vital amine. *Science*, 281(5378), 794–795.
Retrieved from <https://doi.org/10.1126/science.281.5378.794>
- Boucard, C. C., Hoogduin, J. M., van der Grond, J., & Cornelissen, F. W. (2007). Occipital proton magnetic resonance spectroscopy (1H-MRS) reveals normal metabolite concentrations in retinal visual field defects. *PLoS ONE*, 2(2), e222–e222.
- Boussida, S., François, Y., Heintz, A., Saidak, Z., Dakpé, S., Coutte, A., Devauchelle, B., Galmiche, A., Testelin, S., Goudot, P. & Constans, J.-M. (2022). Evaluation of Proton MR Spectroscopy for the Study of the Tongue Tissue in Healthy Subjects and Patients With Tongue Squamous Cell Carcinoma: Preliminary Findings. *Frontiers in Oral Health*, 3(July), 1–9. Retrieved from <https://doi.org/10.3389/froh.2022.912803>
- Bracken, B. K., Jensen, J. E., Prescott, A. P., Cohen, B. M., Renshaw, P. F., & Ongür, D. (2011). Brain metabolite concentrations across cortical regions in healthy adults. *Brain Res.*, 23(13), 89–94. Retrieved from <https://doi.org/10.1016/j.brainres.2010.11.036>.
- Brar, V. S. (2020). *2020-2021 Basic and Clinical Science Course (TM), Section 2 : Fundamentals and Principles of Ophthalmology*. San Francisco, United States: American Academy of Ophthalmology.
- Breitling, R., Cenicerros, A., Jankevics, A., & Takano, E. (2013). Metabolomics for Secondary Metabolite Research. *Metabolites*, 3(4), 1076–1083.
Retrieved from <https://doi.org/10.3390/metabo3041076>
- Bressloff, P. C. (2005). Course 11 Pattern formation in visual cortex. *Les Houches Summer School Proceedings*, 80(C), 477–574. Retrieved from [https://doi.org/10.1016/S0924-8099\(05\)80017-4](https://doi.org/10.1016/S0924-8099(05)80017-4)
- Brief, E. E. (2000). *Proton Magnetic Resonance Spectroscopy Of Human Brain: T1 And T2 Relaxation And Absolute Concentrations Of Metabolites In Patients And Healthy Volunteers*. The University of British Columbia.
- Brown, H. D. H., Woodall, R. L., Kitching, R. E., Baseler, H. A., & Morland, A.

- B. (2016). Using magnetic resonance imaging to assess visual deficits: a review. *Ophthalmic & Physiological Optics: The Journal Of The British College Of Ophthalmic Opticians (Optometrists)*, 36(3), 240–265.
- Brown, R. W., Cheng, Y. N., Haacke, E. M., Thompson, M. R., & Venkatesan, R. (2014). *Magnetic Resonance Imaging*. Wiley. Retrieved from <https://doi.org/10.1002/9781118633953>
- Bruton, A., Conway, J. H., & Holgate, S. T. (2000). Reliability: What is it, and how is it measured? *Physiotherapy*, 86(2), 94–99. Retrieved from [https://doi.org/10.1016/S0031-9406\(05\)61211-4](https://doi.org/10.1016/S0031-9406(05)61211-4)
- Bulakbasi, N. (2004). Clinical applications of proton MR spectroscopy in the diagnosis of brain tumours. *Spectroscopy*, 18(2), 143–153. Retrieved from <https://doi.org/10.1155/2004/381453>
- Bunting, K. V., Steeds, R. P., Slater, L. T., Rogers, J. K., Gkoutos, G. V., & Kotecha, D. (2019). A Practical Guide to Assess the Reproducibility of Echocardiographic Measurements. *Journal of the American Society of Echocardiography*, 32(12), 1505–1515. Retrieved from <https://doi.org/10.1016/j.echo.2019.08.015>
- Buonocore, M. H., & Maddock, R. J. (2015). Magnetic resonance spectroscopy of the brain: A review of physical principles and technical methods. *Reviews in the Neurosciences*, 26(6), 609–632.
- Burgess, K., Rankin, N., & Weidt, S. (2014). Metabolomics. *Handbook of Pharmacogenomics and Stratified Medicine*, 181–205. Retrieved from <https://doi.org/10.1016/B978-0-12-386882-4.00010-4>
- Burtscher, I. M., & Holtas, S. (2001). Proton MR spectroscopy in clinical routine. *Journal of Magnetic Resonance Imaging*, 13(4), 560–567. Retrieved from <https://doi.org/10.1002/jmri.1079>
- Bussel, I. I., Wollstein, G., & Schuman, J. S. (2014). OCT for glaucoma diagnosis , screening and detection of glaucoma progression, 98(Suppl II), 15–19. Retrieved from <https://doi.org/10.1136/bjophthalmol-2013-304326>

- Canavan disease. (n.d.). Retrieved 1 December 2020, from <http://www.n-acetylaspartate.com/canavan.html>
- Castillo, M., Kwock, L., & Mukherji, S. K. (1996). Special Report Clinical Applications of Proton MR Spectroscopy, 1–15.
- Cecil, K. M. (2014). Proton Magnetic Resonance Spectroscopy: Technique for the Neuroradiologist. *Neuroimaging Clinics of North America*, 23(3), 381–392. Retrieved 27 November 2018 from <https://doi.org/10.1016/j.nic.2012.10.003>.Proton
- Cecil, K. M., Lenkinski, R. E., Gur, R. E., & Gur, R. C. (1999). Proton magnetic resonance spectroscopy in the frontal and temporal lobes of neuroleptic naive patients with schizophrenia. *Neuropsychopharmacology*, 20(2), 131–140. Retrieved from [https://doi.org/10.1016/S0893-133X\(98\)00063-3](https://doi.org/10.1016/S0893-133X(98)00063-3)
- Chianca, V., Albano, D., Messina, C., Gitto, S., Ruffo, G., Guarino, S., Del Grande, F. & Sconfienza, L. M. (2021). Sarcopenia: imaging assessment and clinical application. *Abdominal Radiology*, 47(9), 3205–3216. Retrieved 6 October 2023 from <https://doi.org/10.1007/s00261-021-03294-3>
- Choi, C., Ganji, S., Hulsey, K., Madan, A., Kovacs, Z., Dimitrov, I., Zhang, S., Pichumani, K., Mendelsohn, D. Mickey, B., Malloy, C., Bachoo, R., Deberardinis, R. & Maher, E. (2013). A comparative study of short- and long-TE 1 H-MRS at 3T for in- vivo detection of 2-hydroxyglutarate in brain tumors. *NMR Biomed*, 26(10), 1242–1250.
- Christopher, Bowd, Zangwill, L. M., Berry, C. C., Blumenthal, E. Z., Vasile, C., Sanchez-Galeana, C., Bosworth, Charles F., Sample, Pamela A. & Weinreb, R. N. (2001). Detecting Early Glaucoma by Assessment of Retinal Nerve Fiber Layer Thickness and Visual Function. *Investigative Ophthalmology & Visual Science*, 42(9), 1993–2003.
- Conlon, R., Saheb, H., & Ahmed, I. I. K. (2017). Glaucoma treatment trends: a review. *Canadian Journal of Ophthalmology*, 52(1), 114–124. Retrieved from <https://doi.org/10.1016/j.jcjo.2016.07.013>

- Covington, B. P., & Khalili, Y. Al. (2022). *Neuroanatomy, Nucleus Lateral Geniculate - StatPearls - NCBI Bookshelf*. StatPearls Publishing, Treasure Island (FL).
- Craig, J. (2008). Complex Diseases : Research and Applications. *Nature Education*, 1(1), 184.
- Cudalbu, Cristina Ramona; Lanz, B.; Duarte, J. M.; Kunz, N.; Gruetter, R. (2011). Impact of the prior knowledge on the quantification of in vivo ¹³C spectra using two different algorithms : LCMoDel and. *In Vivo*, 4, 131087.
- Currie, S., Hadjivassiliou, M., Craven, I. J., Wilkinson, I. D., Griffiths, P. D., & Hoggard, N. (2013). Magnetic resonance spectroscopy of the brain. *Postgraduate Medical Journal*, 89(1048), 94–106. Retrieved from <https://doi.org/10.1136/postgradmedj-2011-130471>
- Danbolt, N. C. (2001). Glutamate uptake. *Progress in Neurobiology*, 65(1), 1–105. Retrieved from [https://doi.org/10.1016/S0301-0082\(00\)00067-8](https://doi.org/10.1016/S0301-0082(00)00067-8)
- D'Anci, K. E., Allen, P. J., & Kanarek, R. B. (2011). A potential role for creatine in drug abuse? *Molecular Neurobiology*, 44(2), 136–141. Retrieved from <https://doi.org/10.1007/s12035-011-8176-2>
- Dandil, E. (2020). AIMRS: A feature extraction method from MRS signals based on artificial immune algorithms for classification of brain tumours. *IET Signal Processing*, 14(6), 361–373. Retrieved from <https://doi.org/10.1049/iet-spr.2019.0576>
- Danilova, V. M., Grigorieva, M. V., & Komisarenko, S. V. (2023). Discovery of magnetic resonance imaging: Paul Lauterbur and Peter Mansfield. The Nobel Prize in Physiology or Medicine 2003. *Ukrainian Biochemical Journal*, 94(6), 67–73. Retrieved from <https://doi.org/10.15407/UBJ94.06.067>
- Dezortova, M., & Hajek, M. (2008). ¹H MR spectroscopy in pediatrics. *European Journal of Radiology*, 67(2), 240–249. Retrieved from

<https://doi.org/10.1016/j.ejrad.2008.02.035>

- Doganay, S., Cankaya, C., & Alkan, a. (2012). Evaluation of corpus geniculatum laterale and vitreous fluid by magnetic resonance spectroscopy in patients with glaucoma; a preliminary study. *Eye (London, England)*, 26(8), 1044–51. Retrieved from <https://doi.org/10.1038/eye.2012.84>
- Duda, J. M., Moser, A. D., Zuo, C. S., Du, F., Chen, X., Perlo, S., Richards, C. E., Nascimento, N., Ironside, M., Crowley, D. J., Holsen, L. M., Misra, M., Hudson, J. I., Goldstein, J. M., & Pizzagalli, D. A. (2021). Repeatability and reliability of GABA measurements with magnetic resonance spectroscopy in healthy young adults. *Magnetic Resonance in Medicine*, 85(5), 2359–2369. Retrieved from <https://doi.org/10.1002/mrm.28587>
- Dydak, U., Weiger, M., Pruessmann, K. P., Meier, D., & Boesiger, P. (2001). Sensitivity-encoded spectroscopic imaging. *Magnetic Resonance in Medicine*, 46(4), 713–722. Retrieved 6 October 2023 from <https://doi.org/10.1002/mrm.1250>
- Ernst, T., & Linda, C. (2006). *Data Processing and Interpretation. ISMRM*.
- Faghihi, R., Zeinali-Rafsanjani, B., Mosleh-Shirazi, M.-A., Saeedi-Moghadam, M., Lotfi, M., Jalli, R., & Iravani, V. (2017). Magnetic Resonance Spectroscopy and its Clinical Applications: A Review. *Journal of Medical Imaging and Radiation Sciences*, 48(3), 233–253. Retrieved 5 September 2018 from <https://doi.org/10.1016/j.jmir.2017.06.004>
- Faul, F., Erdfelder, E., Lang, A. G., & Buchner, A. (2007). G*Power 3: A flexible statistical power analysis program for the social, behavioral, and biomedical sciences. *Behavior Research Methods*, 39(2), 175–191. Retrieved from <https://doi.org/10.3758/BF03193146>
- Fayad, L. M., Barker, P. B., & Bluemke, D. A. (2007). Molecular Characterization of Musculoskeletal Tumors by Proton MR Spectroscopy. *Seminars in Musculoskeletal Radiology*, 11(3), 240–245. Retrieved 6 October 2023 from <https://doi.org/10.1055/s-2008-1038313>

- Feng, Y., Zhang, C., Wei, Z., Li, G., Gan, Y., Liu, C., & Deng, Y. (2022). Gene variations of glutamate metabolism pathway and epilepsy. *Acta Epileptologica*, 4(1). Retrieved from <https://doi.org/10.1186/s42494-022-00103-2>
- Fiedorowicz, M., Dyda, W., Rejdak, R., & Grieb, P. (2011). Magnetic resonance in studies of glaucoma. *Med Sci Monit*, 17(10), RA227-32. Retrieved from <https://doi.org/881973> [pii]
- Fujita, N., Tanaka, H., Takanashi, M., Hirabuki, N., Abe, K., Yoshimura, H., & Nakamura, H. (2001). Lateral geniculate nucleus: Anatomic and functional identification by use of MR imaging. *American Journal of Neuroradiology*, 22(9), 1719–1726.
- Gandhi, M., & Dubey, S. (2013). Evaluation of the optic nerve head in glaucoma. *Journal of Current Glaucoma Practice*, 7(3), 106–114. Retrieved from <https://doi.org/10.5005/jp-journals-10008-1146>
- Gangeddula, V., Ranchet, M., Akinwuntan, A. E., Bollinger, K., & Devos, H. (2017). Effect of cognitive demand on functional visual field performance in senior drivers with glaucoma. *Frontiers in Aging Neuroscience*, 9(AUG), 1–9. Retrieved from <https://doi.org/10.3389/fnagi.2017.00286>
- Gennatas, E. D., Avants, B. B., Wolf, D. H., Satterthwaite, T. D., Ruparel, K., Ciric, R., ... Gur, R. C. (2017). Age-related effects and sex differences in gray matter density, volume, mass, and cortical thickness from childhood to young adulthood. *Journal of Neuroscience*, 37(20), 5065–5073. Retrieved from <https://doi.org/10.1523/JNEUROSCI.3550-16.2017>
- Giavarina, D. (2015). Understanding Bland Altman analysis. *Biochemia Medica*, 25(2), 141–151. Retrieved from <https://doi.org/10.11613/BM.2015.015>
- Giorgio, A., Zhang, J., Costantino, F., De Stefano, N., & Frezzotti, P. (2018). Diffuse brain damage in normal tension glaucoma. *Human Brain Mapping*, 39(1), 532–541. Retrieved from <https://doi.org/10.1002/hbm.23862>

- Gondim Teixeira, P. A., Ledrich, M., Kauffmann, F., Wamba, J. M., Felblinger, J., Blum, A., & Hossu, G. (2017). Qualitative 3-T Proton MR Spectroscopy for the Characterization of Musculoskeletal Neoplasms: Update on Diagnostic Performance and Indications. *American Journal of Roentgenology*, 208(6), 1312–1319. Retrieved from <https://doi.org/10.2214/AJR.16.17285>
- Gosling, D., & Meyer, J. J. (2022). Normal tension glaucoma. Retrieved from <https://www.ncbi.nlm.nih.gov/books/NBK576377/>
- Govindaraju, V., Young, K., & Maudsley, A. (2000). ¹H-NMR chemical shifts and coupling constants for brain metabolites. *NMR Biomed*, 13(3), 129–53. Retrieved from <https://doi.org/10.1002/9780470034590.emrstm1530>
- Grachev, I. D., & Apkarian, A. V. (2000). Chemical heterogeneity of the living human brain: A proton MR spectroscopy study on the effects of sex, age, and brain region. *NeuroImage*, 11(5 I), 554–563. Retrieved from <https://doi.org/10.1006/nimg.2000.0557>
- Grachev, I. D., & Apkarian, A. V. (2001). Aging alters regional multichemical profile of the human brain: an in vivo ¹H-MRS study of young versus middle-aged subjects. *Journal of Neurochemistry*, 76(2), 582–593. Retrieved from <http://www.blackwell-synergy.com/doi/abs/10.1046/j.1471-4159.2001.00026.x%5Cnpapers2://publication/uuid/67B2D427-C9EA-46C0-940D-A867AC0F3943>
- Graff-Radford, J., & Kantarci, K. (2013). Magnetic resonance spectroscopy in Alzheimer's disease. *Neuropsychiatric Disease and Treatment*, 9, 687–96. Retrieved 15 April 2018 from <https://doi.org/10.2147/NDT.S35440>
- Graveron-demilly, D. (2016). *Help and Documentation for jMRUI Written*.
- Graves, J. M., & Zhu, C. (2015). Basic Principles of Magnetic Resonance Imaging. In R. Trivedi, L. Saba, & J. Suri (Eds.), *3D Imaging Technologies in Atherosclerosis*. Springer, Boston, MA. Retrieved from <https://doi.org/10.1007/978-1-4899-7618-5>

- Grover, V. P. B., Tognarelli, J. M., Crossey, M. M. E., Cox, I. J., Taylor-Robinson, S. D., & McPhail, M. J. W. (2015). Magnetic Resonance Imaging: Principles and Techniques: Lessons for Clinicians. *Journal of Clinical and Experimental Hepatology*, 5(3), 246–255. Retrieved from <https://doi.org/10.1016/j.jceh.2015.08.001>
- Grzybowski, A., Och, M., Kanclerz, P., Leffler, C., & De Moraes, C. G. (2020). Primary Open Angle Glaucoma and Vascular Risk Factors. *Journal of Clinical Medicine*, 9(3), 761. Retrieved from <https://doi.org/10.3390/jcm9030761>
- Gu, M., Kim, D. H., Mayer, D., Sullivan, E. V., Pfefferbaum, A., & Spielman, D. M. (2008). Reproducibility study of whole-brain 1H spectroscopic imaging with automated quantification. *Magnetic Resonance in Medicine*, 60(3), 542–547. Retrieved from <https://doi.org/10.1002/mrm.21713>
- Gujar, S. K., Maheshwari, S., Björkman-Burtscher, I., & Sundgren, P. C. (2005). Magnetic resonance spectroscopy. *Journal of Neuro-Ophthalmology : The Official Journal of the North American Neuro-Ophthalmology Society*, 25(3), 217–26. Retrieved from <https://doi.org/10.1119/1.1974575>
- Guo L, Wang R, Tang Z, Sun X, Wu L, Wang J, Zhong Y, Xiao Z, Zhang Z. (2018). Metabolic Alterations Within the Primary Visual Cortex in Early Open-angle Glaucoma Patients: A Proton Magnetic Resonance Spectroscopy Study. *Journal Of Glaucoma*, 27(12), 1046–1051. Retrieved from <https://doi.org/10.1097/IJG.0000000000001098>
- Gupta, M., Ireland, A., & Bordoni, B. (2022). Neuroanatomy , Visual Pathway. Retrieved from <https://www.ncbi.nlm.nih.gov/books/NBK553189/>
- Gupta, N., Ang, L. C., De Tilly, L. N., Bidaisee, L., & Yücel, Y. H. (2006). Human glaucoma and neural degeneration in intracranial optic nerve, lateral geniculate nucleus, and visual cortex. *British Journal of Ophthalmology*, 90(6), 674–678. Retrieved from <https://doi.org/10.1136/bjo.2005.086769>
- Gupta, N., Greenberg, G., De Tilly, L. N., Gray, B., Polemidiotis, M., & Yücel,

- Y. H. (2009). Atrophy of the lateral geniculate nucleus in human glaucoma detected by magnetic resonance imaging. *British Journal of Ophthalmology*, 93(1), 56–60. Retrieved from <https://doi.org/10.1136/bjo.2008.138172>
- Haddadin, I. S., McIntosh, A., Meisamy, S., Corum, C., Styczynski Snyder, A. L., Powell, N. J., Nelson M.T., Yee D., Garwood M., & Bolan, P. J. (2009). Metabolite quantification and high-field MRS in breast cancer. *NMR in Biomedicine*, 22(1), 65–76. Retrieved from <https://doi.org/10.1002/nbm.1217>
- Haga, K. K., Khor, Y. P., Farrall, A., & Wardlaw, J. M. (2009). A systematic review of brain metabolite changes, measured with ¹H magnetic resonance spectroscopy, in healthy aging. *Neurobiology of Aging*, 30(3), 353–363. Retrieved from <https://doi.org/10.1016/j.neurobiolaging.2007.07.005>
- Hajek, M., & Dezortova, M. (2008). Introduction to clinical in vivo MR spectroscopy. *European Journal of Radiology*, 67(2), 185–193. Retrieved from <https://doi.org/10.1016/j.ejrad.2008.03.002>
- Harris, R. E., Sundgren, P. C., Craig, A. D., Kirshenbaum, E., Sen, A., Napadow, V., & Clauw, D. J. (2009). Elevated insular glutamate in fibromyalgia is associated with experimental pain. *Arthritis and Rheumatism*, 60(10), 3146–3152. Retrieved from <https://doi.org/10.1002/art.24849>
- Harte, M. K., Bachus, S. B., & Reynolds, G. P. (2005). Increased N-acetylaspartate in rat striatum following long-term administration of haloperidol. *Schizophrenia Research*, 75(2–3), 303–308. Retrieved from <https://doi.org/10.1016/j.schres.2004.11.001>
- Hartmann, J., Gellermann, J., Brandt, T., Schmidt, M., Pyatykh, S., Hesser, J., Ott O., Fietkau R., & Bert, C. (2017). Optimization of Single Voxel MR Spectroscopy Sequence Parameters and Data Analysis Methods for Thermometry in Deep Hyperthermia Treatments. *Technology in Cancer Research and Treatment*, 16(4), 470–481. Retrieved from

<https://doi.org/10.1177/1533034616656310>

Hashemi, R. H., Bradley, W. G., & Lisanti, C. J. (2012). *MRI: The basics*. Lippincott Williams & Wilkins.

Hazin, R., Hendrick, A. M., & Kahook, M. Y. (2009). Primary open-angle glaucoma: Diagnostic approaches and management. *Journal of the National Medical Association*, 101(1), 46–50. Retrieved from [https://doi.org/10.1016/S0027-9684\(15\)30811-7](https://doi.org/10.1016/S0027-9684(15)30811-7)

Healthcare, G. E. (2019). When and why was MRI invented | GE Healthcare (United Kingdom). Retrieved 26 September 2023, from <https://www.gehealthcare.co.uk/feature-article/when-and-why-was-mri-invented>

Hesselink, J. R. (2014). Fundamentals of Mr Spectroscopy Fundamentals of Mr Spectroscopy. Retrieved 7 August 2019, from <http://spinwarp.ucsd.edu/neuroweb/Text/mrs-TXT.htm>

Hoa, D. (2016). Single voxel spectroscopy (SVS). *Imaios*.

Hodapp E, Parrish RK II, A. D. (1993). *Clinical decisions in glaucoma*. St Louis: The CV Mosby Co.

Holmes, E., & Nicholson, J. K. (2007). Human Metabolic Phenotyping and MetabolomeWideAssociation Studies. *Ernst Schering Found Symp Proc.*, 4, 227–49. Retrieved from https://doi.org/10.1007/2789_2008_096

Horton, J. C., Landau, K., Maeder, P., & Hoyt, W. F. (1990). Magnetic Resonance Imaging of the Human Lateral Geniculate Body. *Archives of Neurology*, 47(11), 1201–1206. Retrieved from <https://doi.org/10.1001/archneur.1990.00530110059017>

Hudsmith, L. E., & Neubauer, S. (2009). Magnetic Resonance Spectroscopy in Myocardial Disease. *JACC: Cardiovascular Imaging*, 2(1), 87–96. Retrieved from <https://doi.org/10.1016/j.jcmg.2008.08.005>

Huff, T., Mahabadi, N., & Tadi, P. (2022). *Neuroanatomy , Visual Cortex*.

StatPearls, StatPearls Publishing.

- Lester, M., Telani, S., Vagge, A., & Bagnis, A. (2013). *Diagnosis of glaucoma. Glaucoma: Basic and Clinical Perspectives*. www.futuremedicine.com. Retrieved from <https://doi.org/10.2217/EBO.12.375>
- Jansen, J. F. A., Backes, W. H., Nicolay, K., & Kooi, M. E. (2006). 1H MR spectroscopy of the brain: Absolute quantification of metabolites. *Radiology*, 240(2), 318–332. Retrieved from <https://doi.org/10.1148/radiol.2402050314>
- Jonas, J. B., Wang, N., Wang, Y. X., You, Q. S., Yang, D., & Xu, L. (2014). Ocular hypertension: General characteristics and estimated cerebrospinal fluid pressure. The Beijing eye study 2011. *PLoS ONE*, 9(7), 1–8. Retrieved from <https://doi.org/10.1371/journal.pone.0100533>
- Jones, R. S., & Waldman, A. D. (2004). ¹H-MRS evaluation of metabolism in Alzheimer's disease and vascular dementia. *Neurological Research*, 26(5), 488–495. Retrieved from <https://doi.org/10.1179/016164104225017640>
- Joseph P. Hornak. (2020). The Basics of MRI: Imaging Hardware. Retrieved from <https://www.cis.rit.edu/htbooks/mri/chap-9/chap-9.htm#9.6>
- Kaddurah-Daouk, R., Kristal, B. S., & Weinshilboum, R. M. (2008). Metabolomics: A global biochemical approach to drug response and disease. *Annual Review of Pharmacology and Toxicology*, 48, 653–683. Retrieved from <https://doi.org/10.1146/annurev.pharmtox.48.113006.094715>
- Kagawa, T., Yoshida, S., Shiraishi, T., Hashimoto, M., Inadomi, D., Sato, M., Tsuzuki, T., Miwa, K., & Yuasa, K. (2017). Basic principles of magnetic resonance imaging for beginner oral and maxillofacial radiologists. *Oral Radiology*, 33(2), 92–100. Retrieved from <https://doi.org/10.1007/s11282-017-0274-z>
- Kalra, A. (2017). Decoding the Bland–Altman plot: Basic review. *Journal of the*

Practice of Cardiovascular Sciences, 3(1), 36. Retrieved from
https://doi.org/10.4103/jpcs.jpcs_11_17

Kantarci, K., Jack, C. R., Xu, Y. C., Campeau, N. G., O'Brien, P. C., Smith, G. E., Ivnik, R.J., Boeve, B.F., Kokmen, E., Tangalos, E.G., & Petersen, R. C. (2000). Regional Metabolic Patterns in Mild Cognitive Impairment and Alzheimer ' S Disease a 1 H MRS Study. *Neurology*, 55(2), 210–217.

Kapetanakis, V. V., Chan, M. P. Y., Foster, P. J., Cook, D. G., Owen, C. G., & Rudnicka, A. R. (2016). Global variations and time trends in the prevalence of primary open angle glaucoma (POAG): A systematic review and meta-analysis. *British Journal of Ophthalmology*, 100(1), 86–93. Retrieved from <https://doi.org/10.1136/bjophthalmol-2015-307223>

Karen Grace-Martin. (2020). When Unequal Sample Sizes Are and Are NOT a Problem in ANOVA - The Analysis Factor. Retrieved from <https://www.theanalysisfactor.com/when-unequal-sample-sizes-are-and-are-not-a-problem-in-anova/>

Keeler, J. (2010). *Understanding NMR Spectroscopy*. John Wiley & Sons. Retrieved 4 October 2023 from

Khaw, P. T., Shah, P., & Elkington, A. R. (2004). Glaucoma — 1 : Diagnosis Primary open angle glaucoma. *Bmj*, 528, 97–99.

Khazaeni, B., & Khazaeni, L. (2023). Acute closed angle glaucoma. Retrieved from <https://www.ncbi.nlm.nih.gov/books/NBK430857/?report=printable>

King, A., Azuara-Blanco, A., & Tuulonen, A. (2013). Glaucoma. *BMJ*, 346(f3251). Retrieved 13 February 2019 from <https://doi.org/10.1136/bmj.f3518>

Kosior-Jarecka, E., Pankowska, A., Polit, P., Stepniewski, A., Symms, M. R., Kozioł, P., Żarnowski, T., & Pietura, R. (2020). Volume of lateral geniculate nucleus in patients with glaucoma in 7Tesla Mri. *Journal of Clinical Medicine*, 9(8), 1–13. Retrieved from <https://doi.org/10.3390/jcm9082382>

- Kreis, R. (2004). Issues of spectral quality in clinical ¹H-magnetic resonance spectroscopy and a gallery of artifacts. *NMR in Biomedicine*, 17(6), 361–381. Retrieved from <https://doi.org/10.1002/nbm.891>
- Kreis, R., Slotboom, J., Hofmann, L., & Boesch, C. (2005). Integrated data acquisition and processing to determine metabolite contents, relaxation times, and macromolecule baseline in single examinations of individual subjects. *Magnetic Resonance in Medicine*, 54(4), 761–768. Retrieved from <https://doi.org/10.1002/mrm.20673>
- Kumar, M., Singh, S., Rana, P., Kumar, P., Sekhri, T., Kanwar, R., D'Souza, M., & Khushu, S. (2021). Neurometabolite Changes in Hyperthyroid Patients Before and After Antithyroid Treatment: An in vivo ¹H MRS Study. *Frontiers in Human Neuroscience*, 15(November), 1–10. Retrieved from <https://doi.org/10.3389/fnhum.2021.739917>
- Laader, A., Beiderwellen, K., Kraff, O., Maderwald, S., Wrede, K., Ladd, M. E., Lauenstein, T.C., Forsting, M., Quick, H.H., Nassenstein, K., & Umutlu, L. (2017). 1.5 versus 3 versus 7 Tesla in abdominal MRI: A comparative study. *PLoS ONE*, 12(11), 1–18. Retrieved from <https://doi.org/10.1371/journal.pone.0187528>
- Läkens, D. (2022). PsyArXiv Preprints | Sample Size Justification. *Collabra: Psychology*, 1–32.
- Lambert, J., Mazzola, E., & Ridge, C. (2019). *Nuclear magnetic resonance spectroscopy: an introduction to principles, applications, and experimental methods*. John Wiley & Sons.
- Lauterbur, P. C. (1973). Image formation by induced local interactions: Examples employing nuclear magnetic resonance. *Nature*, 242(5394), 190–191. Retrieved from <https://doi.org/10.1038/242190a0>
- Lee, J. Y., Jeong, H. J., Lee, J. H., Kim, Y. J., Kim, E. Y., Kim, Y. Y., Ryu, T., Cho, Z.H., & Kim, Y. B. (2014). An investigation of lateral geniculate nucleus volume in patients with primary open-angle glaucoma using 7 tesla magnetic resonance imaging. *Investigative Ophthalmology and*

Visual Science, 55(6), 3468–3476. Retrieved from
<https://doi.org/10.1167/iovs.14-13902>

- Lee, P., Adany, P., & Choi, I. Y. (2017). Imaging based magnetic resonance spectroscopy (MRS) localization for quantitative neurochemical analysis and cerebral metabolism studies. *Anal Biochem*, 15(529), 40–47. Retrieved from <https://doi.org/10.1016/j.ab.2017.01.007>
- Lewandowska, Z., Steinborn, B., Borkowski, W., Chlebowska, E., & Karmelita-Katulaska, K. (2018). SCL6A8 mutation in female patient resulting in creatine transporter deficiency. *Child Neurology*, 27(55), 69–76. Retrieved from <https://doi.org/10.20966/chn.2018.55.434>
- Lexell, J. E., & Downham, D. Y. (2005). How to assess the reliability of measurements in rehabilitation. *American Journal of Physical Medicine and Rehabilitation*, 84(9), 719–723. Retrieved from <https://doi.org/10.1097/01.phm.0000176452.17771.20>
- Li, B. S. Y., Wang, H., & Gonen, O. (2003). Metabolite ratios to assumed stable creatine level may confound the quantification of proton brain MR spectroscopy. *Magnetic Resonance Imaging*, 21(8), 923–928. Retrieved from [https://doi.org/10.1016/S0730-725X\(03\)00181-4](https://doi.org/10.1016/S0730-725X(03)00181-4)
- Li, M., He, H., Shi, W., Li, J., Lv, B., Wang, C. H., Miao, Q.W., Wang, Z.C., Wang, N.L., Walter, M., & Sabel, B. A. (2012). Quantification of the human lateral geniculate nucleus in vivo using MR imaging based on morphometry: Volume loss with age. *American Journal of Neuroradiology*, 33(5), 915–921. Retrieved from <https://doi.org/10.3174/ajnr.A2884>
- Li, T., Qu, X., Chen, W., Wang, Q., Wang, H., Wang, Y., Huang, C., Zhang, X., Wang, N., & Xian, J. (2020). Altered information flow and microstructure abnormalities of visual cortex in normal-tension glaucoma: Evidences from rest-state fMRI and DKI. *Brain Research*, 1741(146874), 146874. Retrieved from <https://doi.org/10.1016/j.brainres.2020.146874>
- Lin, A., Andronesi, O., Bogner, W., Choi, I. Y., Coello, E., Cudalbu, C., C.,

- Juchem, C., Kemp, G.J., Kreis, R., Krššák, M. & Lee, P. (2021). Minimum Reporting Standards for in vivo Magnetic Resonance Spectroscopy (MRSinMRS): Experts' consensus recommendations. *NMR in Biomedicine*, 34(5), 1–18. Retrieved from <https://doi.org/10.1002/nbm.4484>
- Liu, R., Bao, Z. X., Zhao, P. J., & Li, G. H. (2021). Advances in the study of metabolomics and metabolites in some species interactions. *Molecules*, 26(11). Retrieved from <https://doi.org/10.3390/molecules26113311>
- Liu, Y., Cui, D.-X., Pan, Y., Yu, S.-H., Zheng, L.-W., & Wan, M. (2022). Stem Cells and Cancer Stem Cells, 14(7), 490–502.
- Lynette, G. (2020). History of MRIs and the Evolution of This Life-Saving Technology. Retrieved 26 September 2023, from <https://ezra.com/blog/history-of-mri-scans>
- Machiele, R., Motlagh, M., & Patel, B. C. (2022). Intraocular pressure. Retrieved from <https://www.ncbi.nlm.nih.gov/books/NBK532237/>
- Mandal, P. K. (2007). Magnetic Resonance Spectroscopy (MRS) and its application in Alzheimer's disease. *Concepts in Magnetic Resonance Part A: Bridging Education and Research*, 30(1), 40–64. Retrieved from <https://doi.org/10.1002/cmr.a.20072>
- Mandal, P. K. (2012). In vivo proton magnetic resonance spectroscopic signal processing for the absolute quantitation of brain metabolites. *European Journal of Radiology*, 81(4), e653–e664. Retrieved from <https://doi.org/10.1016/j.ejrad.2011.03.076>
- Markley, J. L., Brüschweiler, R., Edison, A. S., Eghbalnia, H. R., Powers, R., Raftery, D., & Wishart, D. S. (2017). The future of NMR-based metabolomics. *Current Opinion in Biotechnology*, 43, 34–40. Retrieved from <https://doi.org/10.1016/j.copbio.2016.08.001>
- Marshall, I., Wardlaw, J., Cannon, J., Slattery, J., & Sellar, R. J. (1996). Reproducibility of metabolite peak areas in ¹H MRS of brain. *Magnetic*

Resonance Imaging, 14(3), 281–292. Retrieved from
[https://doi.org/10.1016/0730-725X\(95\)02084-7](https://doi.org/10.1016/0730-725X(95)02084-7)

Martucci, A., Nucci, C., & Pinazo-Duran, M. D. (2023). Editorial: New perspectives in glaucoma pathophysiology, diagnosis, and treatment. *Frontiers in Medicine*, 10(3), 1200427. Retrieved from
<https://doi.org/10.3389/fmed.2023.1200427>

Maudsley, A. A., Domenig, C., Govind, V., Darkazanli, A., Studholme, C., Arheart, K., & Bloomer, C. (2009). Mapping of brain metabolite distributions by volumetric proton MR spectroscopic imaging (MRSI). *Magnetic Resonance in Medicine*, 61(3), 548–559. Retrieved from
<https://doi.org/10.1002/mrm.21875>

McGowan, J. C. (2008). Basic Principles of Magnetic Resonance Imaging. *Neuroimaging Clinics of North America*, 18(4), 623–636. Retrieved from
<https://doi.org/10.1016/j.nic.2008.06.004>

McRobbie, D. W., Moore, E. A., Graves, M. J., & Prince, M. R. (2006). *MRI from Picture to Proton. Health Physics* (2nd ed.). United States of America: Cambridge University Press. Retrieved 15 April 2018 from
<https://doi.org/10.1097/00004032-200310000-00020>

Miettinen, P. S., Jauhiainen, A. M., Tarkka, I. M., Pihlajamäki, M., Gröhn, H., Niskanen, E., E., Hänninen, T., Vanninen, R., & Soininen, H. (2015). Long-term response to cholinesterase inhibitor treatment is related to functional MRI response in Alzheimer's disease. *Dementia and Geriatric Cognitive Disorders*, 40(5–6), 243–255. Retrieved from
<https://doi.org/10.1159/000435948>

Minati, L., Aquino, D., Bruzzone, M., & Erbetta, A. (2010). Quantitation of normal metabolite concentrations in six brain regions by in-vivo ¹H-MR spectroscopy. *Journal of Medical Physics*, 35(3), 154. Retrieved from
<https://doi.org/10.4103/0971-6203.62128>

Moffett, J. R., Ross, B., Arun, P., Madhavarao, C. N., & Namboodiri, A. M. A. (2007). N-Acetylaspartate in the CNS: From neurodiagnostics to

neurobiology. *Progress in Neurobiology*, 81(2), 89–131. Retrieved from <https://doi.org/10.1016/j.pneurobio.2006.12.003>

Munemasa, Y., & Kitaoka, Y. (2013). Molecular mechanisms of retinal ganglion cell degeneration in glaucoma and future prospects for cell body and axonal protection. *Frontiers in Cellular Neuroscience*, 6(60), 1–13. Retrieved from <https://doi.org/10.3389/fncel.2012.00060>

Murphy, M. C., Conner, I. P., Teng, C. Y., Lawrence, J. D., Safiullah, Z., Wang, B., Bilonick, R.A., Kim, S.G., Wollstein, G., Schuman, J.S., & Chan, K. C. (2016). Retinal Structures and Visual Cortex Activity are Impaired Prior to Clinical Vision Loss in Glaucoma. *Scientific Reports*, 6(July), 1–12. Retrieved from <https://doi.org/10.1038/srep31464>

Nduaguba, C., & Lee, R. K. (2006). Glaucoma screening: current trends, economic issues, technology, and challenges. *Current Opinion in Ophthalmology*, 17(2), 142–152. Retrieved from <https://doi.org/10.1097/01.icu.0000193088.75432.c9>

Near, J., Harris, A. D., Juchem, C., Kreis, R., Marjańska, M., Öz, G., Slotboom, J., Wilson, M., & Gasparovic, C. (2021). Preprocessing, analysis and quantification in single-voxel magnetic resonance spectroscopy: experts' consensus recommendations. *NMR in Biomedicine*, 34(5), 1–23. Retrieved from <https://doi.org/10.1002/nbm.4257>

Noro, T., Namekata, K., Kimura, A., Azuchi, Y., Hashimoto, N., Moriya-Ito, K., Komaki, Y., Lee, C.Y., Okahara, N., Guo, X., & Harada, T. (2019). Normal tension glaucoma-like degeneration of the visual system in aged marmosets. *Scientific Reports*, 9(1), 1–12. Retrieved from <https://doi.org/10.1038/s41598-019-51281-y>

Nuzzi, R., Dallorto, L., & Rolle, T. (2018a). Changes of visual pathway and brain connectivity in glaucoma: A systematic review. *Frontiers in Neuroscience*, 12(363), 1–21. Retrieved from <https://doi.org/10.3389/fnins.2018.00363>

Nuzzi, R., Dallorto, L., & Rolle, T. (2018b). Changes of visual pathway and

- brain connectivity in glaucoma: A systematic review. *Frontiers in Neuroscience*, 12(363), 1–21. Retrieved from <https://doi.org/10.3389/fnins.2018.00363>
- Öz, G., Alger, J. R., Barker, P. B., Bartha, R., Bizzi, A., Boesch, C., Bolan, P.J., Brindle, K.M., Cudalbu, C., Dinçer, A., & Kauppinen, R. A. (2014). Clinical Proton MR Spectroscopy in Central Nervous System Disorders. *Radiology*, 270(3), 658–679. Retrieved from <https://doi.org/10.1148/radiol.13130531>
- P Mansfield. (1977). Multi-planar image formation using NMR spin echoes. *Journal of Physics C: Solid State Physics*, 10(3), L55. Retrieved from <https://doi.org/10.1088/0022-3719/10/3/004>
- Patel, B. Y. K., & Lighthizer, N. (2022). A Review of the Most Impactful Glaucoma Studies. *Modern Optometry*. Retrieved 3 October 2022 from <https://modernod.com/articles/2022-jan-feb/complex-management-of-a-patient-with-a-coinfection?c4src=article:infinite-scroll>
- Pedrosa de Barros, N., Mckinley, R., Knecht, U., Wiest, R., & Slotboom, J. (2016). Automatic quality control in clinical 1H MRSI of brain cancer. *NMR in Biomedicine*, 29(5), 563–575. Retrieved from <https://doi.org/10.1002/nbm.3470>
- Peichl, L. (2009). Retinal Ganglion Cells. In M. D. Binder, N. Hirokawa, & U. Windhorst (Eds.), *Encyclopedia of Neuroscience* (pp. 3507–3513). Berlin, Heidelberg: Springer Berlin Heidelberg. Retrieved from https://doi.org/10.1007/978-3-540-29678-2_5106
- Poser, B. A., & Setsompop, K. (2018). Pulse sequences and parallel imaging for high spatiotemporal resolution MRI at ultra-high field. *NeuroImage*, 168, 101–118. Retrieved from <https://doi.org/10.1016/j.neuroimage.2017.04.006>
- Pouwels, P. J. W., & Frahm, J. (1998). Regional metabolite concentrations in human brain as determined by quantitative localized proton MRS. *Magnetic Resonance in Medicine*, 39(1), 53–60. Retrieved from

<https://doi.org/10.1002/mrm.1910390110>

- Provencher, S. W. (2001). Automatic quantitation of localized in vivo ¹H spectra with LCModel. *NMR in Biomedicine*, 14(4), 260–264. Retrieved from <https://doi.org/10.1002/nbm.698>
- Puri, B. K., Egan, M., Wallis, F., & Jakeman, P. (2018). Repeatability of two-dimensional chemical shift imaging multivoxel proton magnetic resonance spectroscopy for measuring human cerebral choline-containing compounds. *World Journal of Psychiatry*, 8(1), 20–26. Retrieved from <https://doi.org/10.5498/wjp.v8.i1.20>
- Quigley, H. A. (1999). Neuronal death in glaucoma. *Progress in Retinal and Eye Research*, 18(1), 39–57. Retrieved from [https://doi.org/10.1016/S1350-9462\(98\)00014-7](https://doi.org/10.1016/S1350-9462(98)00014-7)
- Quigley, H., & Broman, A. T. (2006). The number of people with glaucoma worldwide in 2010 and 2020. *British Journal of Ophthalmology*, 90(3), 262–267. Retrieved from <https://doi.org/10.1136/bjo.2005.081224>
- Raininko, R., & Mattsson, P. (2010). Metabolite concentrations in supraventricular white matter from teenage to early old age: A short echo time ¹H magnetic resonance spectroscopy (MRS) study. *Acta Radiologica*, 51(3), 309–315. Retrieved from <https://doi.org/10.3109/02841850903476564>
- Ramadan, S., Lin, A., & Stanwell, P. (2013). Glutamate and glutamine: A review of in vivo MRS in the human brain. *NMR in Biomedicine*, 26(12), 1630–1646. Retrieved from <https://doi.org/10.1002/nbm.3045>
- Reichardt, J. L., Dirks, M., Wirries, A. K., Pflugrad, H., Nösel, P., Haag, K., Lanfermann, H., Wedemeyer, H., Potthoff, A., Weissenborn, K., & Ding, X. Q. (2022). Brain metabolic and microstructural alterations associated with hepatitis C virus infection, autoimmune hepatitis and primary biliary cholangitis. *Liver International*, 42(4), 842–852. Retrieved from <https://doi.org/10.1111/liv.15093>

- Rigotti, D. J., Inglese, M., Babb, J. S., Rovaris, M., Benedetti, B., Filippi, M., Grossman, R.I., & Gonen, O. (2007). Serial Whole-Brain N-Acetylaspartate Concentration in Healthy Young Adults. *American Journal of Neuroradiology*, 28(9), 1650–1651. Retrieved from <https://doi.org/10.3174/ajnr.A0712>
- Rigotti, D. J., Kirov, I. I., Djavadi, B., Perry, N., Babb, J. S., & Gonen, O. (2011). Longitudinal whole-brain N-acetylaspartate concentration in healthy adults. *American Journal of Neuroradiology*, 32(6), 1011–1015. Retrieved from <https://doi.org/10.3174/ajnr.A2452>
- Rombouts, S. A. R. B., Barkhof, F., Van Meel, C. S., & Scheltens, P. (2002). Alterations in brain activation during cholinergic enhancement with rivastigmine in Alzheimer's disease. *Journal of Neurology Neurosurgery and Psychiatry*, 73(6), 665–671. Retrieved from <https://doi.org/10.1136/jnnp.73.6.665>
- Ross, B. D., Chenevert, T. L., Kim, B., & Ben-Yoseph, O. (2015). Magnetic Resonance Imaging and Spectroscopy: Application to Experimental Neuro-Oncology. *Quarterly of Magnetic Resonance in Biology and Medicine*, 1(2), 89–106.
- Ross, B. D., Malyarenko, D., Heist, K., Amouzandeh, G., Jang, Y., Bonham, C. A., C.A., Amirfazli, C., Luker, G.D., & Chenevert, T. L. (2023). Repeatability of Quantitative Magnetic Resonance Imaging Biomarkers in the Tibia Bone Marrow of a Murine Myelofibrosis Model. *Tomography*, 9(2), 552–566. Retrieved from <https://doi.org/10.3390/tomography9020045>
- Rucker, J. C., Biousse, V. V. V. V., Mao, H., Sandbach, J., Constantinidis, I., Newman, N. J., & Anlanta, G. (2003). Detection of Lactate in the Human Vitreous Body using Proton Magnetic Resonance Spectroscopy. *Archives of Ophthalmology*, 121(6), 909–911. Retrieved from <https://doi.org/doi:10.1001/archopht.121.6.909>
- Saman, S., & Jamjala Narayanan, S. (2019). Survey on brain tumor segmentation

and feature extraction of MR images. *International Journal of Multimedia Information Retrieval*, 8(2), 79–99. Retrieved from <https://doi.org/10.1007/s13735-018-0162-2>

Schirmer, T., & Auer, D. P. (2000). On the reliability of quantitative clinical magnetic resonance spectroscopy of the human brain - Schirmer - 2000 - NMR in Biomedicine - Wiley Online Library. *NMR in Biomedicine*, 28–36.

Schmitz, B., Wang, X., Barker, P. B., Pilatus, U., Bronzlik, P., Dadak, M., Kahl, K.G., Lanfermann, H., & Ding, X. Q. (2018). Effects of Aging on the Human Brain: A Proton and Phosphorus MR Spectroscopy Study at 3T. *Journal of Neuroimaging*, 28(4), 416–421. Retrieved from <https://doi.org/10.1111/jon.12514>

Shahida, & Qadir, M. I. (2020). Glaucoma: Etiology, Pathophysiology and Management. *Biomedical Journal of Scientific & Technical Research*, 30(5), 23695–23698. Retrieved from <https://doi.org/10.26717/bjstr.2020.30.005005>

Shampo, M. A., Kyle, R. A., & Steensma, D. P. (2012). Richard ernst-nobel prize for nuclear magnetic resonance spectroscopy. *Mayo Clinic Proceedings*, 87(12), e109. Retrieved from <https://doi.org/10.1016/j.mayocp.2012.01.023>

Sharma, H. A., & Lagopoulos, J. (2010). MRI physics: pulse sequences. *Acta Neuropsychiatrica*, 22(2), 90–92. Retrieved from <https://doi.org/10.1111/j.1601-5215.2010.00449.x>

Sheffield, S. (2022). Visual Cortex Areas. Retrieved from <https://www.getbodysmart.com/the-brain/visual-cortex-areas>

Shevelev, O. B., Illarionova, N. B., Petrovski, D. V., Sarapultsev, A. P., Chupakhin, O. N., & Moshkin, M. P. (2017). Effects of a compound from the group of substituted thiadiazines with hypothermia inducing properties on brain metabolism in rats, a study in vivo and in vitro. *PLoS ONE*, 12(7), 1–12. Retrieved from <https://doi.org/10.1371/journal.pone.0180739>

- Sidek, S., Ramli, N., Rahmat, K., Ramli, N. M., Abdulrahman, F., & Kuo, T. L. (2016). In vivo proton magnetic resonance spectroscopy (1H-MRS) evaluation of the metabolite concentration of optic radiation in primary open angle glaucoma. *European Radiology*, 26(12), 4404–4412. Retrieved from <https://doi.org/10.1007/s00330-016-4279-5>
- Soares, D. P., & Law, M. (2009). Magnetic resonance spectroscopy of the brain: review of metabolites and clinical applications. *Clinical Radiology*, 64(1), 12–21. Retrieved from <https://doi.org/10.1016/j.crad.2008.07.002>
- Soqia, J., Ataya, J., Alhalabi, R., Alhomsy, R., Hamwy, R., Mardini, K., & Hamzeh, A. (2023). Awareness and knowledge of glaucoma among visitors of main public hospitals in Damascus, Syria: a cross-sectional study. *BMC Ophthalmology*, 23(1), 1–8. Retrieved from <https://doi.org/10.1186/s12886-022-02766-4>
- Sprawls, P. (2001). *Magnetic Resonance Imaging: Principles, Methods, and Techniques*. *Radiology* (Vol. 221). Retrieved from <https://doi.org/10.1148/radiol.2212012537b>
- Statistics, L. (2015). Paired-samples t-test using SPSS Statistics. Retrieved from <https://statistics.laerd.com>
- Steen, R. G., & Ogg, R. J. (2005). Abnormally high levels of brain N-acetylaspartate in children with sickle cell disease. *American Journal of Neuroradiology*, 26(3), 463–468.
- Stefan, D., Cesare, F. Di, Andrasescu, A., Popa, E., Lazariev, A., Vescovo, E., Strbak, O., Williams, S., Starcuk, Z., Cabanas, M., & Van Ormondt, D. (2009). Quantitation of magnetic resonance spectroscopy signals: the jMRUI software package. *Measurement Science and Technology*, 20(104035), 9. Retrieved from <https://doi.org/10.1088/0957-0233/20/10/104035>
- Tan, L. L., & Sanders, R. (2013). Classification. In *Glaucoma: Basic and Clinical Perspectives* (pp. 6–17). London: Future Medicine Ltd. Retrieved from <https://doi.org/10.2217/ebo.12.415>

- Teixeira, P., Beaumont, M., Gabriela, H., Bailiang, C., Verhaeghe, J., Sirveaux, F., & Blum, A. (2015). Advanced Techniques in Musculoskeletal Oncology: Perfusion, Diffusion, and Spectroscopy. *Seminars in Musculoskeletal Radiology*, 19(05), 463–474. Retrieved 6 October 2023 from <https://doi.org/10.1055/s-0035-1569250>
- Tham, Y. C., Li, X., Wong, T. Y., Quigley, H. A., Aung, T., & Cheng, C. Y. (2014). Global prevalence of glaucoma and projections of glaucoma burden through 2040: A systematic review and meta-analysis. *Ophthalmology*, 121(11), 2081–2090. Retrieved from <https://doi.org/10.1016/j.ophtha.2014.05.013>
- Tognarelli, J. M., Dawood, M., Shariff, M. I. F., Grover, V. P. B., Crossey, M. M. E., Cox, I. J., Taylor-Robinson, S.D., & McPhail, M. J. W. (2015). Magnetic Resonance Spectroscopy: Principles and Techniques: Lessons for Clinicians. *Journal of Clinical and Experimental Hepatology*, 5(4), 320–328. Retrieved from <https://doi.org/10.1016/j.jceh.2015.10.006>
- Toosy, A. T., Mason, D. F., & Miller, D. H. (2014). Optic neuritis. *The Lancet Neurology*, 13(1), 83–99. Retrieved from [https://doi.org/10.1016/S1474-4422\(13\)70259-X](https://doi.org/10.1016/S1474-4422(13)70259-X)
- Tournier, J. D., Calamante, F., & Connelly, A. (2012). MRtrix: Diffusion tractography in crossing fiber regions. *International Journal of Imaging Systems and Technology*, 22(1), 53–66. Retrieved from <https://doi.org/10.1002/ima.22005>
- Trihadijaya, A. F., Abimanyu, B., & Darmini, D. (2019). Pengukuran Nilai Metabolit Pada Penggunaan Variasi Nilai Time Echo Pemeriksaan Magnetic Resonance Spectroscopy Otak. *Jurnal Imejing Diagnostik*, 5(2), 112–119.
- Trivedi, V., Bang, J. W., Parra, C., Colbert, M. K., O'Connell, C., Arshad, A., Faiq, M.A., Conner, I.P., Redfern, M.S., Wollstein, G., & Schuman, J.S (2019). Widespread brain reorganization perturbs visuomotor coordination in early glaucoma. *Scientific Reports*, 9(1), 1–8. Retrieved

from <https://doi.org/10.1038/s41598-019-50793-x>

- Van Der Graaf, M. (2010). In vivo magnetic resonance spectroscopy : basic methodology and clinical applications, 39(4), 527–540. Retrieved from <https://doi.org/10.1007/s00249-009-0517-y>
- Van Geuns, R. J. M., Wielopolski, P. A., De Bruin, H. G., Rensing, B. J., Van Ooijen, P. M. A., Hulshoff, M., Oudkerk, M., & De Feyter, P. J. (1999). Basic principles of magnetic resonance imaging. *Progress in Cardiovascular Diseases*, 42(2), 149–156. Retrieved from [https://doi.org/10.1016/S0033-0620\(99\)70014-9](https://doi.org/10.1016/S0033-0620(99)70014-9)
- Vanoverberghe, C. (2020, January). The importance of glaucoma research and education.
- Vrabec, J. P., & Levin, L. A. (2007). The neurobiology of cell death in glaucoma. *Eye (Basingstoke)*, 21(1), S11–S14. Retrieved from <https://doi.org/10.1038/sj.eye.6702880>
- Weinreb, R. N., Aung, T., & Medeiros, F. A. (2014). The Pathophysiology and Treatment of Glaucoma: A Review. *JAMA*, 311(18), 1901–1911. Retrieved from <https://doi.org/10.1001/jama.2014.3192>.The
- Wiebenga, O. T., Klauser, A. M., Nagtegaal, G. J. A., Schoonheim, M. M., Barkhof, F., Geurts, J. J. G., & Pouwels, P. J. W. (2014). Longitudinal absolute metabolite quantification of white and gray matter regions in healthy controls using proton MR spectroscopic imaging. *NMR in Biomedicine*, 27(3), 304–311. Retrieved from <https://doi.org/10.1002/nbm.3063>
- Wijtenburg, S. A., Rowland, L. M., Oeltzschner, G., Barker, P. B., Workman, C. I., & Smith, G. S. (2019). Reproducibility of brain MRS in older healthy adults at 7T. *NMR in Biomedicine*, 32(2), 1–8. Retrieved from <https://doi.org/10.1002/nbm.4040>
- Wilson, M., Andronesi, O., Barker, P. B., Bartha, R., Bizzi, A., Bolan, P. J., Brindle, K.M., Choi, I.Y., Cudalbu, C., Dydak, U., & Emir, U.E. (2019).

A Methodological Consensus on Clinical Proton MR Spectroscopy of the Brain: Review and Recommendations. *Magn Reson Med*, 82(2), 527–550. Retrieved from <https://doi.org/10.1002/mrm.27742.A>

Wishart, D. S. (2008). Quantitative metabolomics using NMR. *TrAC - Trends in Analytical Chemistry*, 27(3), 228–237. Retrieved from <https://doi.org/10.1016/j.trac.2007.12.001>

Wishart, D. S., Cheng, L. L., Edison, A. S., Eghbalnia, H. R., Hoch, J. C., Gouveia, G. J., Pathmasiri, W., Powers, R., Schock, T.B. & Sumner, L.W. (2022). NMR and Metabolomics — A Roadmap for the Future, 1–20.

Wootla, B., Denic, A., Watzlawik, J. O., Warrington, A. E., & Rodriguez, M. (2015). A single dose of a neuron-binding human monoclonal antibody improves brainstem NAA concentrations, a biomarker for density of spinal cord axons, in a model of progressive multiple sclerosis. *Journal of Neuroinflammation*, 12(1), 2–7. Retrieved from <https://doi.org/10.1186/s12974-015-0303-y>

Wormald, R. P. L., & Jones, E. (2015). Glaucoma: acute and chronic primary angle-closure. *BMJ Clinical Evidence*, 2015(12:703), 1–13.

Yang, Z.-X., Huo, S.-S., Cheng, X.-F., Xu, Z.-F., Cao, Z., Zeng, J.-X., Xiao, Y.Y., You, K.Z., Chen, W., Liu, Y.Y., & Wu, R.-H. (2011). Quantitative multivoxel proton MR spectroscopy study of brain metabolites in patients with amnesic mild cognitive impairment: a pilot study. *Neuroradiology*, 54(5), 451–8. Retrieved from <https://doi.org/10.1007/s00234-011-0900-0>

Yaquob, M. (2012). Visual fields interpretation in glaucoma: a focus on static automated perimetry. *Community Eye Health Journal Issues*, 25(79 & 80), 1–8. Retrieved 29 January 2018 from https://www.ncbi.nlm.nih.gov/pmc/articles/PMC3678209/pdf/jceh_25_79-80_001.pdf

You, M., Rong, R., Zeng, Z., Xia, X., & Ji, D. (2021). Transneuronal Degeneration in the Brain During Glaucoma. *Frontiers in Aging Neuroscience*, 13(643685), 1–10. Retrieved from

<https://doi.org/10.3389/fnagi.2021.643685>

- Yücel, Y. H., Zhang, Q., Weinreb, R. N., Kaufman, P. L., & Gupta, N. (2003). Effects of retinal ganglion cell loss on magno-, parvo-, koniocellular pathways in the lateral geniculate nucleus and visual cortex in glaucoma. *Progress in Retinal and Eye Research*, 22(4), 465–481. Retrieved from [https://doi.org/10.1016/S1350-9462\(03\)00026-0](https://doi.org/10.1016/S1350-9462(03)00026-0)
- Zandavar, H., & Babazad, M. A. (2023). Secondary Metabolites: Alkaloids and Flavonoids in Medicinal Plants. *IntechOpen*. Retrieved from <https://doi.org/10.5772/intechopen.108030>
- Zeisel, S. H., & Da Costa, K. A. (2009). Choline: An essential nutrient for public health. *Nutrition Reviews*, 67(11), 615–623. Retrieved from <https://doi.org/10.1111/j.1753-4887.2009.00246.x>
- Zhang, N., Wang, J., Chen, B., Li, Y., & Jiang, B. (2021). Prevalence of Primary Angle Closure Glaucoma in the Last 20 Years: A Meta-Analysis and Systematic Review. *Frontiers in Medicine*, 7(624179), 1–10. Retrieved from <https://doi.org/10.3389/fmed.2020.624179>
- Zhang, Y., Chen, X., Wen, G., Wu, G., & Zhang, X. (2013). Proton Magnetic Resonance Spectroscopy (1H-MRS) Reveals Geniculocalcarine and Striate Area Degeneration in Primary Glaucoma. *PLoS ONE*, 8(8), 8–13. Retrieved from <https://doi.org/10.1371/journal.pone.0073197>
- Zhou, Y., & Danbolt, • N C. (2014). Glutamate as a neurotransmitter in the healthy brain. *J Neural Transm*, 121, 799–817. Retrieved from <https://doi.org/10.1007/s00702-014-1180-8>

APPENDIX A: PUBLICATION AND PRESENTATION

PUBLISHED PAPER:

Musa, L., Sidek, S., Yusof @ Alias, F., Hanafiah, M., Musa, A. A., & Mohd Razalli, M. (2021). Proton Magnetic Resonance Spectroscopy (1H-MRS) in Studies of Glaucoma: A Scoping Review. *Science Letters*, 15(2), 135–146.
<https://doi.org/10.24191/sl.v15i2.13835>

ORAL PRESENTATION:

International Conference on Research and Practices in Science, Technology and Social Sciences 2020, Universiti Teknologi MARA, Cawangan Selangor, Kampus Dengkil, Dengkil Selangor, MALAYSIA. 4th July 2020. Proton Magnetic Resonance Spectroscopy (1H-MRS) in Studies of Glaucoma: A Scoping Review. (Oral presentation).

APPENDIX B: INFORMATION SHEET

Subjects Information Sheet

CHARACTERISATION OF METABOLITES CONCENTRATION IN GLAUCOMATOUS EYES USING NARROWER SCAN AREA OF PROTON MAGNETIC RESONANCE SPECTROSCOPY (1H-MRS)

Introduction of Study

Glaucoma is one of the most common diseases that could lead to blindness. Commonly, it is a disease that people will only notice after certain area of their normal visual field has become limited. The screening methods that are currently used to detect the early stage of the disease are not as good as we would like them to be. Early detection of this disease is important to enable early treatment given to the patient. There is a technique that would use an imaging modality that may work better to detect the glaucoma at an early stage.

Purpose of Study

The reason we are doing this research is to find out if the technique could give information that would signify that a person would develop glaucoma.

Study Procedure

This research will involve a single imaging procedure of head area using Magnetic Resonance Imaging.

Participant selection

We are inviting all glaucoma patients from the Pusat Pakar Perubatan UITM to participate in the research on the new technique to detect a developing glaucoma. We are also inviting aged matched healthy individuals who are concerned with their eye condition to participate in this research.

Procedures and Protocol

For healthy participants, it is because we do not know if you are really free from this glaucoma disease, we will assess your eyes using several instruments to enable us categorizing you in the healthy control group.

For participants who are already diagnosed with glaucoma or other certain ocular disease, it is because your eyes condition might change, we will also assess your eyes using several instruments to allow us obtaining the accurate conditions of your eyes prior the imaging procedures.

Eye assessment

The tests will be performed by qualified optometrists and ophthalmologists. You will be asked to sit before the instrument or the assessors for the eye assessment.

Your details of eye condition would be obtained from the tests prior the imaging procedure. The several instruments for the eye assessment are safe and not harmful; hence should not worry you.

Imaging procedure

This imaging procedure does not use x-rays or radiation but use magnetic field and radio waves to create an image of internal body structure.

You will be asked to lie down on the MRI table while your test is being performed. Your head will be cradled on a headrest and your arms at your sides. The table will slowly move into the magnetic field. While the scanner is performing your scan, you will hear some humming and thumping sounds for several minutes at a time. These are normal and should not worry you.

Exam times may range from as short as 15 minutes to as long as 40 minutes, depending on the cooperation from you; to be relax and lie as still as possible. Any movement during the scanning will blur the image and interrupt the signals that that should be received by the system.

Duration

The research takes place over nine months in total. However, each participant will only need to come for eye assessment once and for imaging procedure in the radiology unit once. In total you will be asked to come 2 times to the hospital within the 9 months.

Participation in Study

Your participation in this research is entirely voluntary. It is your choice whether to participate or not. Nothing will change and all the services that you receive in the clinics of this hospital will continue whether you choose to participate or not. Even if you agreed earlier, you may stop participating anytime if you change your mind.

Benefit of Study

Information obtained from this study will benefit the researchers, Government of Malaysia, doctors and individuals for the advancement of knowledge and practice of medicine in future.

The outcome of this research will hopefully guide us to use MRI as a diagnosing tool for glaucoma, which in turn could provide better care for glaucoma patient.

If you have any question about this study or your rights, please contact the investigator at the following:

Researcher's Name: Liyana Musa

Contact Number: 013-9952346

Address : Department of Diagnostic Imaging and Radiotherapy,
Kulliyah of Allied Health Sciences,
International Islamic University Malaysia
Kuantan Campus,

25200 Kuantan, Pahang

Email : liyanamusamumtaz@gmail.com/ liyanamusa@iium.edu.my

OR

Supervisor's Name : Asst. Prof. Dr. Firdaus bin Yusof@Alias

Contact Number: 09-571 6400

Address : Department of Optometry and Vision Science,
Kulliyah of Allied Health Sciences,
International Islamic University Malaysia
Kuantan Campus,
25200 Kuantan, Pahang

Email : yfirdaus@iium.edu.my

OR

Co-Supervisor's Name: Dr. Sabrilhakim bin Sidek

Contact Number: 03-6126 5000

Address : Medical Imaging Unit,
Faculty of Medicine,
Universiti Teknologi MARA,
Sungai Buloh Campus, Selangor Branch,
47000, Jln Hospital, Sungai Buloh
Selangor.

Email : bhkimy_7@hotmail.com

Study Risk

Because of the magnetic field and radio frequencies, people with a heart pacemaker, brain aneurysm clips and some implanted metallic or electrical devices should not have an MRI. It is important that you inform the researcher or the technologist if you have any of these metallic appliances.

Other than that, there are no risks involved in this research itself.

Confidentiality

Your medical information will be kept confidential by the investigators and will not be made public unless disclosure is required by law.

By signing this consent form, you will authorize the review of records, analysis and use of the data arising from this study.

APPENDIX C: CONSENT FORM

Consent Form

To become a subject in the research, you or your legal guardian is advised to sign this Consent Form.

I herewith confirm that I have met the requirement of age and am capable of acting on behalf of myself /* as a legal guardian as follows:

1. I understand the nature and scope of the research being undertaken.
2. I have read and understood all the terms and conditions of my participation in the research.
3. All my questions relating to this research and my participation therein have been answered to my satisfaction.
4. I voluntarily agree to take part in this research, to follow the study procedures and to provide all necessary information to the investigators as requested.
5. I may at any time choose to withdraw from this research without giving reasons.
6. I have received a copy of the Subjects Information Sheet and Consent Form.
7. Except for damages resulting from negligent or malicious conduct of the researcher(s), I hereby release and discharge UiTM and all participating researchers from all liability associated with, arising out of, or related to my participation and agree to hold them harmless from any harm or loss that may be incurred by me due to my participation in the research.

_____ Name of Subject/Legal Guardian	_____ Signature
_____ I.C No	_____ Date
_____ Name of Witness	_____ Signature
_____ I.C No	_____ Date
_____ Name of Consent Taker	_____ Signature
_____ I.C No	_____ Date

APPENDIX D: MRI PATIENT SAFETY SCREENING FORM

MAGNETIC RESONANCE IMAGING (MRI) SAFETY CHECKLIST

NAME:	
ID:	PHONE NO:
WEIGHT	HEIGHT:

Please complete the questions by circling YES or NO

Do you (or have ever had) any of the following?			
Heart Attack	Y / N	Intravascular coils, filters or stents	Y / N
Stroke	Y / N	Vascular clips or wires	Y / N
Peripheral Vascular Disease	Y / N	Brain shunt tube	Y / N
Pacemaker	Y / N	Metal pins, plates, rods, screws, prosthesis	Y / N
Pacing Wires/Defibrillator	Y / N	Ocular (eye) prosthesis	Y / N
Artificial Heart Valve	Y / N	Implanted pain relief pump	Y / N
Brain aneurysm clip	Y / N	Any other form of implant	Y / N
Cochlear implant	Y / N	Ear Surgery	Y / N
Stapes (ear) implant	Y / N	Brain Surgery	Y / N
Neurostimulator / Biostimulator	Y / N	Heart Surgery	Y / N
Claustrophobia	Y / N	Any previous MRI examination?	Y / N

Do you have any of the following?			
Hearing aid	Y / N	Shrapnel or bullet wounds	Y / N
Currently have transdermal (skin) patches? e.g. nicotine patches	Y / N	Dentures, braces including magnetically activated dentures	Y / N
A tattoo (or tattooed makeup)	Y / N	Any type of body piercing	Y / N
Have you had an operation in the last 6 weeks? If <u>YES</u> , what?			Y / N
Female patient: Could you be pregnant?			Y / N

I acknowledge to the best of my understanding; the answers are true.
I have had the MRI scan explained to me and been given the opportunity to ask questions about this scan. I give my consent to undergo this procedure.

Date / / Signature

Date / / Signature of Radiographer



**PLEASE REMOVE ALL JEWELLERY (WATCHES, CHAINS, EARRINGS ETC) IN
PREPARATION FOR YOUR EXAMINATION.**

APPENDIX E: ETHICS APPROVAL

www.irmi.uitm.edu.my

Institut Pengurusan Penyelidikan & Inovasi
Institute of Research Management & Innovation

Universiti Teknologi MARA
Aras 3, Bangunan Wawasan
40450 Shah Alam, Selangor, MALAYSIA
Tel: (+603) 5544 2094 Faks: (+603) 5544 2096
E-mel: irmi@uitmsalam.uitm.edu.my



**UNIVERSITI
TEKNOLOGI
MARA**

Reference : 600-IRMI (5/1/18)
Our reference : REC/450/18
Date : 25 February 2019

Dr Sabrihakim Sidek
Faculty of Medicine
Universiti Teknologi MARA
Sungai Buloh Campus
Jalan Hospital
47000 Sungai Buloh
Selangor

Dear Dr Sabrihakim,

ETHICS APPROVAL BY UITM RESEARCH ETHICS COMMITTEE

Title: Characterisation of Metabolites Concentration in Glaucomatous Eyes Using Narrower Scan Area of Proton Magnetic Resonance Spectroscopy.

Trial Site: Faculty of Medicine, UiTM Shah Alam

Thank you for your research ethics application on 29 November 2018 and your amendment for the above study on 11 January 2019. We would like to inform that the UiTM Research Ethics Committee had deliberated your proposal on the 19 February 2019 and it is our pleasure to inform you that the Committee has agreed to grant an ethics approval for the said study. This ethics approval is valid from 19 February 2019 until 31 August 2020.


Please submit progress report of the study to the REC Secretariat 12 months after the date of approval letter and annually until the study has completed. Please kindly notify the REC for any amendments to the relevant documents for this study. Notification should be made to the REC for any protocol deviation and in case of serious adverse event, please notify the REC within 48 hours from the time known. A summary of the final report should be submitted at the end of your study.

The UiTM Research Ethics Committee operates in accordance to the ICH Good Clinical Practice Guidelines, Malaysia Good Clinical Practice Guidelines and the Declaration of Helsinki.

Attached is the list of members of the Committee.


Thank you.


Yours faithfully,




PROFESSOR DR. HADARIAH BAHRON
Assistant Vice Chancellor (Research & Innovation)
Chairman of UiTM Research Ethics Committee

Research with Integrity & Accountability.

 Peghat Call : Tel : (+603) 5544 8289/8254
Faks : (+603) 5544 8280

 Peghat RMC : Tel : (+603) 5544 8072/8070
Faks : (+603) 5544 2096

 Peghat RIBU : Tel : (+603) 5544 2747/2746
Faks : (+603) 5544 2790

c.c.: Dr Firdaus Yusof @ Alias
Department of Optometry and Vision Science
Kuliyah of Allied Health Sciences
International Islamic University Malaysia

Liyana Musa
Department of Diagnostic Imaging and Radiotherapy
Kuliyah of Allied Health Sciences
International Islamic University Malaysia



APPENDIX F: DETAILED SAMPLE SIZE CALCULATION

File Edit View Tests Calculator Help

Central and noncentral distributions Protocol of power analyses

Analysis: A priori: Compute required sample size

Input:

- Tail(s) = One
- Effect size d = 1.1666667
- α err prob = 0.05
- Power (1-β err prob) = 0.8
- Allocation ratio N2/N1 = 1

Output:

- Noncentrality parameter δ = 2.6087460
- Critical t = 1.7340636
- Df = 18
- Sample size group 1 = 10
- Sample size group 2 = 10
- Total sample size = 20

Test family: t tests

Statistical test: Means: Difference between two independent means (two groups)

Type of power analysis: A priori: Compute required sample size – given α, power, and effect size

Input Parameters:

- Tail(s): One
- Effect size d: 1.1666667
- α err prob: 0.05
- Power (1-β err prob): 0.8
- Allocation ratio N2/N1: 1

Output Parameters:

- Noncentrality parameter δ: 2.6087460
- Critical t: 1.7340636
- Df: 18
- Sample size group 1: 10
- Sample size group 2: 10
- Total sample size: 20
- Actual power: 0.8061747

Secondary Window: n1 != n2

- Mean group 1: 0.38
- Mean group 2: 1.29
- SD σ within each group: 0.78

Secondary Window: n1 = n2

- Mean group 1: 0
- Mean group 2: 1
- SD σ group 1: 6.24
- SD σ group 2: 4.8

Calculate Effect size d 1.166667

Calculate and transfer to main window

Close

X-Y plot for a range of values Calculate

What is a good power sample size?

The number of participants recruited for this study was calculated using mean and standard deviation of Glx/Cr ratio in lateral geniculate body from glaucoma group (1.29 ± 1.21) and healthy group (0.38 ± 0.35) in the study by Doganay, Cankaya, & Alkan, (2012). The calculation was done using Power and Sample Size Calculation software (version 3.9.1.4) (Faul, Erdfelder, Lang, & Buchner, 2007).

$$\begin{aligned} \text{SD within each group} &= (\text{SD group 1} + \text{SD group 2})/2 \\ &= (1.21 + 0.35)/2 \\ &= 0.78 \end{aligned}$$